Guiding the design of heterogeneous electrode microstructures for Li-ion batteries: microscopic imaging, predictive modeling, and machine learning

Hongyi Xu[1], Juner Zhu[2,3], Donal P. Finegan[4], Hongbo Zhao[3], Xuekun Lu[5,6,7], Wei Li[2], Nathaniel Hoffman[8], Antonio Bertei[9], Paul Shearing[5,6], Martin Z. Bazant[3,10]

[1] Department of Mechanical Engineering, University of Connecticut, Storrs, CT 06269, USA
[2] Department of Mechanical Engineering, Massachusetts Institute of Technology, Cambridge, MA 02139, USA
[3] Department of Chemical Engineering, Massachusetts Institute of Technology, Cambridge, MA 02139, USA
[4] Center for Integrated Mobility Sciences, National Renewable Energy Laboratory, Golden, CO, 80401, USA
[5] The Electrochemical Innovation Lab, Department of Chemical Engineering, University College London, Torrington Place, WC1E 7JE, London, United Kingdom
[6] The Faraday Institution, Quad One, Becquerel Ave, Harwell Campus, Didcot OX11 0RA
[7] National Physical Laboratory, Hampton Road, Teddington, Middlesex, TW11 0LW, UK
[8] Advanced Manufacturing for Energy Systems, University of Connecticut, Storrs, CT 06269, USA
[9] Department of Civil and Industrial Engineering, University of Pisa, Pisa, 56122, Italy
[10] Department of Mathematics, Massachusetts Institute of Technology, Cambridge, MA 02139, USA

Abstract

Electrochemical and mechanical properties of lithium-ion battery materials are heavily dependent on their 3D microstructure characteristics. A quantitative understanding of the role played by stochastic microstructures is critical for the prediction of material properties and for guiding synthesis processes. Furthermore, tailoring microstructure morphology is also a viable way of achieving optimal electrochemical and mechanical performances of lithium-ion cells. To facilitate the establishment of microstructure-resolved modeling and design methods, here we present a review covering spatially and temporally resolved imaging of microstructure and electrochemical phenomena, microstructure statistical characterization and stochastic reconstruction, microstructure-resolved modeling for property prediction, and machine learning for microstructure design. This review is concluded with our perspectives on the unresolved challenges and opportunities in applying experimental data, modeling, and machine learning to improve our understanding of materials and identify paths towards enhanced performance of lithium-ion cells.

Keywords: Lithium-ion battery; Stochastic microstructure; Microscopic imaging; Multi-physics modeling; Electrochemical property; Mechanical property; Computational design; Machine learning.

1. Introduction

Lithium-ion (Li-ion) batteries show great potential in achieving societal impact in terms of electrified transportation, grid-level energy storage, consumer electronics, military, and aerospace applications. Despite progress in Li-ion battery technologies in recent years, major challenges in energy density, durability, safety, and cost remain. Research efforts are primarily focused on two aspects to provide prospective solutions. On one hand, new chemistries are developed to obtain electrochemical properties that cannot be found in existing materials. On the other hand, significant efforts are also made to achieve a quantitative understanding of the relationship between the electrochemically coupled transport processes and the microstructures of cathode, anode, and separator [1-3], which is the focus of this review paper. The heterogeneous microstructural morphologies induce heterogeneity in mass transport, electrochemical, and mechanical performances of the battery materials. Here “microstructures” refer to the stochastic geometrical characteristics at the micron and submicron scales (larger than the atomic scale). It is to be noted that structures at this length scale are also referred to as “mesostructures” in some works [4].

Microstructure-resolved predictive modeling and machine learning enable rational discovery and design of new materials for Li-ion battery applications. Computational microstructural material design tools, including Integrated Computational Materials Engineering (ICME) [5, 6], enable forward property prediction and backward process and microstructure design based on the process-microstructure-property (P-S-P) link. Microstructure plays a central role in predicting material properties and guiding synthesis processes. A computational microstructural material design framework consists of four major components:

- **Microscopic imaging and microstructure characterization:** the purpose is to measure microstructural features and describe the observed features quantitatively. As most heterogeneous materials embody certain degrees of randomness in microstructures (microstructural uncertainties), the microstructure characterization methods should also achieve statistical significance.
- **Stochastic reconstruction:** is the process of generating a set of digital microstructures that are equivalent to the target microstructure's statistical functions, which are obtained by statistical characterization of experimental data. Stochastic reconstruction also enables exploration of the vast microstructure design space by generating microstructure designs beyond the limit of empirical datasets.
- **Predictive modeling:** physical laws are implemented into the microstructural model and the governing equations are solved computationally. The electrochemical performance and mechanical integrity are predicted, which serve as an important input for microstructural design and health prognostics.
- **Material informatics and computational design:** the focus is to make sense of the vast image/simulation data to provide guidance for rational discovery and design. Machine learning and deep learning-driven methods accelerate the process of generating new microstructure designs from large parameter spaces to achieve target properties.

Here, we provide an in-depth review of the microscopic imaging and computational methods that have an impact on the predictive modeling and design of microstructural materials for Li-ion battery applications. This review is structured following the typical procedure of computational material design, as shown in Figure 1. Section 2 introduces the state-of-the-art microscopic imaging techniques that are applied to collect image data of Li-ion battery materials as well as recent insights achieved into heterogeneous microstructures and lithium transport that are important for model accuracy. Section 3 introduces image-based statistical characterization and stochastic reconstruction methods, which provide structural information for the property prediction models introduced in Section 4. In Section 5, studies on the computational design of Li-ion battery microstructures are reviewed. Section 6, the final section, outlines our perspectives on new opportunities and challenges in microstructure design and manufacturing of Li-ion battery microstructures.

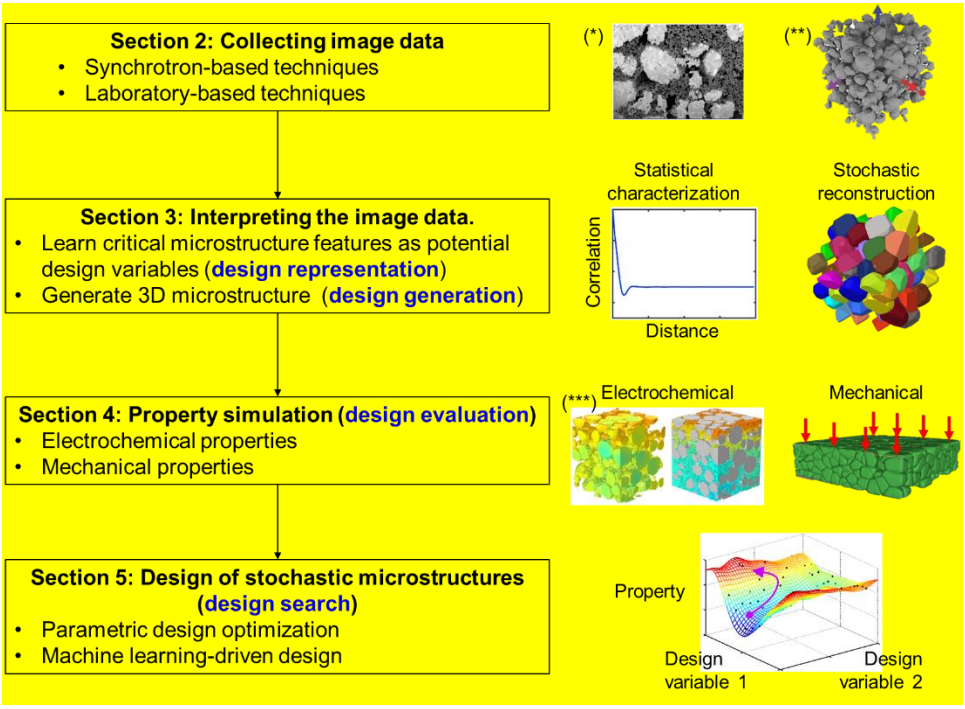

Figure 1: Organization of this paper follows the process of designing a new stochastic microstructural material for battery applications. Section 2 discusses techniques for data collection, Section 3 discusses methods for interpreting the image data to generate quantitative representations of the stochastic microstructures, and methods for generating microstructures based on design variable values. Section 4 discusses methods for evaluating design performances (electrochemical and mechanical properties), and Section 5 discusses how to utilize the aforementioned techniques to search microstructure designs of desired properties. Subplots (*) and (***) are from [7], and subplot (**) is from [8].

2. Microscopic imaging of the heterogeneous microstructures

Accurately capturing the microstructure of lithium-ion battery components is a critical first step towards simulating the behavior of a realistic system. However, further dynamic chemical data is needed to help guide and validate cutting-edge models. Ideally, a researcher would have tools to capture chemical, mechanical, crystallographic, and morphological details nondestructively, across a range of temporal and spatial resolution, and in relevant operating environments. However, existing techniques are constrained by systematic and physical limits, often having benefits and drawbacks for a particular purpose when compared to each other. A spectrum of techniques are available for measuring chemical, mechanical, and/or crystallographic changes ex-situ, in-situ, or in operando [9]. These techniques across multiple length scales use X-rays, electrons, neutrons and ion beams, as well as optical, infrared, and other wavelengths of light to probe chemical heterogeneities and dynamics during the operation of batteries. Here, we focus on techniques that can provide valuable information for informing microstructure models, i.e. with resolutions within the range of 10's of nanometers to around 1 micrometer, and can measure spatial and/or temporal chemical changes that can inform cutting-edge microstructure modeling.

The rapid development of tomography tools over the past twenty years has provided researchers with the toolbox for routine characterization of heterogeneous microstructures for battery electrodes. At the length scales of relevance to this article, the two primary methods are based on X-ray probes (using laboratory and synchrotron sources), and variants of FIB-SEM. These tools provide the balance of spatial resolution and Representative Volume Element (RVE) required to successfully characterize continuum behavior in battery

electrodes, and to successfully establish quantitative relationships between electrode microstructure and performance. X-ray tomography benefits from the ability to non-destructively characterize battery materials and devices; and consequently provides opportunities to explore microstructural evolution effects, which contribute to electrode and device degradation. Numerous examples from the literature include investigations of electrochemical [10-13] and mechanical [7, 14] driving forces for microstructure evolution, and are summarized in recent reviews [15, 16]. Emerging techniques, predominantly using synchrotron facilities, are also subjects of recent review articles [17].

Whilst the suite of tools using FIB-SEM are characterized by their destructive nature, they provide an alternative probe, typically with different contrast generation mechanisms, and higher spatial resolution [18] Moreover the routine ability for combined chemical [19, 20] and crystallographic [21] analysis provides valuable correlative insight.

In concert, and as part of a correlative microscopy toolbox, these tools provide the ability to understand and quantify electrode heterogeneities, and through combination with relevant modelling tools, to provide a platform for rational electrode design.

In the following sections we will explore X-ray and electron imaging techniques that will be broken down to synchrotron techniques [22] and lab-based techniques. The advantage of synchrotron techniques is that measurements with much higher temporal resolution than lab-based techniques can be acquired, thus presenting opportunities for operando measurements. But while synchrotron techniques offer this advantage, their access is limited and often bespoke data-processing methods make data analysis very time-consuming with steep learning curves.

Here we focus our discussion on synchrotron and lab-based techniques that can give insight into the complex and heterogeneous chemical, mechanical, and crystallographic information and guide our departure from conventional models that carry numerous simplified assumptions like chemical homogeneity. We will focus on recent progress in answering key questions on how lithium transports through solid materials, how the crystallographic and stoichiometric properties of electrode materials vary in space and time, and how heterogeneous chemical dynamics influence strain field and contribute to performance limitations and degradation.

2.1 Laboratory-based techniques

The accessibility and relatively low cost of laboratory-based techniques compared to synchrotron sources make them more favorable for researchers to use. There are numerous lab-based techniques that can reveal useful information to guide modelling techniques; here, we will focus on a few recent developments that help provide information on material properties including morphological, crystallographic, chemical, and electrical heterogeneities within electrodes. These properties will be discussed in sequence.

For morphological measurements, the portfolio of laboratory X-ray CT instrumentation has grown substantially over the past decade and provides a toolbox for studying batteries from the particle [23, 24] to the electrode [25] and device [26] level; and indeed, there are numerous examples of the correlation across these scales [18, 27]. These examples illustrate the flexibility of the laboratory technique for non-destructive, multi-scale characterization: whilst the temporal resolution of synchrotron facilities is substantially better, the spatial resolution of laboratory tools is competitive. A comprehensive review of the principles of X-ray CT, applied to battery materials, is provided by Pietsch et al. [28].

Early studies predominantly focused on the ability to extract key microstructural information (porosity, surface areas, geometrical tortuosity etc.) [1, 29], but the potential for in-situ studies was quickly realized,

and applied to both commercial [30], and bespoke [31] cells, to explore the evolution of electrode morphology as a function of state of charge and cycle life. With increasing sophistication, the ability to demarcate solid phases within composite electrodes has also been realized [7, 25, 32, 33]. Moreover, the ability to quantify the changing electrode morphology, as an indicator of cell degradation has also been demonstrated [34-36]. However, even the highest-resolution X-ray CT systems are limited in their ability to distinguish sub-particle features like the grains within NMC particles, and does not have the ability to characterize crystallographic properties or the orientation of grains that influence sub-particle lithium transport.

For grain and crystallographic properties, electron backscatter diffraction (EBSD) has recently been applied to quantify the sub-particle grain structure of NMC electrode particles. This technique is particularly powerful for model guidance because very often, models assume a homogeneous structure within single particles and a uniform radial diffusion of lithium. The resolution of EBSD is dependent on the spot size of the electron beam as well as the size of the steps between each measurement, and since images are reconstructed from a series of point measurements the field of view is only limited by the time that the user is willing to commit to the measurement and perhaps their data storage capabilities. Quinn et al. [37] applied EBSD to NMC particles with a resolution of about 50 nm (Figure 2a) and quantified the orientation of grains within NMC particles while also showing through basic modeling that the orientation of grains within particles will greatly affect the transport dynamics of lithium during operation. While this work presented opportunities for EBSD in 2D, gathering the grain information in 3D is essential to accurately model transport within full particles. Extending EBSD to 3D was later achieved by the same group in a paper by Furat et al. [21] where they applied FIB-EBSD with a similar resolution of about 50 nm to map the grain structure of a single NMC particle (Figure 2b) and quantify the morphological features of sub-particle grains. This work provided a rich 3D dataset for input to finite element multi-physics models to understand lithium transport limitations and sub-particle strains.

For exploring elemental distributions within electrodes, energy-dispersive spectroscopy (EDS) is commonly used but is limited in resolution and detection capability of light elements in low concentrations like lithium, whereas time-of-flight secondary ion mass spectrometry (TOF-SIMS) and FIB-SIMS [38] have higher detection capabilities. TOF-SIMS has been applied to cross sections of lithium-ion battery electrodes to map elemental distributions of lithium and other metals within particles with resolutions of 10's of nanometers (Figure 2c) [39, 40]. The fields of view for these techniques are also variable depending on the time and data-storage capabilities available, but are generally applied with field of view of micrometers or 10's of micrometers. The techniques can be combined through correlative metrology due to the possibility of multiple electron measurement techniques being housed in a single laboratory system. Correlative FIB-SEM, EDS, and TOF-SIMS was demonstrated by Sui et al. [40], and showed the power of these techniques for identifying lithium trapping sites within particles and heterogeneous elemental distributions within particles that would affect lithium transport and rate of degradation of cells.

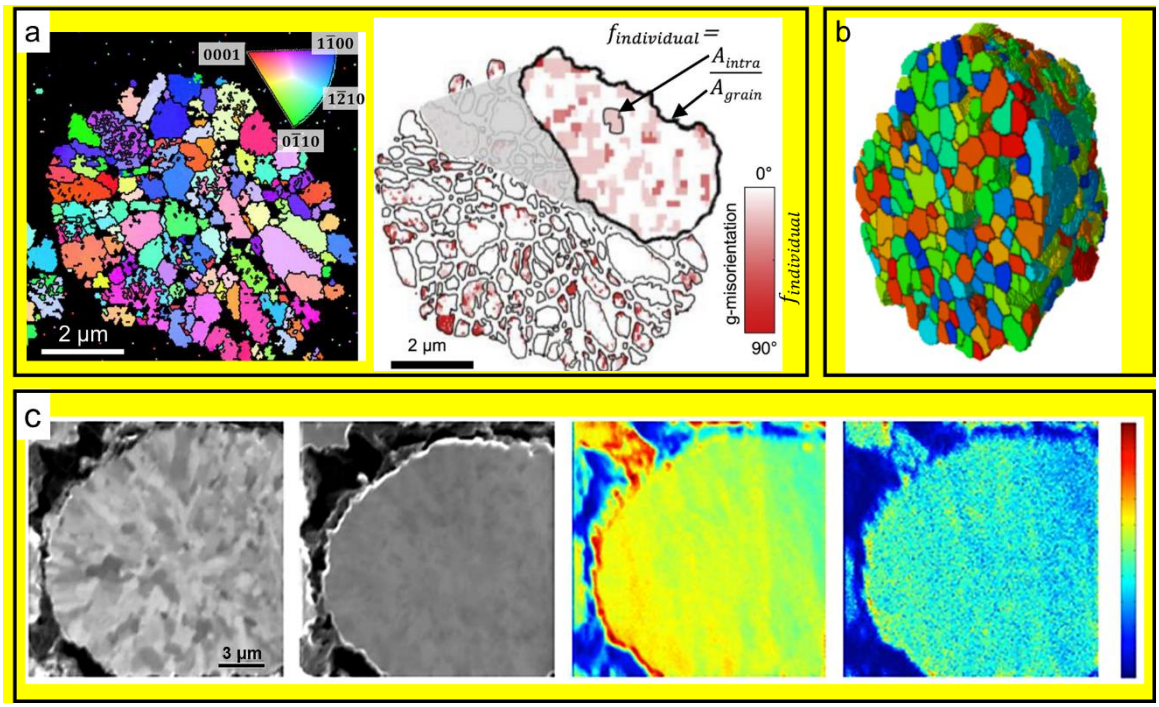

Figure 2: (a) EBSD cross-section of an NMC particle showing the orientation of individual grains in addition to sub-grain defects, extracted from [37]. (b) 3D image of the grain structure within an NMC particle quantified using FIB-EBSD, extracted from [21]. (c) Images from SEM and SIMS showing the elemental distribution of lithium and manganese on the cross-section of an NMC particle, extracted from [39].

With resolution in the range of nanometers, X-ray photoelectron spectroscopy can be applied for depth-profiling of composition which is particularly useful for characterizing the thickness and composition of the solid electrolyte interphase (SEI). For example, Niehoff et al. [41] used XPS in combination with sputter depth profiling to show variations in the thickness and composition of the SEI on graphite with lateral resolution of 3 µm and showed a multi-layer composition of inorganic and organic constituents. Bjorklund et al. [42] applied XPS to NMC particles and showed that the surface layer formed on the NMC cathode is influenced by the choice of the anode, with lithium-metal anodes causing the greatest difference in surface layer thickness and composition on NMC. Understanding the influence of SEI and surface layers is also important to improving the accuracy of models because the SEI will influence the life of the cell as well as the impedance of the cell.

Finally, for exploring the spatial electrical properties of electrode materials, scanning spreading resistance microscopy (SSRM) has been applied to measure the resistivity of surface layers on electrodes in 3D with

spatial resolution of nanometers for fields of view of 10's of micrometers

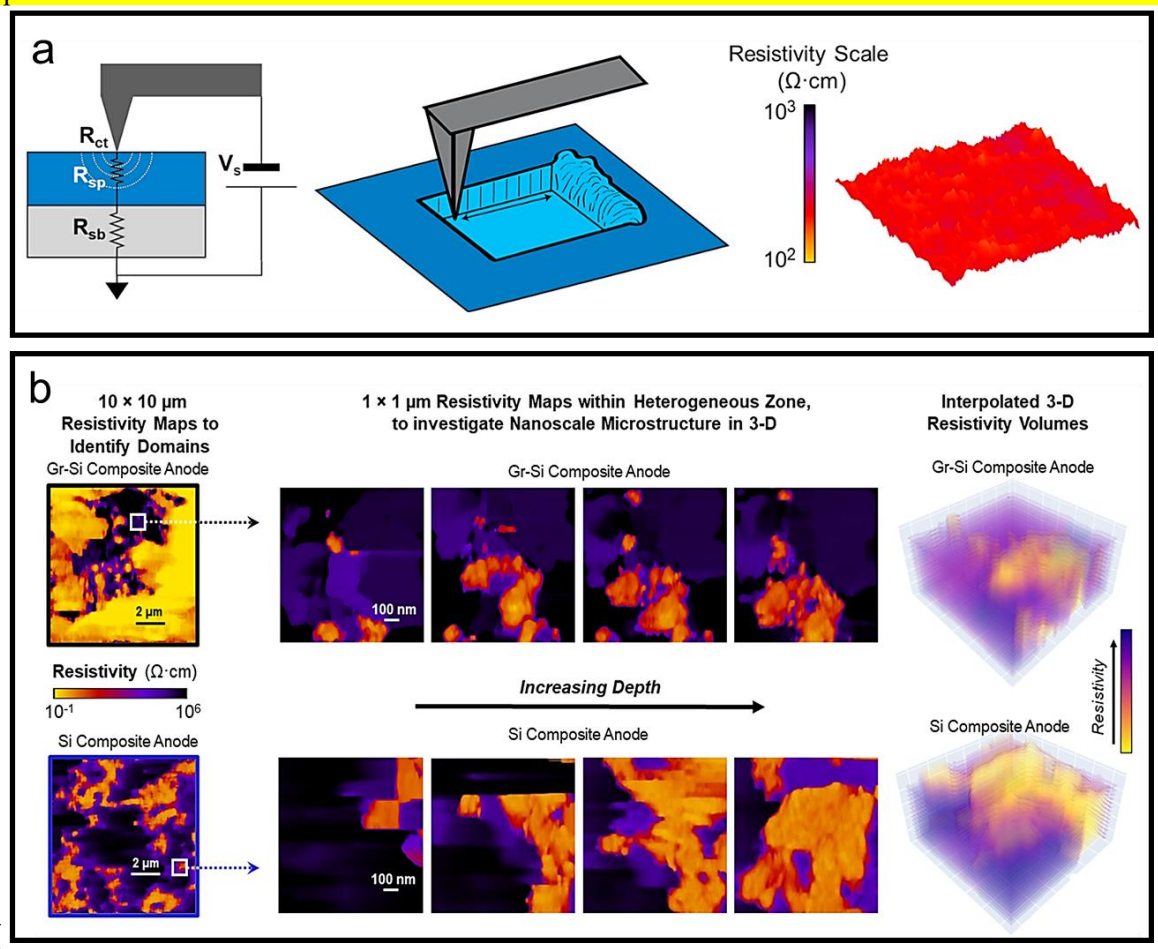

(

Figure 3) [43, 44] and holds great potential for understanding the influence of different operating conditions, formation conditions, electrolyte additives, and electrode materials on the thickness and electrical resistivity of surface layers on electrodes, thus providing valuable impedance information for modelling techniques. These heterogeneities at the electrode and particle scales incur consequences for the operation of cells and must be reflected in modelling methods to achieve a high degree of accuracy and be able to predict degradation and optimal operating conditions.

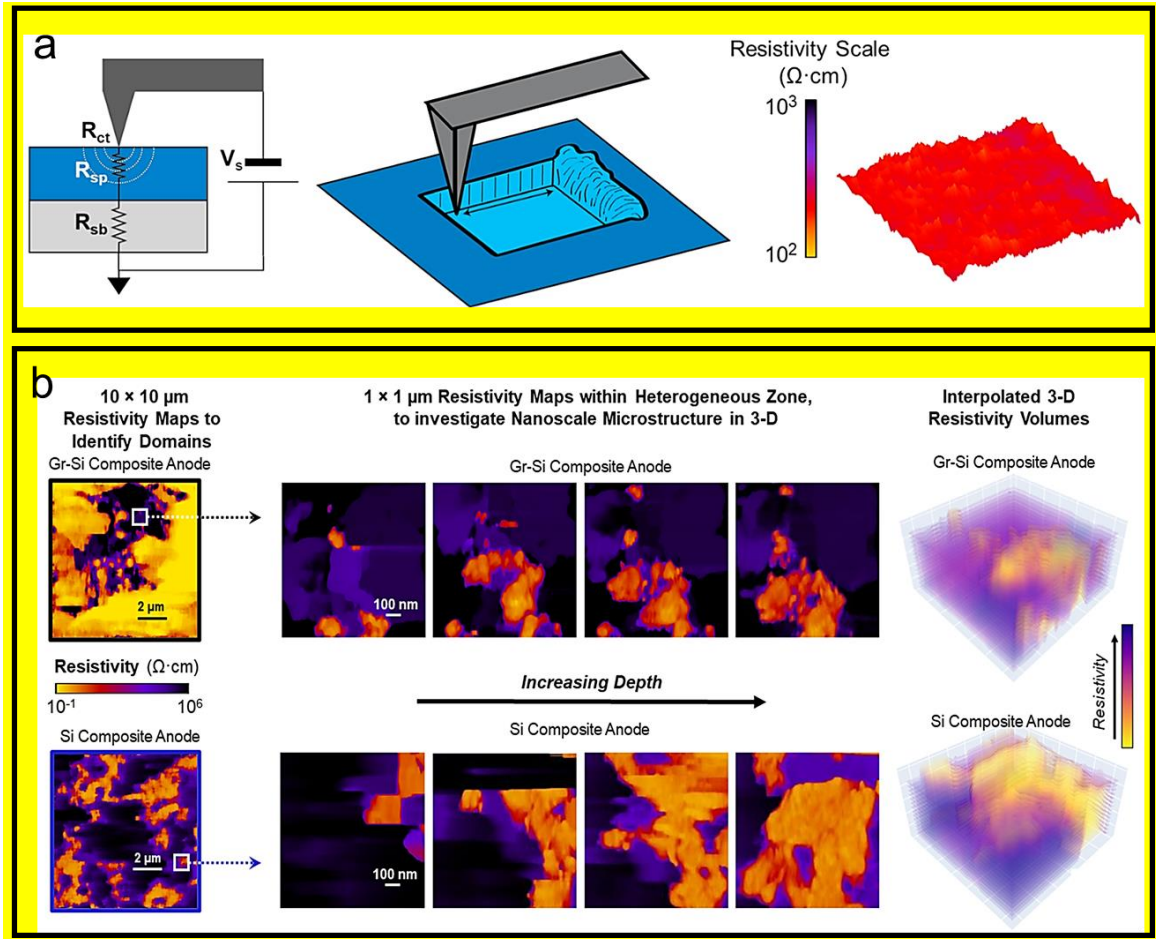

Figure 3: (a) Example of how SSRM can be used to construct 3D resistivity maps of electrode materials, extracted from [43]. (b) SSRM applied to Si-graphite electrodes showing a 3D reconstruction of resistivity within the Si-graphite composite, extracted from [44].

2.2 Synchrotron-based techniques

Over the past decade, non-destructive synchrotron X-ray techniques have revealed numerous new insights into the spatial and temporal function of lithium-ion battery materials. Most notably, synchrotron X-ray techniques have elucidated the complexities that influence how lithium and electrons transport through electrodes, such as phase-field dynamics, reaction kinetics, concentration gradients, mechanical strains, and certain defects in active materials.

The application of synchrotron based absorption tomography across multiple length scales is widespread, and the enhanced flux offered by synchrotron sources makes in-situ and operando studies more routine; consequently it has been applied widely to a range of materials including NMC [8], graphite [12] and silicon [10, 13], as well as a range of emerging battery electrode materials and chemistries [45-47]. Alongside laboratory data, these have been widely applied as the basis for image-based models [8, 48-50]. The routine application of X-ray phase contrast modalities in synchrotron environments has also been widely applied to visualize low atomic number materials [51, 52].

Moreover the versatility in synchrotron imaging enables the tandem application of imaging, diffraction and spectroscopy, which coupled with high signal to noise capabilities provide an opportunity to push both spatial and temporal resolution: these insights are crucial to guide modeling methods to a higher degree of

accuracy. For example, with 50 nm resolution X-ray absorption near-edge spectroscopy (XANES), local chemical information within single $LiFePO_4$ particles was measured and nanonetworks of a segregated Fe-phosphide phase were detected [53]. X-ray diffraction computed tomography (XRDCT) also showed heterogeneous crystal structures and compositions within spinel $LiMn_2O_4$ particles [54] (Figure 4a) as well as core-shell structures of amorphous lithiation and crystalline delithiated Si particles in graphite-Si electrodes [55]. Tian et al. [56] applied transmission X-ray microscopy (TXM) and XANES to explore heterogeneities through single $LiNi_{0.6}Mn_{0.2}Co_{0.2}O_2$ (NMC) particles, finding radial gradients in Ni oxidation states showing evidence of surface reconstruction and a core-shell structure of particles. By looking at the oxidation states of the transition metals within the particle crystal structures, this work also showed lithiation gradients within particles (Figure 4b). These heterogeneous stoichiometries and crystal structures will affect the effective diffusion coefficient of particles and cause local diffusion rates within the particle, diverging from standard assumptions of a single diffusion coefficient applied to particles for finite element modelling. Features like surface reconstructions and lithiation heterogeneities can impact the mechanical integrity of particles and dictate the rate of degradation of electrodes. For example, consequences of surface reconstructions and lithiation heterogeneities for sub-particle mechanical strain were revealed by Li et al. [57] where, through the application of TXM and soft X-ray absorption spectroscopy, the surface chemistry was linked to sub-particle cracking through TXM and finite element modelling (Figure 4c).

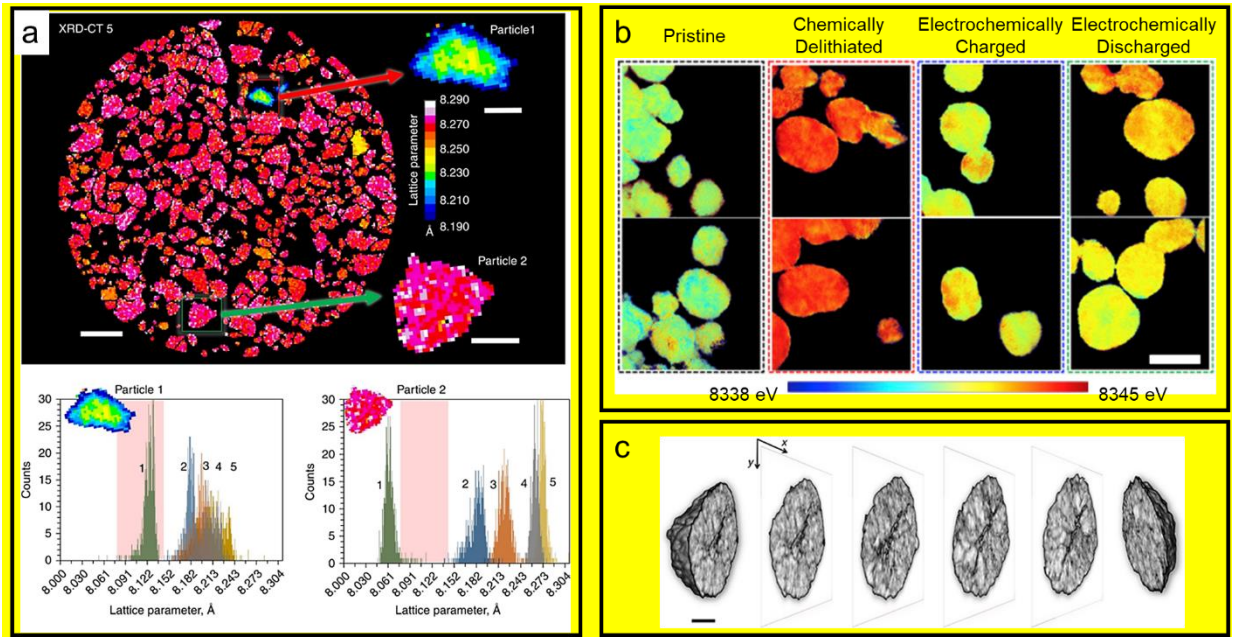

Figure 4: (a) Reconstructed XRDCT slice showing the lattice parameter of numerous LiMn2O4 particles in a lithium-ion electrode and evidence of chemical heterogeneity. Extracted from [54]. (b) Ni K-edge maps of NMC622 under different lithiation states, extracted from [56] and (c) Renderings from a 3D tomographic reconstruction of a single NMC811 particle showing internal cracks and granular structure, extracted from [57].

Even if particles were homogeneous single crystal particles without complexities of the aforementioned defects, chemical heterogeneities, and polycrystallinity, the mechanisms in which lithium distributes itself at open circuit, and moves throughout the material during operation, are still not well understood. For example, where classic Newman-style models assume a constant diffusion coefficient for layered electrode materials, more recent physics-based models apply phase change thermodynamics and kinetics to more accurately predict the distribution and transport of lithium through layered materials [58-61]. Proof of phase

separation within single particles has recently been revealed in electrode materials. For example, ptychographic tomography with 11 nm spatial resolution explored phase co-existence within individual particles of $LiFePO_4$ [62]. Rather than the concentration of lithium relaxing to a homogeneous state within particles, the lithium segregates into lithiated and delithiated states supporting the most thermodynamically stable state predicted for the crystal structure (Figure 5a). Similarly Ulvestad et al.[63, 64] applied Bragg coherent diffraction imaging (BCDI) to single $LiNi_{0.5}Mn_{1.5}O_4$ particles to study the nanomechanics and phase separation that influence cell performance and degradation (Figure 5b). Related work by Singer et al. [65] on $LiNi_{0.5}Mn_{1.5}O_4$ used XRD to clarify the interplay of solid solution kinetics and phase transformation during lithiation and delithiation, finding for example that the solid solution kinetics dominate transport during delithiation, whereas the two-phase reaction dominates during lithiation, again indicating hysteresis in kinetics and lithium transport. The data demonstrated that there is hysteresis in the lithium transport mechanisms between lithiation and delithiation due to asymmetry of energy barriers for phase transformation to occur. This also led to asymmetric crystallographic strain being experienced by the particles during lithiation and delithiation. Ptychographic tomography and XRD were also applied to study the relationship between crystallographic strain and the formation of cracks within particles [66] as a result of gradients in lithium concentration. BCDI also revealed sub-particle strain fields [67, 68], and in particular shed light on how strain concentrates around crystallographic defects and that mechanical properties and susceptibility to cracking vary with state of charge.

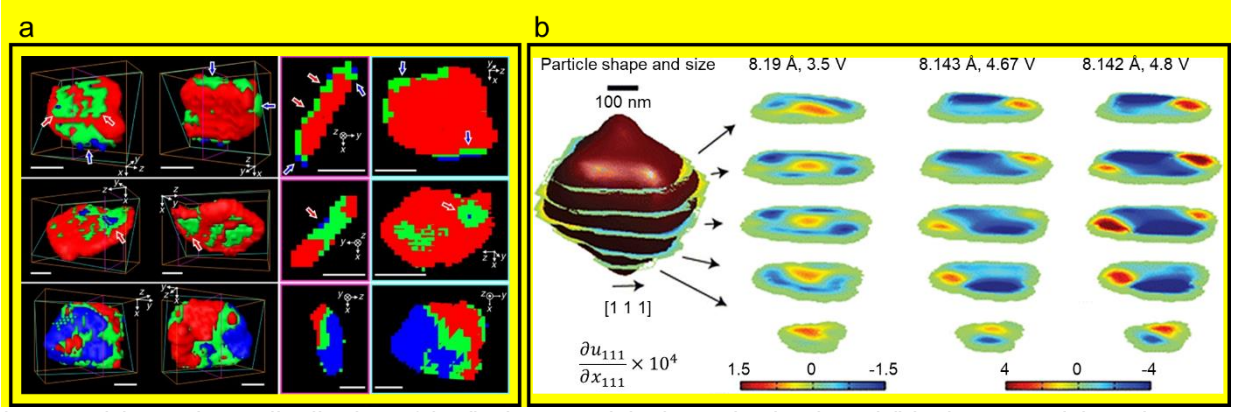

Figure 5: (a) 3D phase distribution of (red) $LiFePO_4$-rich, (green) mixed, and (blue) $FePO_4$-rich regions within a particle from ptychographic tomography, extracted from [62]. (b) Interior strain distribution within a $LiNi_{0.5}Mn_{1.5}O_4$ measured using coherent X-ray diffraction, extracted from [63].

When a cell is operational, not all regions of the cell behave the same and are exposed to the same voltage and current conditions. This may arise from inhomogeneous distributions of materials, like conductive carbon and binder that will create regional electrical connectivity on particle surfaces. The uneven coverage of conductive carbon and binder on particle surfaces was captured in 3D using a combination of ptychography computed tomography and transmission X-ray CT by Muller et al. [69]. The respective phases of electrode, conductive carbon, and pore were segmented within an electrode matrix (Figure 6a) and the 3D geometry of materials were used in an electrochemical model to correlate coverage of conductive carbon with the presence of SEI and charge heterogeneity that is expected to arise during operation. For this particular case, the combination of ptychographic X-ray CT and transmission X-ray CT enabled relatively easy distinct segmentation of the conductive carbon and binder domain, active material, and pore, by leveraging the benefits in contrast provided by the respective technique (ptychography X-ray CT for the conductive carbon, and transmission X-ray CT for graphite and Si phase). Segmentation of the respective phases with either one of the two techniques would have been much more challenging, making this work an excellent example of synergy created by combining multi-modal techniques. Furthermore,

lithium concentration gradients in the electrolyte can cause localized lithiation rates which become particularly prevalent at high charge and discharge rates where lithium depletion in electrolytes as a function of depth into the electrode can become severe. With small beam spot sizes at synchrotron sources, depth profiling XRD has recently been shown to effectively quantify such resultant lithiation gradients in electrodes [70, 71]. Finegan et al. [70] conducted high-speed XRD depth profiling with a resolution of 3 µm in a graphite electrode during fast charging and discharge (Figure 6b). Severe lithiation gradients were revealed and lithium plating occurred at the regions closest to the separator where the highest current densities were measured due to lithium depletion in the electrolyte. This study also showed that phase-transition energy barriers influence regional lithiation and that lithiation stages can co-exist in the same regions, which further supports the aforementioned phase-field models over the conventional Newman-type models with a single diffusion coefficient.

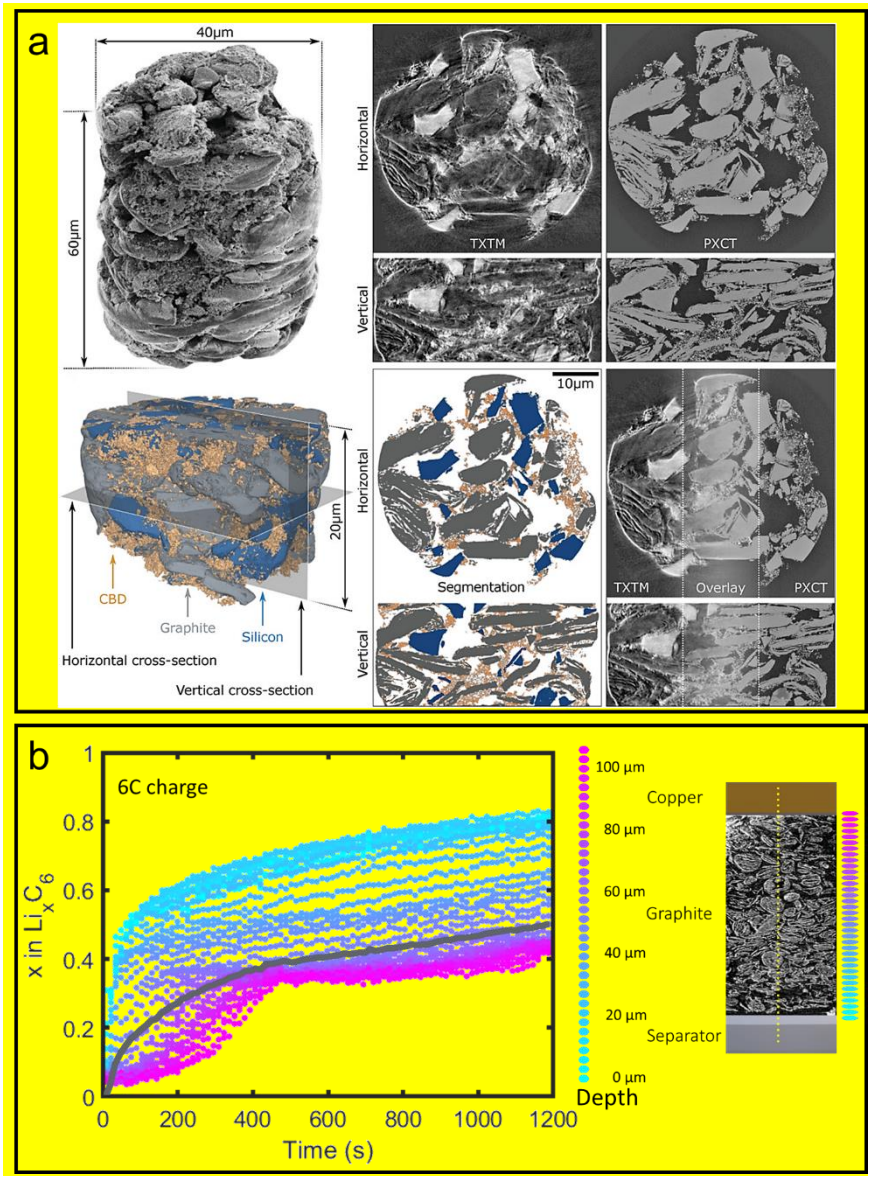

Figure 6: (a) SEM image alongside TXM and ptychographic tomography reconstructions capturing the detailed distribution of conductive carbon around graphite and silicon particles in a composite anode, extracted from [69]. (b)Scatter plots of XRD point measurements color-coded by depth in a graphite electrode during a 6C charge, extracted from [70].

Synchrotron sources provide a wealth of opportunity for understanding the function of electrode materials and for providing rich time- and space-resolved datasets for modelling, but they are not readily accessible to researchers and in even less accessible to industry. Laboratory based techniques are also being developed to provide information like the above.

3. Statistical representation and stochastic reconstruction

Material modeling based on the tomographic reconstruction data has the advantage of accurate representation of the true microstructure, but this approach is limited by the available material samples. Computational modeling based on statistical microstructure characterization and reconstruction (MCR) enables design freedom of generating new microstructures that are beyond the existing sample set. MCR provides (i) a quantitative representation of the stochastic microstructure, which can be potentially used as microstructure design variables, and (ii) statistically equivalent microstructures in 2D or 3D digital space, which can be converted to a numerical model for material property prediction. By generating virtual microstructure designs, MCR enables systematic investigation of the microstructure-property relationship beyond existing material samples. MCR has been widely applied in material property prediction [72, 73], identification of critical microstructure features [74], and microstructure design optimization for desired properties [75]. The quantitative microstructure features obtained by statistical characterization also facilitate a meaningful mapping to the synthesis process parameters. In this section, we firstly review the state-of-the-art of MCR for Li-ion battery materials, and then introduce several MCR methods that have been successfully applied to other material systems and will potentially benefit the modeling of battery microstructures.

3.1 Statistical characterization of Li-ion battery microstructures

Statistical microstructure descriptors, including both statistical parameters and stochastic functions, have been widely used to characterize the heterogeneous microstructures of electrodes and separators based on the image data obtained by the techniques reviewed in the Section 2 or from open-access databases (e.g. Battery Microstructures Library by National Renewable Energy Laboratory [76]). As summarized in Table 1, statistical microstructure descriptors can be classified into three categories based on the length scale: composition, dispersion/agglomeration, and geometry. At the top level, composition descriptors, such as the volume fraction of each material phase, provide a homogenized description of the microstructure. For example, the compositional descriptors of porous electrodes include porosity, volume fraction of the active material particles, percentages of carbon binders and additives, etc. The second category is the dispersion/agglomeration descriptors, which quantify the spatial distribution of a certain material phase. Dispersion/agglomeration descriptors for characterizing general heterogeneous microstructure include surface area, interfacial area, surface-to-volume ratio, 2-point correlation function, connectivity, tortuosity, etc. Furthermore, a large set of dispersion/agglomeration descriptors were also proposed specifically for the random particle systems, because a significant amount of studies focus on electrodes that consist of densely packed particles. Those descriptors include contact probability, nearest neighbor distance, spatial arrangement pattern, probability of finding conductive binders on the surface of active particles, particle-particle contact area, radial distribution function, etc. At the lowest level, geometry descriptors are defined to capture the morphological features of a single particle or local pore sizes. The geometry descriptors include particle size, pore size, particle shape, particle sphericity, particle orientation, surface roughness, etc. The above-mentioned parametric descriptors can be either deterministic parameters or statistical distribution functions.

It is to be noted that some statistical descriptors contain information of all three levels. For example, *N*-point correlation functions (Figure 7) capture both volume fractions of the phase of interest and the detailed

dispersion and geometrical features. The 2-point correlation function is the most widely used statistical descriptor for microstructural material analysis and design [77-79]. For a two-phase stochastic microstructure, the 2-point correlation function is defined as:

$$S_2^i(x_1, x_2) \equiv \langle I^{(i)}(x_1) I^{(i)}(x_2) \rangle \tag{1}$$

where I is an indicator function:

$$I^{(i)}(x) = \begin{cases} 1, & x \in \text{phase } 1 \\ 0, & x \in \text{phase } 0 \end{cases} \tag{2}$$

The physical meaning of the two-point correlation function is the probability of finding two points with a given distance r in the same phase of the random media. Therefore, 2-point correlation is a function of distance r, and it can be denoted as $S_2^i(r)$. r can be any value from 0 to $+\infty$, so the 2-point correlation function has an infinite length, which is usually truncated to a finite length by the microstructure image window size. According to its definition, a 2-point correlation function should satisfy three boundary conditions [79]:

(1) If $r = 0$, $S_2^i(r)$ equals to the volume fraction of composite, so the first point of the 2-point correlation function captures the composition information;
(2) As $r \to \infty$, $S_2^i(r)$ approaches the square of volume fraction;
(3) The derivative of $S_2^i(r)$ at $r = 0$ is equal to the surface area per unit volume, which contains the dispersion and geometry information.

In our previous work, we observed that the fluctuation patterns of the 2-point correlation functions are related to the spatial correlation length of the material phase (dispersion/agglomeration) [80].

A variety of correlation functions can be defined in a similar way to provide additional information about the microstructure features (Figure 7). A 2-point cluster function [81] is defined as the probability of finding two points with a given distance r in the same pixel/voxel cluster. A 2-point surface function [82] is defined as the probability of finding two points with a given distance r on the boundary of the phase of interest. A 3-point correlation function [83] is defined as the probability of finding all three corners of an equilateral triangle with side length r in the phase of interest. The major limitation of *N*-point correlation functions is their vague physical meaning. The *N*-point correlation functions, which are curves by nature, are difficult to use as design variables. Compared with parametric microstructure descriptors such as volume fraction, particle number, particle radius, neighbor distances, etc., establishing the mapping relationship between the *N*-point correlation functions and physics-based material processing parameters is challenging.

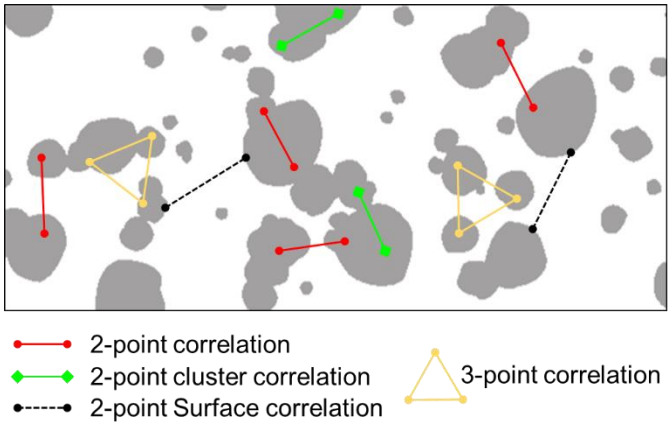

Figure 7: Definition of different types of correlation functions

Table 1: Statistical descriptors for Li-ion battery microstructure characterization

Category	Statistical descriptors	References
Composition	Volume fraction of active materials, binders, additives, pores, etc.	[3, 50, 84-102]
	Porosity	[7, 11, 50, 84, 96, 100, 103-112]
Dispersion/ agglomeration	Specific surface area	[1, 84, 87-91, 94, 106, 113, 114]
	Specific interfacial area	[50, 108]
	2-point correlation/distance correlation function	[109-112, 114, 115]
	Surface to volume ratio (volume-specific surface area), surface area density	[107]
	Connectivity	[89, 95]
	Tortuosity	[1, 3, 7, 87, 89, 90, 95, 97, 106, 108, 114]
	Contact probability	[3]
	Spatial arrangement of particles	[88, 98, 99]
	Probability of finding conductive binders on the surface of active particles	[100, 116]
	Particle-particle contact area	[97, 102, 113]
	Nearest neighbor distance	[92, 101]
	Radial distribution function (RDF): the number of particles v.s. the distances between the particles and the carbon surface	[117]
Geometry	Particle size (volume, equivalent diameter, diameter/radius along different axes)	[7, 11, 50, 84, 87-89, 92, 93, 96, 98-105, 109-122]
	Type of particle shape/morphology/profile (sphere, ellipsoid, cylindrical, elliptic cylinder, etc.)	[86, 111, 112, 121, 123]
	Sphericity	[7]
	Particle orientation	[7, 86, 98, 99, 111, 112]
	Surface roughness	[119]
	Pore size/radius/diameter	[7, 90, 93, 100, 106, 107]

3.2 Stochastic reconstruction of Li-ion battery microstructures

The purpose of stochastic reconstruction is to generate 2D or 3D microstructures in the digital space based on the input statistical microstructure descriptor values. The microstructure reconstruction is random but statistically equivalent to the input (target) statistics. A stochastic reconstruction method generally follows either or both of the following two strategies (Figure 8):

(1) Statistical sampling. The microstructure features are generated by sampling the statistical functions of the microstructure descriptors obtained by statistical characterization.
(2) Optimization. The reconstruction process is to optimize the morphology of the microstructure in order to minimize the differences between the reconstructed microstructure descriptor values and the target values obtained by statistical characterization.

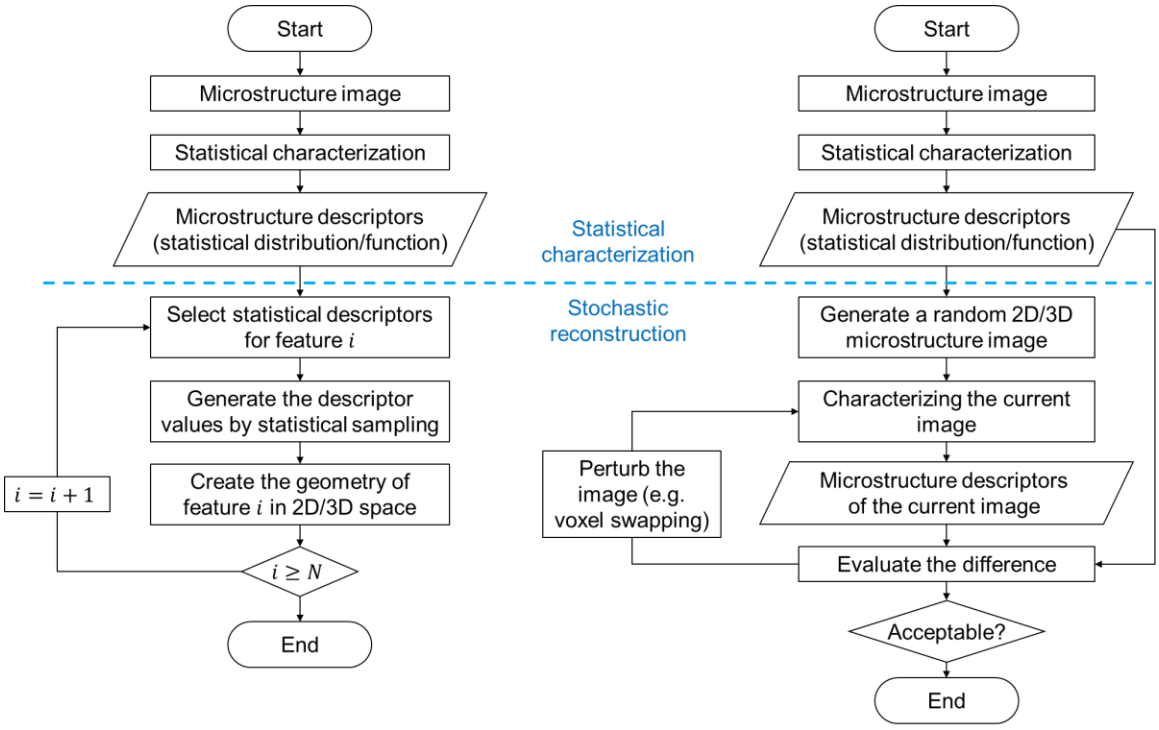

Figure 8: Two strategies for stochastic reconstruction. The target microstructure descriptor values are either obtained by statistical characterization of sample images, or generated by microstructure design. (a) Statistical sampling strategy. The descriptor values of each microstructure feature are generated by sampling the target statistical distributions/functions. (b) Optimization strategy. The microstructure morphology is perturbed until the target descriptor values are fully matched.

Four categories of microstructure reconstruction methods used in Li-ion battery material modeling are summarized in Table 2. A significant amount of previous works adopt the random particle packing approach, which is especially suitable for the particle systems. A simple way of reconstructing particle systems is to randomly distribute spherical/ellipsoidal particles in the 3D space, allowing overlap between particles. The particle sizes are either deterministic or stochastic by sampling a predefined statistical function. However, the overlapping issue may lead to unrealistic microstructure morphologies or interfacial interactions. The overlapping issue can be resolved by integrating the particle packing process with optimization algorithms (e.g. Simulated Annealing and Genetic Algorithm) or Monte Carlo algorithms. By adjusting the locations and orientations of the particles interactively, the overlaps and gaps between particles are minimized to achieve a densely packed particle system without interferences. A representative work on this method is shown in Figure 9a. Yang and Mai [98, 99] proposed an optimization framework that perturbs the location of the particles until the target 2-point correlation function is fully matched. For each particle, the size is obtained by sampling a lognormal distribution, and its geometry is selected from a library that consists of real particle geometrical data obtained by X-ray CT.

Hierarchical reconstruction methods have been developed to reconstruct microstructure features at different length scales in a sequential manner. At the upper scale, the center locations of the particles/clusters are determined by spatial tessellation or simulated annealing optimization to match the target dispersion descriptor values. At the lower scale, the shape of the particle/cluster boundary is reconstructed by sampling a realization from a random process model, which is established to characterize the geometrical statistics. Figure 9b shows a representative work published by Hein et al. [121]. The locations of all particles are

determined using random Laguerre tessellation, which decomposes the region into convex polytopes, one for each particle. Then the shape of each particle's boundary is generated by sampling a Gaussian random field model. The hierarchical reconstruction method has also been applied to reconstruct the 3D anisotropic microstructures of polymer separators based on 2D image data [72]. The center locations of the voids are created randomly in the 3D space, then the geometry of the voids are generated by sampling a Gaussian Copula random process model.

Pixel/voxel swapping methods are applicable to the reconstruction of general random media. Zhang et al. [114] reconstructed the anisotropic microstructures of Ni-YSZ electrodes for solid oxide fuel cells by swapping voxels using the Simulated Annealing algorithm (Figure 9c). The optimization objective is to match the target 2-point correlation function. The SA optimization-driven pixel-voxel swapping is generally applicable to all kinds of stochastic microstructures, including Li-ion battery materials. Stephenson et al. [3] proposed a Markov Chain Monte Carlo (MCMC) approach to guide the voxel swapping process. Starting from a random configuration (a random voxel image), one pair of voxels of different colors are swapped each time, and then MCMC is applied to accept or reject this swapping step. The radial distribution function, which is a normalized probability of finding neighbors at distance r, was used as the criterion to evaluate the reconstruction's accuracy. The reconstruction process is terminated when the target radial distribution function is matched.

Physics-inspired Monte Carlo methods have been developed to mimic the material fabrication process. The reconstruction process starts with "seeds" that are randomly distributed in the 3D space, followed by sequential growth of materials at the seeds (adding more voxels to the voxel cluster). At each growth step, the growth site is defined by sampling a predefined probability function, which reflects the tendency of agglomeration. When the "backbone" of the microstructure is obtained (active particles), the carbon binder and additive phases are added in a similar manner: choose the growth site on surfaces by a predefined probability function, and add voxels of the material phase of interest to that site (Figure 9d). Two microstructures reconstructed with different control parameter values are compared in Figure 19d, Section 5.1. The control parameter ω, which is in the range of [0, 1], is a ratio of conductive binder's preference to deposit on pre-deposited carbon binder domain versus an uncovered active material surface. When ω is close to 0, film-like conductive binder structures will be created on the active material surfaces; when ω is close to 1, finger-like conductive binder structures will be created in the space between active material particles. ω can be potentially used as a microstructure design variable. It is observed that a conductive binder network made up of film-type deposits ($\omega = 0$) leads to a higher conductivity than the finger-like structures ($\omega = 1$).

Table 2: State-of-the-art stochastic reconstruction methods

Category	Reconstruction methods	Reference
Particle moving and packing	Particle random dispersion without optimization	[93, 102, 104, 117, 120]
	Particle packing and moving by optimization or Monte Carlo perturbation	[88, 98, 99, 107, 109-112, 115]
Hierarchical reconstruction	Hierarchical reconstruction: from dispersion to geometry	[72, 121]
Pixel/voxel swapping	Voxel moving by optimization	[114]
	Markov chain Monte Carlo (MCMC)-based statistical sampling approach	[3]
Physics-inspired	Monte Carlo simulation of material growth	[84, 85, 100]

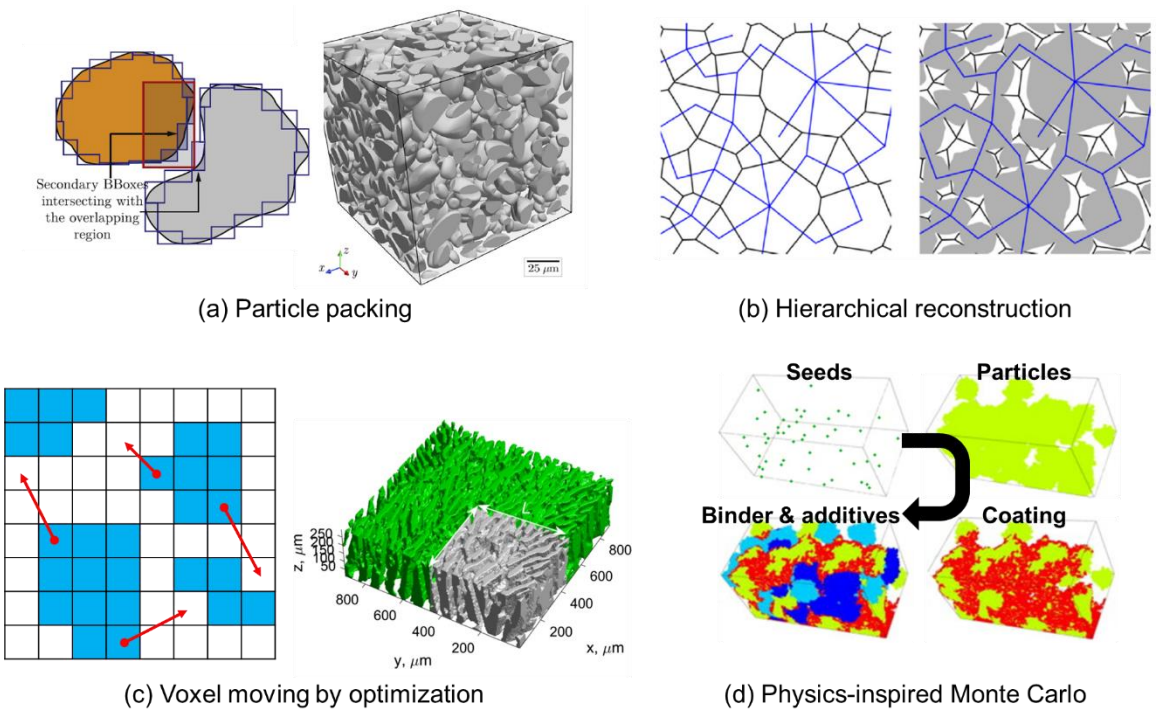

Figure 9: Stochastic reconstruction methods that have been employed in Li-ion battery electrode modeling (a) Particle packing with optimization [99], (b) Hierarchical reconstruction: spatial tessellation and random process sampling [121], (c) voxel swapping by optimization [114], (d) physics-inspired Monte Carlo method for electrode [100].

3.3 Advanced MCR methods that can benefit the numerical modeling of complex, evolving Li-ion battery microstructures

With the advancements in Li-ion material synthesis techniques, we observed various complex microstructures of electrodes that cannot be fully captured by the above mentioned MCR methods. As shown Figure 10a-c, electrode particles of irregular shapes (e.g. platelets [105]), inkjet-printed random fiber-like electrodes [124], and coral-like anisotropic $LiFePO_4$ (LFP) cathode microstructures made by directional ice templating (DIT) [125] have been reported. A simplified microstructure representation by spherical particles is not appropriate for those materials, as it will introduce a significant error in the prediction of material properties. It can be proven by the comparative study reported by Mai et al. [98], where significant differences in the Li insertion reaction-induced stress distribution with particles are observed between a numerical model of simplified, spherical particle shapes and a model of realistic microstructure morphologies. This observation reemphasizes the importance of incorporating realistic microstructure features in a numerical model for the prediction of electrodes' behaviors during charge/discharge cycles.

Another challenge is to capture the degrading microstructure during the charging/discharge cycles (Figure 10d,e). The pristine particles may have spherical or near-spherical shapes, but the geometrical irregularity increases with the cycle number due to fracturing and deformation as a result of lithiation and de-lithiation [94]. The particle-based MCR methods might be sufficiently accurate for modeling the microstructure for the first few cycles, but a significant error will occur for the simulation of the later cycles.

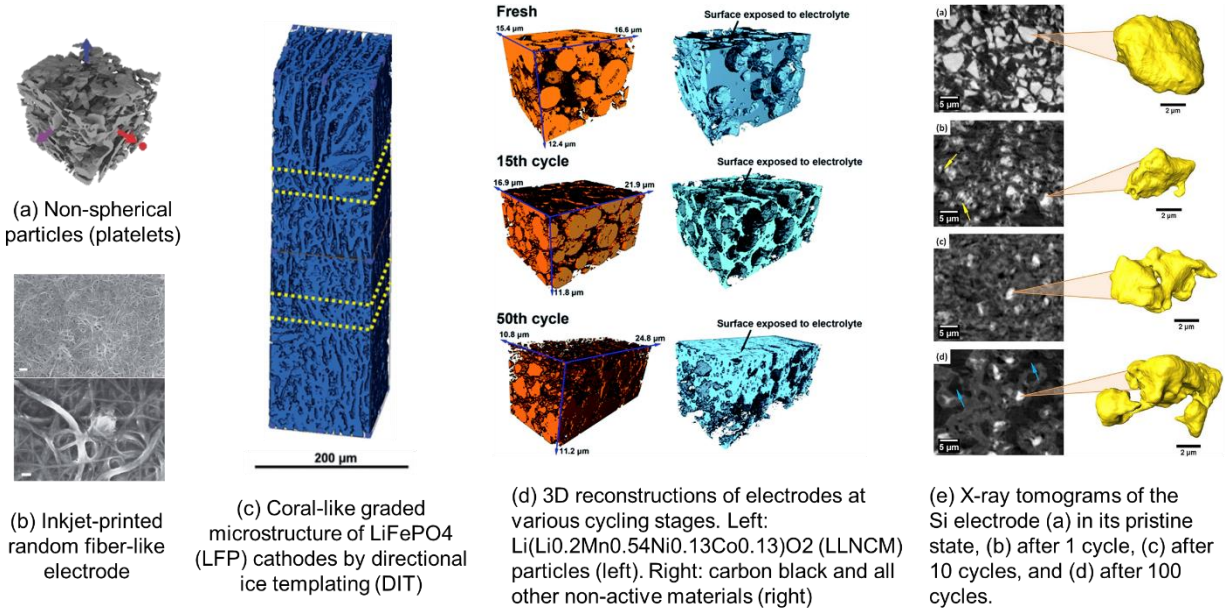

Figure 10: Complex Li-ion electrode microstructures that cannot be fully captured with simple descriptors. (a) Irregular particle shape [105]. (b) Random fiber-like microstructures by inkjet printing [124]. (c) Coral-like graded microstructures by DIT [125]. (d) Microstructure evolution as a function of charge/discharge cycle number [126]. (e) Increasing irregularity in particle geometry due to the increasing number of charge/discharge cycles [94].

Here we provide an overview on two categories of advanced MCR methods that have been successfully applied to a wide range of complex microstructural material systems. In our perspective, these methods have great potential for modeling and design of Li-ion battery microstructures with non-particle-like, time-evolving morphologies.

3.3.1 Spectrum density function (SDF)-based MCR

SDF is a spatial frequency function and represents spatial correlations of material phases in the frequency domain. For a 2-dimensional, bi-phase heterogeneous microstructure image that is modeled as a function $Z(\boldsymbol{r})$ with pixel locations denoted by $\boldsymbol{r}$ and pixel values of 0 or 1, the Fourier spectrum of the microstructure can be obtained by taking the Fourier transform of $Z(\boldsymbol{r})$:

$$\mathcal{F}\{Z(\boldsymbol{r})\} = \int_{\mathbb{R}^n} Z(\boldsymbol{r}) e^{-2\pi i \boldsymbol{r}\cdot\mathbf{k}} \, \mathrm{d}\boldsymbol{k} = A_{\boldsymbol{k}} \cdot e^{i\phi_k} \tag{3}$$

where $A_{\boldsymbol{k}}$ and ϕ_k represent the magnitude and phase information at each location $\boldsymbol{k}$ of the Fourier spectrum. A microstructure's SDF, $\rho(\boldsymbol{k})$, is defined as the squared magnitude of its Fourier transform:

$$\rho(\boldsymbol{k}) = |\mathcal{F}\{Z(\boldsymbol{r})\}|^2 = {A_{\mathbf{k}}}^2 \tag{4}$$

For an isotropic microstructure, the vector $\boldsymbol{k}$ can be reduced to a scalar k; for an anisotropic microstructure, it can be defined as a function of the polar angle. The mathematical connection between SDF and 2-point correlation function has been established by Chatfield [127]. The SDF has been successfully applied to characterize the channel-type, quasi-random microstructures (Figure 11a), which are very similar to the coral-like microstructures of cathodes synthesized by DIT. When applied to characterize isotropic microstructures, another advantage of SDF is that it can be easily fitted with analytical functions like

Gaussian, step functions, or linear functions (Figure 11a), which can be fully captured by one or two fitting parameters.

Two efficient approaches have been proposed to reconstruct 3D microstructures based on an input SDF. The first approach is to simulate a random field by Cahn's method. The n-dimensional microstructure $Z(\boldsymbol{r})$ is represented by a Gaussian random field (GRF) $Y(\boldsymbol{r})$, which can be fully characterized by a field-field correlation function $g(\boldsymbol{r}_1, \boldsymbol{r}_2)$. The analytical relationship between $Y(\boldsymbol{r})$, $Z(\boldsymbol{r})$, and $g(\boldsymbol{r}_1, \boldsymbol{r}_2)$ is provided in the equations below:

$$g(\boldsymbol{r}_1, \boldsymbol{r}_2) = \mathrm{E}[Y(\boldsymbol{r}_1)Y(\boldsymbol{r}_2)] = \int_0^\infty \frac{J_{(n-2)/2}(k\Delta r)}{(k\Delta r)^{(n-2)/2}} \cdot k^{n-1} \cdot \rho(k)dk \tag{5}$$

$$\Delta r = |\boldsymbol{r}_1 - \boldsymbol{r}_2| \tag{6}$$

$$Z(\boldsymbol{r}) = \begin{cases} 1, & Y(r) \le \alpha \\ 0, & Y(r) > \alpha \end{cases} \tag{7}$$

J are Bessel functions of the first kind, and $\rho(k)$ is the SDF. In numerical implementation, a realization of the GRF for a targeting SDF is constructed using the wave-form method [128]:

$$Y(r) = \sqrt{\frac{2}{N}} \cdot \sum_{i=1}^{N} \cos(k_i \boldsymbol{k}_i \cdot r + \phi_i) \tag{8}$$

N is the number of terms in the truncated series; ϕ_i is generated by sampling uniform distribution in the range of $[0, 2\pi]$; $\boldsymbol{k}_i$ is a vector uniformly distributed on a unit sphere, and k_i is a scalar obtained by sampling the probability density function $\rho(k) \cdot k$ in the range of $(0, \infty)$. After a realization of the GRF $Y(\boldsymbol{r})$ is simulated in the pixel/voxel space, a binarization operation is conducted by setting a threshold α on the pixel/voxel values. Pixels/voxels with a value smaller than α represent the material phase of interest, and other pixels/voxels represent other phases in the material.

The second, an Inverse Fourier Transform-based reconstruction approach, has been proposed by Iyer et al. [129] to reconstruct anisotropic microstructures based on SDF. Considering a microstructure as a digital signal, the reconstruction process is formulated as an Linear Time Invariant (LTI) system [130] that takes in a random white noise image and then transforms it into an image with the desired SDF. Denoting the reconstructed, target, and white noise images as Y_R, Y_T, and Y_W, respectively, the reconstructed image can be obtained by:

$$Y_R = \left|\mathcal{F}^{-1}\left\{\sqrt{\rho_T(\boldsymbol{k})} \cdot \mathcal{F}\{Y_W\}\right\}\right| = \left|\mathcal{F}^{-1}\left\{|\mathcal{F}\{Y_T\}| \cdot \mathcal{F}\{Y_W\}\right\}\right| \tag{9}$$

Where $\mathcal{F}\{\cdot\}$ represents the Fourier transform operator, $\rho_T(\boldsymbol{k})$ is the SDF of the target image. Denoting the SDFs of the reconstructed image and white noise image as $\rho_R(\boldsymbol{k})$ and $\rho_W(\boldsymbol{k})$, respectively, we have:

$$\rho_R(\boldsymbol{k}) = \rho_T(\boldsymbol{k}) \cdot \rho_W(\boldsymbol{k}) \tag{10}$$

After obtaining the reconstructed image Y_R, the corresponding microstructure $Z(\boldsymbol{r})$ can be obtained by level cutting Y_R to the desired volume fractions of two phases. A major advantage of this approach is that Eq. (9) can be directly applied to reconstruct both isotropic and anisotropic microstructures without any modification. Given non-spherical symmetric SDF as the input, channel-type heterogeneous microstructures of different levels of anisotropy have been reconstructed (Figure 11b).

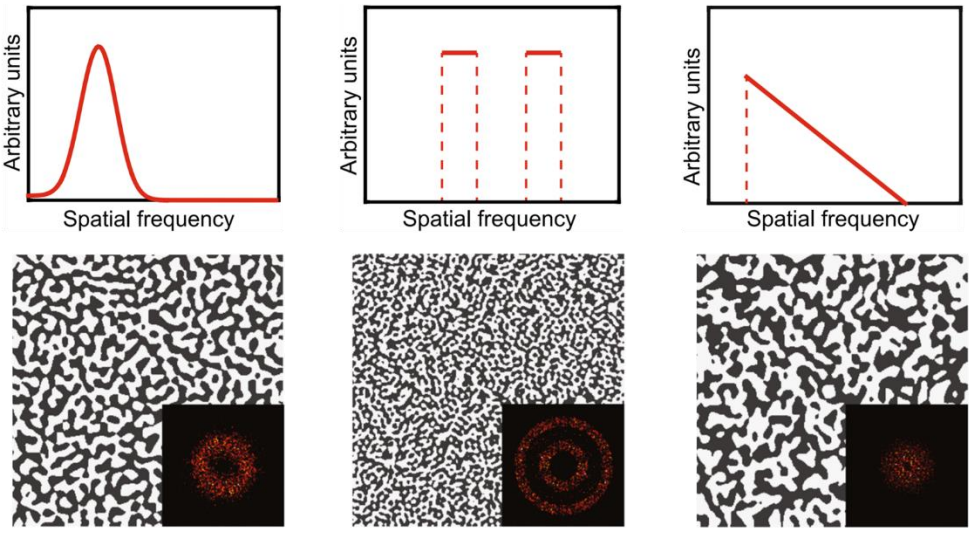

(a) Microstructure images and the corresponding spectrum density functions

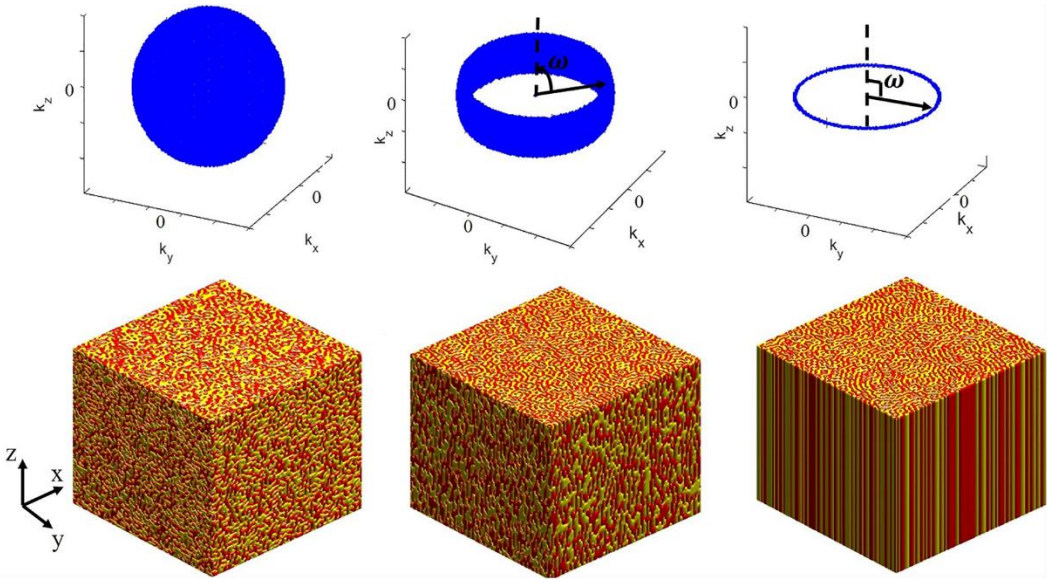

(b) Reconstruction of 3D isotropic and anisotropic microstructures based on target spectrum density functions

Figure 11: Spectrum density function-based MCR methods for channel-type, quasi-random microstructures. (a) 2D heterogeneous microstructures and their corresponding SDFs [131]. (b) Reconstruction of 3D isotropic and anisotropic microstructures with SDFs [129].

3.3.2 Machine learning and deep learning-based MCR

Machine learning and deep learning-based methods have also been developed to (i) obtain a reduced dimensional representation of the complex microstructure images, (ii) gain the flexibility to reconstruct various types of microstructures, and (iii) enable 2D-to-3D reconstruction, which means reconstructing 3D microstructures based on one or a few 2D images when 3D microstructure image data is not available for statistical characterization.

Unsupervised learning methods (Figure 12a) based on variational autoencoder (VAE) [132] and convolutional deep belief network (CDBN) model [133] has been proposed to extract implicit features

from multi-scale anisotropic alloy microstructure images. A VAE consists of an encoder that converts the input microstructure image into a set of statistical distributions in the latent feature space (statistical characterization), and a decoder that reconstructs the microstructure image based on the latent feature vector (stochastic reconstruction). The training process minimizes the reconstruction error and the Kullback-Leibler (KL) divergence. The CDBN model consists of stacked layers of convolutional restricted Boltzmann machine (CRBM), which is a generative artificial neural network model that learns the probability distribution from image data. Embedding layers are extracted from the trained models as a reduced dimensional, parametric feature representation of the microstructure images (statistical characterization). To reconstruct statistically equivalent microstructures, one starts from the last layer of the trained CDBN by assigning binary values (0 or 1) randomly to each node, and inversely sample the previous layers through deconvolution. CDBN has demonstrated its effectiveness on multiple types of microstructures, including granular microstructures of alloys, irregular pore structures of sandstone, and suspension that is featured by random dispersion of spherical colloids.

Markov Random Field (MRF) texture synthesis, which has been widely studied in the area of computer vision, provides another way of reconstructing non-repetitive microstructures based on a small "exemplar" image (Figure 12b). The term "texture" refers to images containing repeated patterns with certain randomness [134]. By modeling the microstructure image as MRFs, the probability of a pixel/voxel's value is conditioned on the values of its neighbor pixels/voxels, and conditionally independent of all the other pixels/voxels. This method has been employed in 2D microstructure reconstruction based on 2D exemplar images [135, 136], and 3D microstructure reconstruction based on 2D orthogonal images [137, 138]. The MRF-based reconstruction methods are applicable to a wide range of microstructures, including both stochastic microstructures and deterministic periodical patterns.

Another reconstruction method that enables 2D-to-3D reconstruction is deep transfer learning-based reconstruction (Figure 12c). Transfer learning [139, 140] is a strategy that migrates knowledge for a new task from a related task that has already been learned. Transfer learning has been applied to microstructure reconstruction to resolve the issue of lacking microstructure image data for training deep feature learning models. Pre-trained deep learning models on benchmark computer vision problems (e.g. VGG-19) are adopted in full or in part as the microstructure characterization model, which generates a reduced dimensional implicit feature representation of the microstructure (embedding layers). With target microstructure feature values, stochastic microstructure reconstructions are created by optimizing the pixel/voxel values to minimize the loss function, which is the sum of Gram-matrix differences between the reconstructed feature layers and the target values. Gradient-based optimization is adopted, and the optimization process can be decomposed into two major steps: (i) Forward-propagation, which generates the feature layer values of the input microstructure image for loss function evaluation, and (ii) backward-propagation, which computes the gradient of the loss function value with respect to each pixel/voxel in the reconstructed image. The gradient information is used to guide the direction of optimization search in the next iteration. In [141], the deep transfer learning-based method was employed to reconstruct a variety of 2D microstructures, including carbonate, particle-dispersed polymer composites, porous sandstone, ceramics, fingerprint-like copolymer, granular alloy, and three-phase rubber composites. In a more recent work [142], the deep transfer learning method has been adapted for 2D-to-3D reconstruction. Anisotropic 3D granular microstructures with color have been reconstructed based on three orthogonal 2D exemplar images. Deep learning-based reconstruction method starts to gain attention in the area of battery material modeling. Gayon-Lombardo et al. [143] applied Generative Adversarial Networks (GAN) in 2D-to-2D and 3D-to-3D reconstruction of multi-phase electrode microstructures (the reconstructed microstructure has the same dimensionality as the input microstructure image), while a periodic boundaries can be achieved in the reconstructions.

The machine learning and deep learning-based methods have two unique advantages that benefit their application on Li-ion battery microstructure modeling. First, the microstructure images can be directly used as inputs without morphological approximations, so the information loss in microstructure characterization (e.g. coral-like graded electrodes or irregular particles) can be minimized. Second, the input microstructure images can be encoded to obtain a 3-channel representation which can distinctly separate multiple material phases. This 3-channel representation will benefit the characterization and reconstruction of Li-ion microstructures that consist of multiple phases such as active material particles, carbon binder, additive, pores, etc. However, the disadvantage of the deep learning-based method is that it is not easy to find an intuitive mapping relationship between the implicit features and the physically meaningful processing/material parameters.

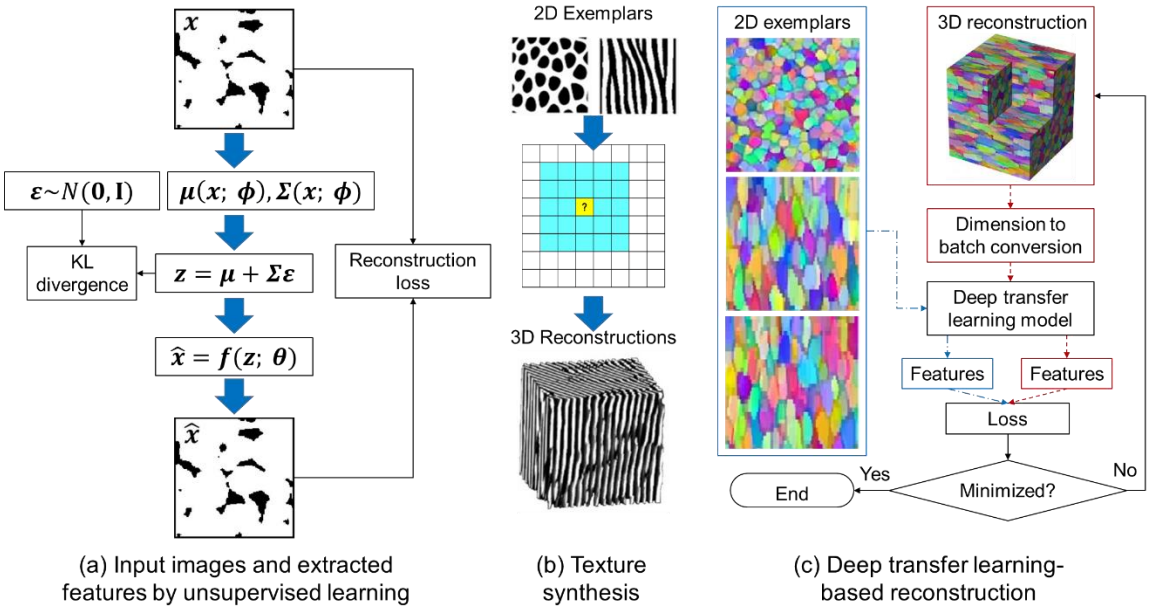

Figure 12: Machine learning and deep learning-based MCR methods. (a) Unsupervised learning by variational autoencoder, an unsupervised learning method [132]; (b) Markov random field texture synthesis for 2D-to-3D reconstruction [135]. (c) Deep transfer learning workflow for 2D-to-3D reconstruction [142].

4. Prediction of multi-physics properties by microstructure-resolved modeling

Both the deterministic reconstruction based on the tomographic data described in Section 2 and the stochastic reconstruction based on microstructure statistics discussed in Section 3 provide the geometrical information for the material models that predict multi-physics properties. While tomographic data ensures high fidelity to real microstructures, stochastic reconstruction enables a seamless integration of microstructure generation and property simulation, which is required by the automatic search of new microstructure designs for optimal properties. In any case, microstructural information, at different levels of sophistication, is a necessary input to physics-based modeling.

Physics-based modeling is a valuable tool to provide additional insights into physical processes that are only partially accessible or totally inaccessible by experiments through the mathematical description of phenomena such as reaction kinetics, heat, mass, and charge transport dynamics as well as mechanics. Depending on the aim and degrees of accuracy and complexity required, there is a variety of battery models,

where the traditional zero-dimensional (0D), 1D, and pseudo-2D (P2D) models, which treat the microstructure as a macro-homogeneous continuum, have been widely used for predictions of performance, cycle life and degradation [144-148], being their computational demand low enough to be parametrized for developing reduced-order semi-empirical models (e.g., equivalent circuits [149]) used in battery management systems (BMSs). However, treating the microstructure as a continuum via volume-averaged parameters is a clear disadvantage because it ignores the complex interplay between electro-chemo-mechanical phenomena and the 3D microstructure. Moreover, microstructural heterogeneity, which has a significant impact on battery performance particularly at high C-rate operating conditions [150-153], is only roughly captured [154, 155] if not completely overlooked. Instead, microstructure-resolved physics-based modeling, albeit undoubtedly more computationally intense, enables the direct use of reconstructed electrode 3D volumes from FIB-SEM, X-ray CT, and stochastic methods described in the previous sections. Such microstructure-resolved models are able to complement and go beyond reduced-order models and thus serve as an "evaluator tool of design performances" to guide material design and battery health prognostics.

Microstructure-resolved models for electrochemical devices have been recently reviewed with a specific focus on physical equations and numerical approaches [156, 157]. In this section, the emphasis is on microstructural heterogeneity and how microstructure-resolved models have been able to investigate its implications in effective transport properties (Section 4.1), electrochemical properties (Section 4.2), and mechanical integrity (Section 4.3).

4.1 Prediction of effective transport properties

One of the most popular applications of microstructure-resolved modeling is the determination of effective transport properties, which are reviewed here with a specific focus on the role of microstructure heterogeneity in the anisotropic effective properties. This also offers the chance to discuss about the modeling of the carbon-binder domain (CBD) and how it affects effective transport properties, eventually escalating to determining electrode performance.

The tortuosity factor is a key parameter which characterizes mass transport resistance of the electrolyte in 3D convoluted pathways of the pore phase [158], thus greatly determining the rate capability of the battery. The tortuosity factor is sensitive to the shape and orientation of active material particles, as investigated by Ebner et al. [105], who used microstructure-resolved diffusion simulations to evaluate the electrode tortuosity factor for NMC (Figure 13a), LCO (Figure 13b), and graphite (Figure 13c) electrodes. It was found that the NMC cathode with spherical particles has the lowest tortuosity factor (i.e., the least mass transport resistance in the pore phase) compared to LCO with randomly-aligned non-spherical particles, while the graphite electrode shows the highest tortuosity factor due to the horizontally-aligned flake-shaped particles. Moreover, electrodes composed of non-spherical particles exhibit different extents of anisotropic tortuosity, depending on the aspect ratio of the particle geometry: in the graphite electrode the through-plane tortuosity factor is significantly larger than the in-plane tortuosity (Figure 13c) while the NMC electrode shows almost isotropic tortuosity (Figure 13a). These features are hardly captured by the Bruggeman equation (in black in Figure 13a-c), which is widely adopted to estimate tortuosity from porosity in battery continuum modeling. These findings are complemented by a later study conducted by the same group [159, 160], who investigated the tortuosity anisotropy on four types of graphite anodes with distinct particle morphologies (Figure 13d-g). All the anodes were fabricated with flake-shaped particles except for the second sample made with synthetic graphite particles, which appear more spherical. The results confirm that the through-plane tortuosity factor in all of the flake-shaped electrodes is larger than the in-plane direction, with smaller particles that weaken this anisotropy (Figure 13f); the electrode with spherical-shaped graphite particles only exhibits trivial tortuosity anisotropy. Similar conclusions were

reached by He et al. [110], who used microstructures generated via stochastic reconstruction. These results indicate that volume-averaged tortuosity in continuum models should be used with caution, especially for graphite electrodes. Alternative metrics to capture a more meaningful tortuosity factor in battery electrodes have been recently presented [161].

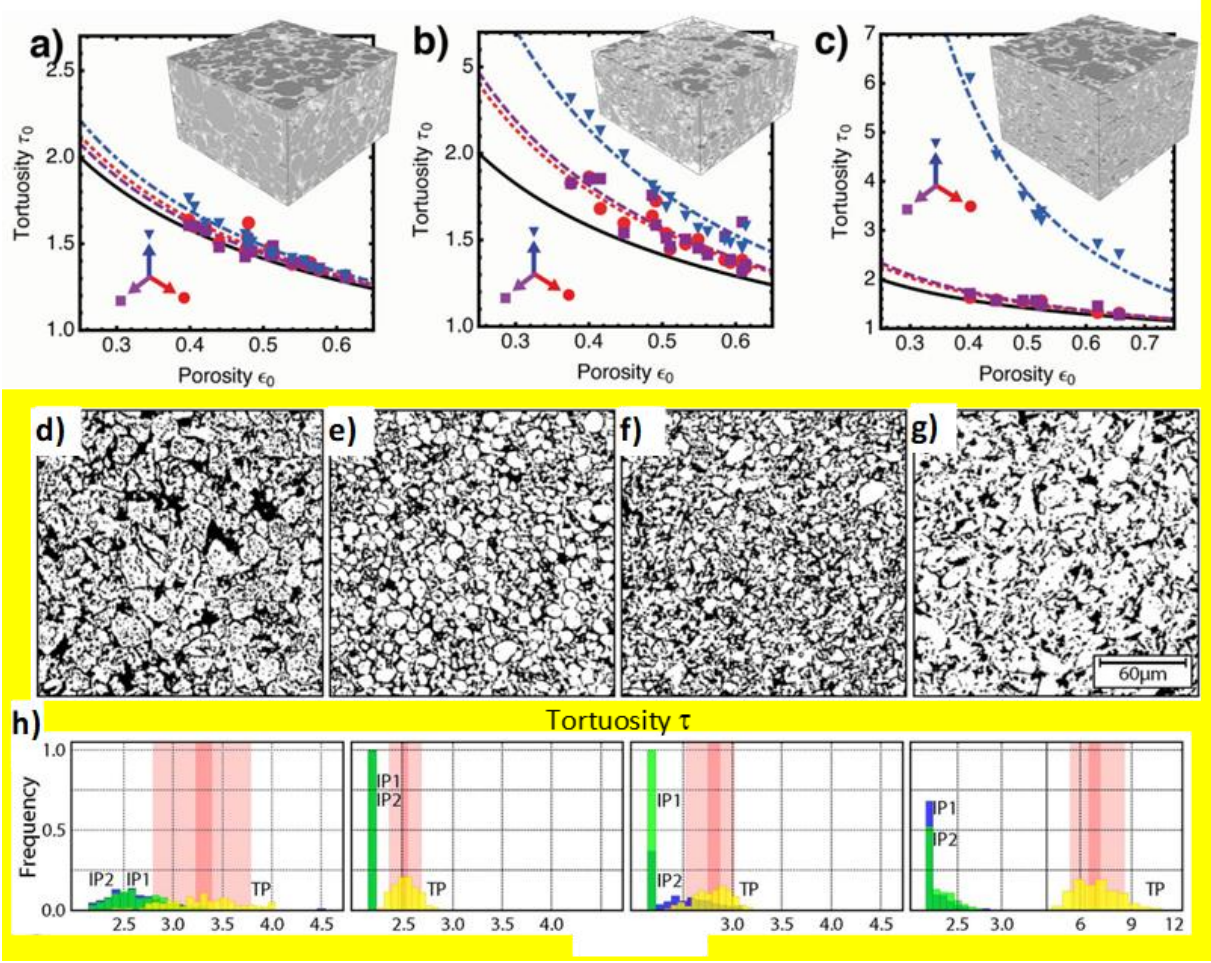

Figure 13: Investigating the effect of particle shape and orientation on anisotropic tortuosity in (a) NMC (b) LCO (c) graphite electrodes [105]; (d) – (g) comparison of the directional tortuosity in graphite electrodes with distinct particle microstructure [159]. The graphite particles are flake-shaped in (d), (f), and (g) while spherical in (e). The particle size in (f) is much smaller than (d) and (g); (h) anisotropic tortuosity of the four graphite microstructures in (d) – (g). IP and TP stand for in-plane and through-plane direction, respectively.

Apart from the active material particles, the non-intercalating carbon and binder additives, used to improve electronic conductivity and mechanical integrity, also play an important role in the mass transport in the pore phase. In fact, the carbon-binder domain (CBD), alongside active material particles, can form a complex network of pores with a wide distribution of pore diameter, thus significantly contributing to microstructural heterogeneity [160, 162, 163]. However, since the contrast between pore and CBD has been generally insufficient in X-ray CT scans to resolve CBD details, several microstructure-resolved models treat pores and CBD as a lumped continuum phase for electrolyte transport [98, 113, 119], thus missing the CBD contribution to electrode tortuosity. As a workaround for this issue, CBD is often introduced by using different types of secondary-phase stochastic reconstructions [164-166] as discussed in Section 3.2.

Ngandjong et al. [167] generated 3D microstructures from coarse-grained molecular dynamics (CGMD) simulation of the electrode fabrication process, where a slurry of active material and additives is mixed in a solvent and then the solvent evaporates while the solid particles equilibrate to form a microstructure (see also the review by Franco et al. [168], Figure 14a). Their simulations show that, by increasing the active material-to-CBD ratio, the electrode porosity increases while the coverage of active material with CBD decreases; the corresponding microstructure-resolved electrochemical simulations show that, when the resulting CBD network facilitates Li-ion transport in the pores, the accessible capacity increases. A different approach was proposed by Mistry et. al. [100], who generated microstructure models with film-like or finger-like arrangements of the CBD (Figure 14b,c): film-like CBD deposits were found to detrimentally affect the reaction kinetics whereas finger-like CBD poses a slightly higher resistance to electrolyte transport (Figure 14d,e). By accounting for such extra resistance posed by the CBD, the study identified a porosity threshold of 31% below which mass transport in the electrolyte becomes rate-limiting. The effect of CBD morphology was also investigated by Zielke et. al. [48], who compared the effect of stochastically-generated cluster-shaped (Figure 14f) and fiber-shaped (Figure 14g) CBD on the tortuosity of the pore phase. Based on these simulations, the fiber CBD arrangement reduced the tortuosity factor of the porous phase (Figure 14h) and shows up to three times higher electronic conductivity at the same CBD content of the cluster-shaped design.

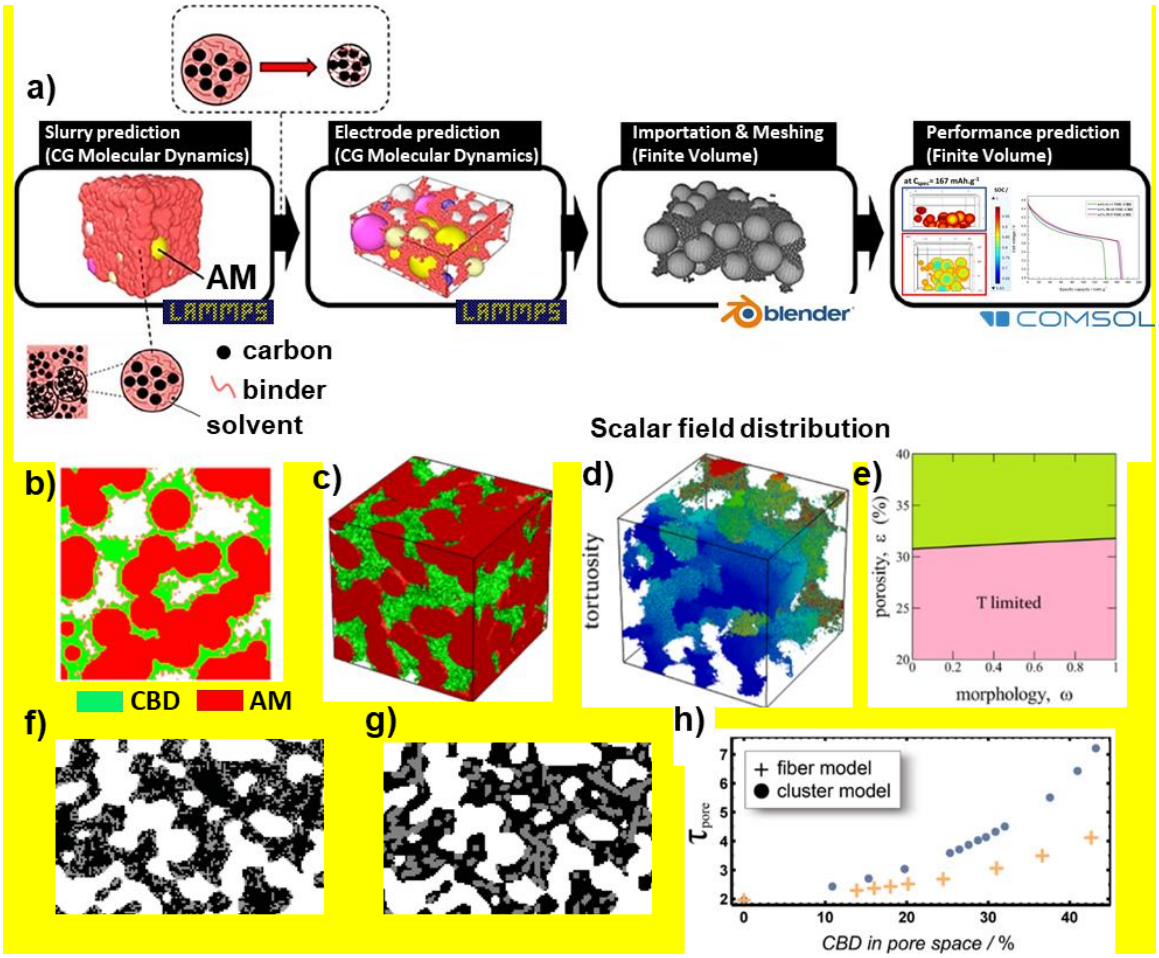

Figure 14: (a) Coarse-grained molecular dynamics (CGMD) is used to simulate the fabrication of the electrode, the resulting microstructure consisting of both active material and CBD is then used to simulate the electrochemical performance [168]; (b) CBD (green) is artificially generated by energy-based

optimization method alongside the active material (red); (c) 3D rendering of the generated electrode structure; (d) scalar field distribution as a result of diffusion simulation to obtain the tortuosity of the fluid domain; (e) suggested mass transport limited zone (pink) as a function of the CBD control parameter ω and porosity [100]. ω = 0 and 1 correspond to the film-type and the finger-like CBD structures respectively. (f)-(g) Artificially generated cluster-shaped and fiber-shaped CBD (grey) and (h) the resultant tortuosity of the pore phase [48].

Nevertheless, the knowledge obtained from the artificially-generated CBD microstructures needs to be treated with caution since the resulting CBD is not authentic, thus it may not capture correctly its effects on pore tortuosity, microstructural heterogeneity, and eventually electrochemical performance. The recent progress in the application of correlative microscopy approaches provides new methodologies for resolving the CBD phase [7, 18]. Hutzenlaub et al. [19] performed the simulation of an LCO electrode resolving the electrolyte, active material, and CBD based on microstructures obtained from focused ion-beam/scanning electron microscopy (FIB/SEM) imaging (Figure 15a-c), finding that the carbon binder coverage enhances the inhomogeneity in lithium composition. Lu et. al. [7] used a dual-scan superimposition (DSS) technique that replaces the low-resolution CBD in the full electrode with a stand-alone CBD scan of higher resolution and contrast (Figure 15d-h) to fully reconstruct the 3D microstructure of the electrode. The embedment of the authentic CBD morphology enabled the development of a microstructure-resolved electrochemical model (see Section 4.2 for more details), which was used to investigate the mechanism of reaction heterogeneity and uneven state-of-lithiation (SoL) distribution among particles of different sizes as induced by the complex microstructural features. In addition, this allowed for the comparison of different microstructural designs, among which electrodes featuring graded porosity and graded particle size (Figure 15i), which improve the rate performance while maintaining a high energy density because of the enhanced transport properties at the separator side. Notably, better effective transport properties in the electrolyte guarantee a more homogeneous distribution of SoL in the active material particles throughout the electrode thickness (Figure 15j). Hence, all these findings indicate the importance of capturing microstructure heterogeneity and authentic CBD details to assess the effect of anisotropic effective transport properties on electrode design.

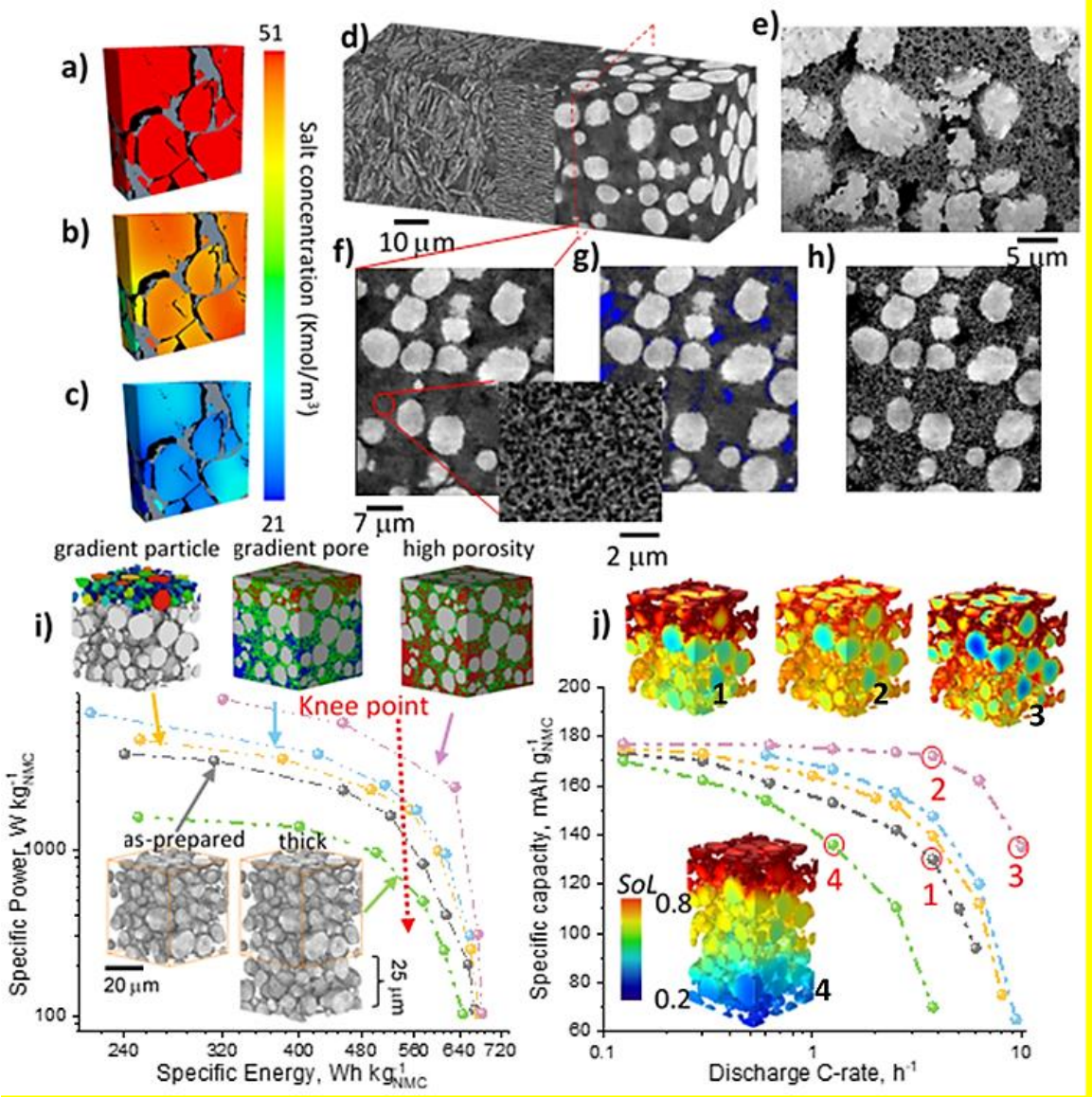

Figure 15: Microstructure-resolved battery modelling using faithful 3D reconstruction of the electrode architecture. (a), (b) and (c) show the lithium concentration within active material (LCO) at state of charge equal to (a) 0, (b) 0.1, and (c) 1 upon charge based on FIB-SEM data [19]; (d) Micro-CT data of the cell components; (e) SEM image showing the active material (NMC) alongside the CBD morphology; (f) a virtual slice of the NMC cathode showing the unresolved CBD phase (grey). The inset is the authentic CBD structure scanned without the inclusion of NMC particles; (g) macro-pores are highlighted in blue and kept untouched whereas the low-resolution CBD phase is replaced with the stand-alone CBD scan using DSS technique [7] (h); (i) Ragone plot obtained from the electrochemical simulation based on the fully-reconstructed 3D microstructure, comparing the energy and power performance for different electrode designs; (j) rated capacity plot corresponding to the electrodes in (i), where the insets show the SoL distribution for each circled data point on the curve (the separator side is at the top).

4.2 Prediction of electrochemical properties

Using microstructure-resolved electrochemical models to understand the relationship between architectural heterogeneity and performance has received wide attention [50, 85, 156, 166]. Microstructure-resolved electrochemical models solve for the electrochemical reactions as well as mass and charge transport within their respective phases. Typically, these microstructure-resolved models use the same elementary equations developed for low-order continuum models, such as Butler-Volmer kinetics for intercalation reactions, concentrated solution [165, 167] or Nernst-Planck equations [7, 113] for ion transport in the electrolyte, Fick law for diffusion in the active materials.

In most of these studies, the microstructure-resolved simulations are used to predict macroscopic descriptors of the electrochemical performance, such as discharge curves [169] at different C-rates or the impedance response of the electrode [170]. In such a context, electrochemical modeling is used to inform the design of more efficient microstructures, for example focusing on the identification of optimal volume fractions of active material, binders and pores [93, 167], or on specific indications for thick electrodes [165]. Some of these studies focus specifically on the effect of heterogeneous microstructures, such as the non-uniform distribution of binders [165], the effect of particle polydispersion [88, 98] or the design of graded electrodes [7] (as in Figure 15i,j). Studies related to the optimization of microstructures are reviewed in detail in Section 5.1.

All these studies generally point out that microstructure-resolved simulations improve the accuracy in the investigation of electrochemical processes compared to continuum pseudo-2D models, especially when considering phenomena that are localized in nature, such as hot spots and degradation phenomena. Yan et al. [118] simulated the heat generation in LCO cathodes, mapping the three-dimensional distribution of ohmic, entropic, and reaction heat within the reconstructed microstructure. The analysis shows that a continuum pseudo-2D model overestimates the electronic ohmic heat while underestimates the ionic ohmic heat (which is two orders of magnitude larger than the electronic one) compared to a microstructure-resolved model. In fact, uneven pore/particle distributions leads to uneven SoL distribution, capacity underutilization, and non-uniform current and temperature profiles, which may be correlated with regions of higher stress and accelerated degradation [93]. Danner et al. [165] studied in which conditions lithium plating in thick graphite electrodes is thermodynamically possible. Simulations show that charging a 300 μm-thick graphite anode at 1C and beyond can create localized zones where the onset of lithium plating is thermodynamically possible, even though the cell voltage is well below 4 V. Lithium plating and lithium stripping are also considered by Feinauer et al. [171], who point out the large simulation time required by microstructure-resolved degradation simulations and propose order reduction methods to speed up the computation. In all these cases, capturing the heterogeneity of the electrode microstructure in electrochemical simulations is proved to be key to overcome the limitations of continuum models.

Another source of heterogeneity may stem from the active materials themselves, irrespective of the microstructure heterogeneity. In fact, many active materials, such as LFP, LCO and graphite, are phase-separating materials [172]; this means that, upon lithiation/delithiation, lithium is distributed within each particle into Li-poor and Li-rich phases (e.g., the ordered stages in graphite [58, 173]), whose compositions are dictated by thermodynamics [174]. Such a phase-separation phenomenon is a source of instability in a population of particles which undergo particle-by-particle separation, also known as mosaic instability [175]. This can sometimes result in a bimodal distribution of the state of lithiation throughout the electrode at low charge/discharge rates, as experimentally visualized in LFP [176, 177] and graphite [58] and then explained by physics-based theories [60, 174, 175, 178, 179]. Compositional heterogeneities have been reported also in NMC and nickel cobalt aluminum oxide (NCA) [180-182], both at high C-rates [182] and in agglomerate particles as a consequence of internal stress [183, 184].

There exist at least two consolidated theories to model phase-separating materials, namely the sharp interface model and the phase-field model. The sharp interface model considers Li-rich and Li-poor areas as individual phases, separated by a sharp interface that moves as one phase grows at the expenses of the other one; in pseudo-2D battery modeling, this approach has largely been framed in terms of shrinking core modeling [148, 185-187] which, however, does not capture the physics of phase separation realistically. The alternative approach, the phase-field model, assumes that lithium composition varies continuously across the two phases, so that the interface between Li-rich and Li-poor phases is diffuse [188]; the phase-field model has been proved to be successful in simulating battery phase-separating materials in reduced-order and single-particle models [61, 189-191]. However, a systematic study of phase-separating materials, mosaic instability, and heterogeneous composition distribution in microstructure-resolved simulations is still lacking; to date, the most comprehensive application of phase-field modeling in 3D microstructures is the electro-chemo-mechanical model presented by Hofmann et al. [192], who focused on mechanics (see Section 4.3). Preliminary investigations were made by Orvananos et al. [193, 194], who simulated phase separation of LFP and LCO in microstructure-resolved simulations (Figure 16a,b) by employing the smoothed boundary method [195], which is a phase-field-like approach that uses a continuous parameter to distinguish different domains, including the electrolyte and solid materials. Simulations showed that, when particles do not touch each other, intra-particle phase separation and sequential transformation occur at low current [196] (Figure 16a), while a simultaneous phase separation occurs at high C-rates, in agreement with the predictions of reduced-order phase-field models [60, 175, 178, 179, 197-199]. On the other hand, when LFP particles are more densely packed, inter-particle phase separation occurs for a greater range of C-rates [193] because lithium can be exchanged directly by contacting particles without being mediated by the electrolyte via interfacial reactions (Figure 16b). In other studies, the dynamics of phase separation was roughly captured by considering the non-monotonic open-circuit voltage and by introducing a thermodynamic factor to lithium solid diffusivity to represent the non-ideal solution behavior of the active material [50, 200]. For example, by using this simplified approach, Kashkooli et al. [50] found a wider distribution of physical properties and state of lithiation in microstructure-resolved simulations than what continuum pseudo-2D models would predict (Figure 16c).

Lastly, composition heterogeneity can emerge also in reaction-limited electrodes, for example when LFP nanoparticles are considered. In such a case, the lithium solid diffusion (which generally obeys a Cahn-Hilliard equation for phase-separating materials) is relatively fast compared to the rate of the intercalation reaction at the particle surface. In such a case, as shown by Bazant and co-workers [61, 190], an Allen-Cahn reaction model is sufficiently descriptive, so that composition heterogeneity is determined by the interplay between phase-separation thermodynamics and reaction kinetics [201]. Besides, while in microstructure-resolved models the Butler-Volmer equation is typically used to describe the intercalation kinetics [7, 88, 165], recent studies [202-205] have shown that Marcus-Hush-Chidsey kinetics is more suited especially at high overpotentials, while electro-autocatalysis, a term used to describe a reaction rate that increases with increasing lithium concentration [206], can be another source of composition heterogeneity. To date, Marcus-Hush-Chidsey and electro-autocatalytic effects have not yet been implemented in microstructure-resolved simulations, so that reaction-driven inhomogeneity and its interplay with microstructure heterogeneity are missed by the current state-of-the-art of physics-based 3D models.

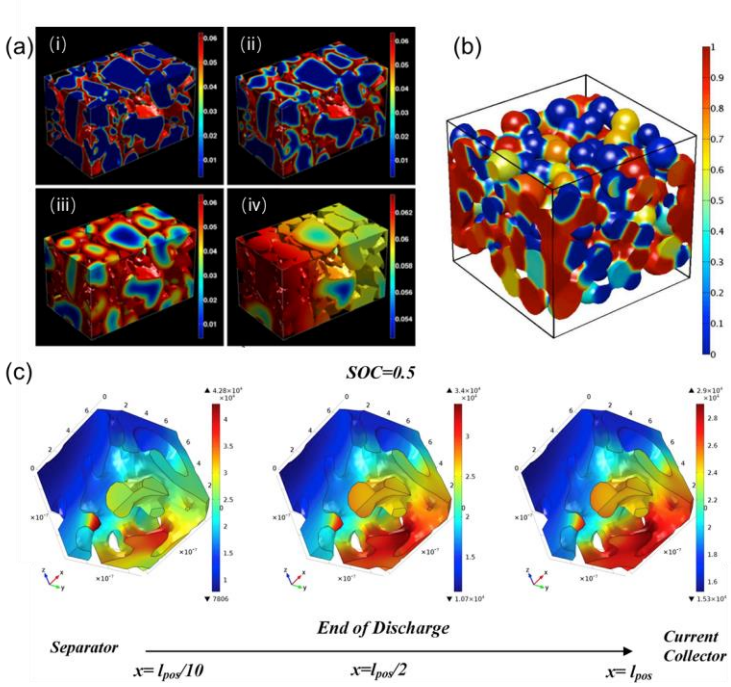

Figure 16: (a) Lithium concentration (mol/cm^3) evolution in time (a to d) shows solid-solution behavior (as observed in a portion of concentration range in LCO) as lithium inserts into LCO particles at a constant voltage, simulated using an experimentally obtained microstructure [194]. (b) A snapshot of the lithium concentration in an aggregate of 200 LFP particles during charge at 10C [193], showing inter-particle phase separation as lithium is exchanged directly via particle contacts. (c) Distribution of lithium concentration (mol/m^3) within representative microstructural elements of an LFP electrode from near the separator to the current collector side at state of charge equal to 0.5 (end of discharge at 1C) when using a thermodynamic factor in lithium solid diffusion [50].

4.3 Prediction of mechanical properties

Apart from the electrochemical performance, long-term mechanical integrity is another critical concern in developing high-performance batteries. Vast experimental and theoretical studies showed that mechanical deformation could significantly influence the mass transport and reactions of the battery systems in many ways such as diffusion-induced stresses, volume expansion, formation and propagation of inner-particle cracks, inter-particle and electrode-level delamination, and structural instability, to name a few. The studies on electro-chemo-mechanical modeling of lithium-ion batteries have been reviewed in several papers: Grazioli et al. [207] summarized the numerical developments of battery modeling; Zhao and Cui [208] outlined the role of mechanics and fundamental issues in energy materials; Xu and Zhao [209] provided a brief but rather in-depth theoretical summary; and, more recently, Zhao et al. [210] performed a comprehensive overview from a combined theoretical-numerical point of view. In addition, safety-focused mechanical modeling efforts are summarized by Zhu et al. [211] and Liu et al. [212]. In this Section, we focus on how microstructure-resolved modeling has a great potential to characterize deformations occurring during battery operation and upon external loads, thus potentially leading to reduced-order and less computational intense mechanical modeling frameworks.

During battery cycling, the overall deformation of the particles is usually decomposed, either additively [210] or multiplicatively [213, 214], into four portions – elastic, plastic, thermal, and diffusion-induced. Microstructure-resolved models enable the quantification of the contributions of these effects for different electrode materials and thus make it possible to go beyond homogenized electrode models and to simplify

the electro-chemo-mechanical theories accordingly, along with in-situ and operando characterization tools which provide a quantitative insight that can be used to validate emerging models [86, 90, 94]. Kim et al. [215] demonstrated on a 2D reconstructed section of a LFP cathode that the thermal strain is negligible compared to diffusion-induced strain during normal charge-discharge and that the experimental capacity fade of the battery cell and the averaged stress in the particles have a positive correlation. In the NMC622 model developed by Xu et al. [101], the plastic deformation was treated as a trivial term based on the author's serial experimental investigations on single particles and electrodes [216-218], which show brittle fracture of the material before large plastic deformation could accumulate. Microstructure-resolved models also enable the investigation of the mechanical interaction between particles and the effect of contact pressure on the electrochemical reaction rate. Wu et al. [219] established a coupled mechanical-electrochemical modeling framework on a simplified 3D geometry of regularly packed particles. The same team used this framework to show that a small electrochemically inactive region can cause large stress in its vicinity [220].

The stress buildup within and among active material particles is a significant factor for electrode lifetime, thus concerted effort has been recently made to study the mechanical properties of various cathode and anode materials [221-224]. Various mechanical degradation mechanisms have been identified experimentally [126, 225-228], among which active material particle cracking/fracture and conductive network debonding are the two most impactful factors. While particle-level investigations have shown that large local strain and stress concentration could happen when a single particle is lithiated [61, 229, 230], Roberts et al. [231] used their multi-particle microstructure-resolved model to demonstrate that the inter-particle contact can cause even larger stresses. Xu et. al. [101] used an electro-chemo-mechanical model to investigate the stress distribution across the NMC electrode under cycling conditions, assuming isotropic strain at the secondary particle level. It was observed that NMC particles near the separator experience more serious mechanical damage than the ones at the current collector, due to different lithium reactivity at these regions (Figure 17a). The particle shape, size and local pore size also cause uneven lithium intercalation rate that can cause heterogeneous stress distribution within and between particles. Thus, the accuracy of local strain predictions can benefit from the information on crystalline size and orientation of NMC primary grains as recently enabled by FIB-EBSD [32]. In addition to the stress within active material particles, the stress distribution in the CBD is highly dependent on the local morphology as well, where narrow regions demonstrate large stress concentration as shown by Xu et. al. [101] (Figure 17b). The mismatch of the strain between particles and CBD inevitably results in a gap at the interfacial area (Figure 17c) and detrimentally affects the conductive network, capacity underutilization, and uneven aging between NMC particles. Thus, improving the mechanistic understanding and mitigating microstructural heterogeneity in all of the three constituents of the electrode is critical in suppressing mechanical degradation and prolonging the cycle life of the batteries.

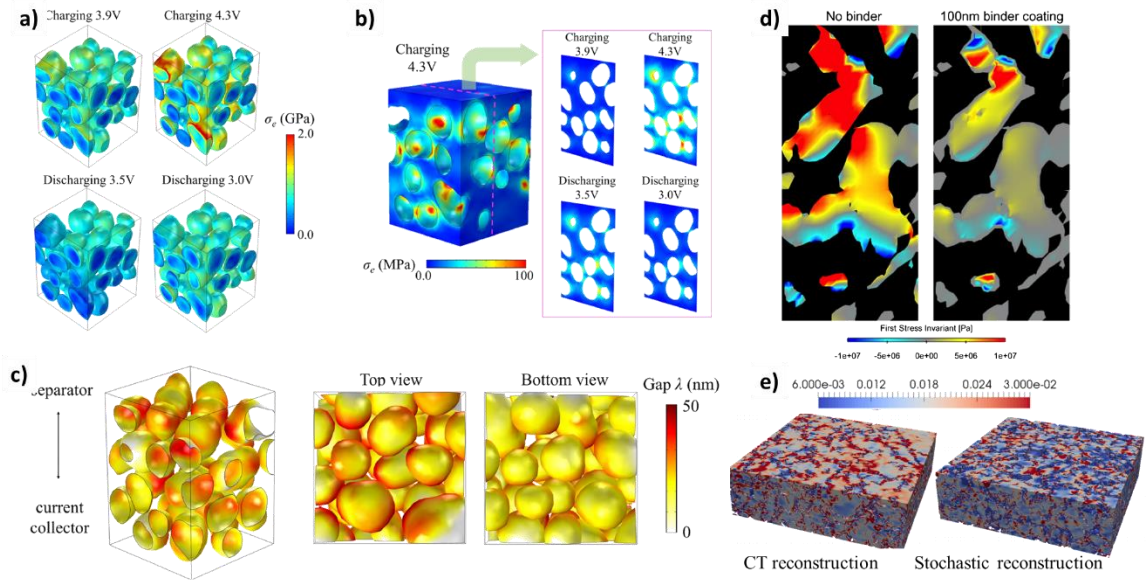

Figure 17: Heterogeneous stress distribution of NMC cathode cycled at 5C. (a) and (b) visualize the spatial distribution of stress developed in NMC particles and CBD matrix respectively under different charge/discharge conditions; (c) the predicted gap between NMC particles and CBD matrix as a result of the stress/strain difference at the interface [101]. (d) Difference in stress distribution between CBD matrix with and without binder [200]. (e) Comparison of predictions by the CT model and the stochastic model [192].

Some efforts have been dedicated to compare modeling results in microstructures obtained via computed tomography or generated via stochastic reconstruction. Roberts et al. [231] pointed out that, when anisotropic swelling is simulated, microstructures obtained via particle packing enable an easier assignment of lattice orientation to each individual particle. In a recent study, Hofmann et al. [192] produced a stochastic 3D microstructure with the information obtained from tomographic data of an LFP cathode. A phase-field model was implemented and coupled with the von Mises J_2 plasticity model and isotropic hardening law. The predictions obtained with the stochastic microstructure turned out to significantly differ from those of the simulation with the tomographic structure in a point-by-point comparison (Figure 17e), but the important statistical features agree well with each other in terms of the mean value and the distribution of the hydrostatic stress and the von-Mises stress.

The downside of microstructure-resolved electro-chemo-mechanical modeling is the high computational cost. Not only there are additional difficulties to handle the contact and boundary conditions compared to continuum models, but also the number of mesh elements is significantly larger, especially when the CBD is explicitly resolved. As an example, up to 30 million tetrahedral elements were used by Lu et al. [7] to mesh a $43 \times 43 \times 50$ μm^3 domain with realistic CBD features included. Treating pores and CBD as a lumped continuum phase is a typical strategy to reduce the computational cost [101, 231], but this simplification does not allow to account for the CBD heterogeneity. An intermediate strategy consists in assuming a uniform binder coating on the interfaces of the particles as reported by Mendoza et al. [200], who showed that adding a binder coating can cause a significant difference in the stress distribution (Figure 17d). In addition to this, the computational stability is highly dependent on how CBD is modeled and how boundary conditions with particles are treated. Hofmann et al. [192] is one of the few studies that reported a convergence difficulty of the electro-chemo-mechanical model at the particle-to-particle contact surface.

To overcome this issue, the authors performed geometric regularization of the neighboring particles to smooth the sharp contact region; however, this practice unifies the discrete particles into one connected domain and, therefore, poses the risk of losing the real physics of frictional contact and cohesion.

Besides the internal deformation triggered by the normal service life of batteries, there are many scenarios where the electrode materials may deform subject to external mechanical loads and consequently change the electrochemical performance and safety. One of these scenarios is the calendering (compression) process during the manufacturing of standardized electrodes. Conventional methods to investigate this effect include equivalent circuit models of the experimental data [232] and discrete element methods (DEMs) [233-235]. DEM is an effective computational tool for characterizing a large number of particles by including different particle shapes and sizes into the microstructure generation, being particularly useful for predicting the porosity of the electrode during compression [236, 237]. There are attempts to extend the DEM approach for multi-physics modeling by relating its predictions with porous electrode theories and empirical equations [235, 238]. But for a fully coupled theory to investigate the underlying mechanisms, it is still not sufficient because important electrochemical processes take place at the interfaces, which are usually not modeled by DEM approaches.

Microstructure-resolved physics-based models show great potential in rationalizing the calendering process of battery electrodes. Kang et al. [239] performed microstructural reconstruction of NMC111 cathodes with different calendering conditions based on the synchrotron transmission X-ray CT data. The geometric properties of the electrode such as porosity, pore size distribution, particle size distribution, specific surface area, and tortuosity were obtained, and the electrochemical performance was investigated experimentally. With a parametric study, the authors suggested the optimum electrochemical performance of the studied NMC at 94:3:3 (NMC: binder: carbon black) could be achieved by calendering to 3.0 g/cm^3 electrode density. Lu et al. [240] investigated the microstructural evolution of NMC cathodes under incremental calendering using 4D X-ray nano-CT and the 3D reconstructed electrode data were directly meshed for electrochemical performance simulation. The experimental setup is shown in Fig. S1 in the Supplementary Information. It was found that solid-state diffusion predominantly restricts the energy and power performance especially for the electrode composed of large particles (AM_L), as evidenced by intra and inter-particle difference of state-of-lithiation (SoL) in Figure 18a-c. In contrast, electrodes made of small particles (AM_S) have more uniform SoL across the depth (Figure 18d-f). The activation overpotential is larger and more heterogeneous in the AM_L electrode (Figure 18g-i) due to the low-specific reaction area and non-uniform distribution of porosity compared to AM_S (Figure 18j-l). The overpotential heterogeneity was observed to exacerbate with calendering, which further reduced the active reaction sites at the electrode-electrolyte interface. For a thin electrode (uncalendered thickness < 50 μm), Li-ion transport in the electrolyte did not primarily govern the battery performance even under 24% calendering as the electrolyte concentration at the current collector was far from being depleted for both types of electrodes (Figure 18m-r). Due to the coarse structure of AM_L, the percolated pore network is more susceptible to the porosity drop by calendering, consequently, the average current flux in the pore phase is much larger in AM_L (Figure 18s-u) than in AM_S (Figure 18v-x). This could pose a higher risk of temperature-induced degradation and shorter lifetime.

Other potential applications of microstructure-resolved models for characterizing the deformation of electrodes subject to external loads include modeling the effect of stack pressure on battery performance [241-244], predicting the initiation of mechanical failure [233, 245], and characterizing the mechanical tests such as nanoindentation [216-218, 246]. There have not been many existing publications on these aspects using microstructure-resolved models, but more usage can be expected.

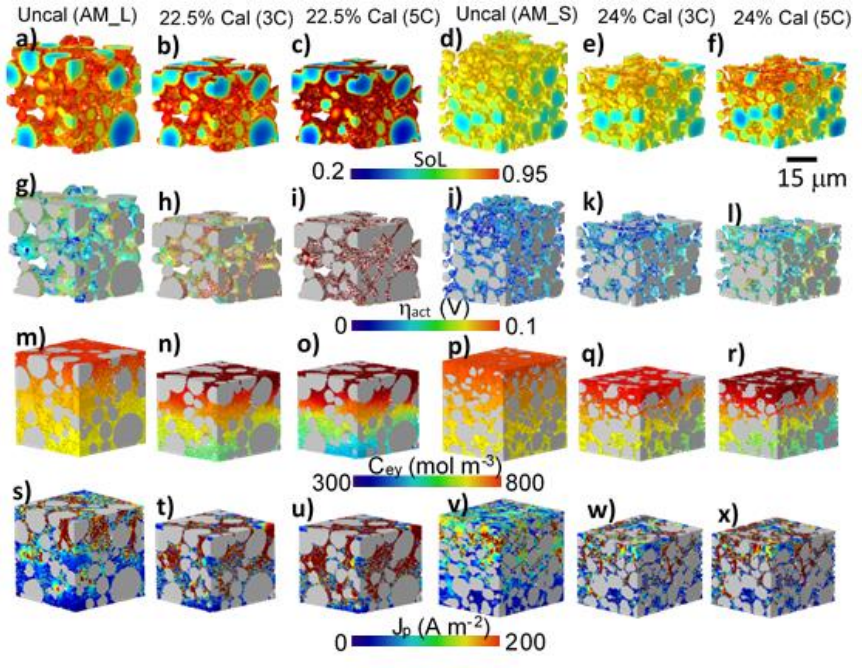

Figure 18: Correlating microstructural evolution with electrochemical performance to guide calendering. The setup of the in-situ calendering experiment by X-ray CT is shown in Fig. S1 in the Supplementary Information. (a-c), (d-f) Spatial distribution of SoL in large-particle electrode (AM_L) and small-particle electrode (AM_S) respectively; (g-i), (j-l) spatial distribution of activation overpotential η_{act} at the active particle/electrolyte reacting interface in AM_L and AM_S; (m-o), (p-r) spatial distribution of electrolyte concentration C_{ey} in AM_L and AM_S; (s-u), (v-x) spatial distribution of Li-ion flux J_p in AM_L and AM_S. The separator side is at the top [240].

The microstructure-resolved modeling also relates the microscale characteristics to macroscale behaviors. The reconstructed microstructure can be treated as the representative volume element (RVE) of the battery electrode. A continuum macroscale model developed on the basis of the microstructural modeling will provide an efficient tool with both high computation efficiency and accuracy for battery design in terms of electrochemical and mechanical performance. Differently from electrochemical modeling, for which the porous electrode theory based on volume averaging as in the pseudo-2D approach is successful to some extent, for mechanical behaviors deriving a continuum model from microstructure-resolved (or RVE) modeling is more challenging. The main difficulties lie in two aspects: (1) finding proper mechanical material models and input properties for each component of the RVE, and (2) formulating the stress-strain relation (mechanical constitutive model) of the RVE.

The RVE of an electrode mainly consists of particles of active material or graphite/silicon and the binder. The mechanical experimental data of secondary particles is quite limited in the literature due to the difficulties in preparing and loading the sample, as well as measuring the force and deformation at the microscale. Zhao's team has made great efforts in developing the in-situ nanoindentation platform for batteries [4]. They observed almost linear elastic behavior of the tested NMC secondary particle and Si anode, and reported some essential mechanical properties, including the elastic modulus, hardness, and interfacial fracture strength [218, 247, 248]. Jia et al. [249] have recently reported the in-situ mechanical AFM-FEM experiment for a porous silicon structure anode to evaluate its mechanical strength. Besides the experimental studies, Qi et al. [250, 251] estimated the mechanical elastic modulus of various active materials through Density Functional Theory (DFT) simulations.

The other important component is the binder, which is typically a viscous hyperelastic material. Chen et al. [252] investigated the adhesion strength of binder by the micro-scratch test, which however cannot fully calibrate a material model for the binder. Santimetaneedol et al. [253] made samples of binder on a larger scale and performed uniaxial loading-unloading tests at macroscale to calibrate and validate the time-dependent deformation behavior of the binder. Since the interface behavior between particle and binder also affects the behavior, Luo et al. [254] designed lap-shear specimens and conducted tension tests along different directions to calibrate the interface behavior.

Thus, by coupling accurately reconstructed microstructure with mechanical material models along with proper input properties for each component, it is possible to develop a macroscale continuum constitutive model (stress-strain relation) of the RVE. To the authors' best knowledge, no such models are reported in the literature for battery electrodes, except for the attempt made by Zhu et al. [233], who investigated the mechanical behavior of cylindrical anode samples and developed a DEM model to predict the force-displacement response of uniaxial and lateral compression tests. Similar work has been widely conducted for the granular materials in the geotechnical field, pharmaceutical industry, and powder forming industry by using DEM [255] or discrete finite element simulations [256], thus indicating that micro-to-macro relations for mechanical modeling can be obtained. In addition, it is worth noting that the same strategy also applies to coupled electro-chemo-mechanical characterization to bridge the gap between the particle-model and the electrode-level model [219].

5. Computational design of Li-ion battery microstructures

As described in the previous section, physics-based modeling enables for the prediction of functional properties given an electrode microstructural design. This capability can be coupled to the statistical characterization and reconstruction methods described in Section 3 to enable the optimization of microstructures to meet target material properties. In particular, statistical characterization (Section 3) plays the role of design representation, which defines the design space quantitatively through microstructure descriptors, while multi-physics modeling (Section 4) computes the resulting transport, electrochemical and mechanical properties. Thus, by integrating stochastic reconstruction (Section 3) and multi-physics modeling (Section 4), we can establish a design evaluation module, which predicts the responses of microstructure designs. The focus of this section is to review computational design methods that inversely find microstructure designs (in the form of microstructure descriptor values) based on target material properties. Both parametric optimization and machine learning approaches have been investigated for the design of Li-ion battery material microstructures.

5.1 Parametric design optimization

With a parameterized microstructure design space, digital microstructure designs can be generated by changing the input microstructure descriptor values for stochastic reconstruction. The microstructural parameters that have been investigated in microstructure-resolved simulations are volume fractions, particle size and shape, spatial arrangement of particles, graded distributions, phase morphology and combinations thereof, as summarized in Figure 19.

Ngandjong et al. [167] analyzed the ratio between active material and CBD in an NMC cathode; simulations showed that by increasing the NMC-to-CBD ratio the porosity increases, which facilitates mass transport in the electrolyte and thus increases the accessible capacity. Nevertheless, decreasing the CBD fraction must be taken with care, especially in thick electrodes, where the inhomogeneous distribution of the CBD may negatively affect the electrochemical performance as reported by Danner et al. [165]. The particle size

has been widely investigated as a design variable since it can be easily varied in particle packing algorithms. By coupling DEM and microstructure-resolved simulations, Chung et al. [119] found that a broad particle size dispersion, following a Gaussian distribution, has the potential to deliver up to two times higher energy density than monodispersed particle systems for low C-rates. The effect of particle size was investigated also by He et al. [110] for graphite anodes (Figure 19a), focusing on effective properties such as pore phase tortuosity and effective electronic conductivity. The study also analyzed the effect of particle shape by varying the ratio of principal axes of ellipsoidal graphite particles: as particles become flatter, the through-plane tortuosity factor of the pore phase becomes larger. The influence of size and shape of particles (namely, LFP particles) was also discussed by Mai et al. [98] on both electrochemical and mechanical responses (Figure 19b). The microstructure morphology determines the spatial distribution of mechanical stresses, which is directly linked to the spatial distribution of Li insertion reaction. For the same particle volume fraction, the microstructure models with realistic particle shapes (ellipsoids) and size distributions lead to a much higher internal stress and sharper voltage drop when increasing the C-rate, compared to the microstructures with monosized spherical particles.

The spatial arrangement of particles is another widely used design variable that is compatible with the particle packing algorithms. Kespe et al. [88] investigated bidisperse size particle systems of three different spatial arrangements: two-layered arrangements of opposite packing sequences and a mixed arrangement (Figure 19c). The three arrangements have similar total particle surface areas, but the spatial distributions of surface areas in the through-plane direction are different, thus affecting lithium distribution within the solid electrode microstructures over the course of discharge. As also reported by other studies [7, 98, 167], due to slow solid diffusion, larger particles are underutilized while smaller particles show elevated lithiation, resulting in an accumulation of intercalated lithium in the corresponding regions. It is found that putting the layer of small particles close to the separator is beneficial to improve the electrochemical performance, especially for high-rate applications. This effect is further intensified for structures of higher porosities. Similar conclusions were reached by a more recent work by Lu et al. [7], who also investigated graded NMC cathode microstructure designs, by erosion of the original particle geometry, followed by gap filling with smaller particles to maintain the same volume fraction (Figure 19e). The study investigated also graded porosity designs, where enlarged pores were created by applying morphological erosion filters on the CBD. Graded microstructure designs with larger pore sizes at the separator side lead to more uniform electrolyte distribution, reduced Li-ion transport resistance, more homogenous charge transfer distribution, and thus more homogeneous lithiation, resulting in better utilization of active material and larger accessible capacity. Notably, homogeneous lithiation also reduces temperature gradients and thermal/mechanical stress [227, 257], preventing cracking and delamination that reduce the life of battery [155].

Compared with single-factor parametric studies, larger design freedom can be obtained by considering multiple microstructure design variables simultaneously. Habte et al. generated four cathode microstructure designs by changing the size of active material particles and porosity [111], and 48 anode microstructure designs by changing particle shape, size, porosity, and volume fraction of active additive [112]. All microstructure designs were created by particle packing reconstruction algorithms and the electrochemical response was assessed via impedance spectroscopy simulations. In general, the simulated results show that small and ellipsoidal particles in highly porous electrodes reduce the charge transfer resistance. Mistry et al. [100] adopted a physics-inspired Monte Carlo algorithm to design CBD microstructures. The design variables include porosity, the volume fraction of active materials, and a CBD morphology control factor, which represents the ratio of “depositing/growing” new conductive binders on pre-deposited conductive binders versus an uncovered active material surface during the reconstruction process (Figure 19d). While the film-like CBD arrangement hinders the intercalation reaction, the finger-like CBD morphology offers

higher mass transport resistance in the porous phase. The main outcome of the analysis is the identification of a porosity threshold, equal to 31%, below which mass transport in the porous phase becomes rate-limiting.

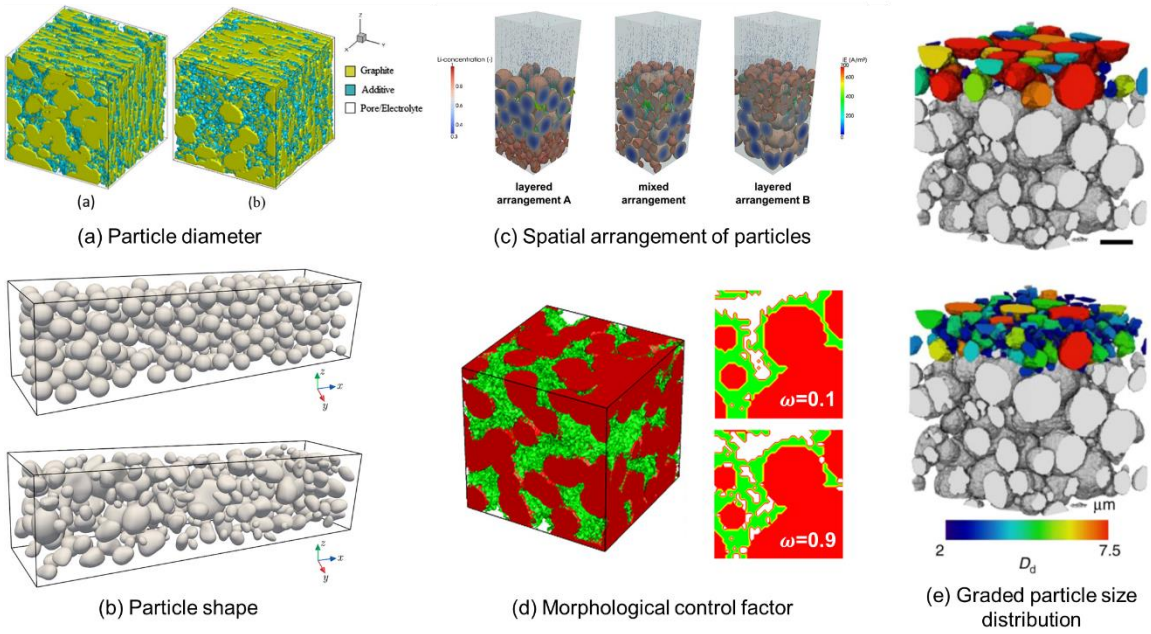

Figure 19: Parametric microstructure design optimization. (a) Particle diameter as the design variable [110]. (b) Particle shape as the design variable [98]. (c) Three designs of different particle arrangements [88]. (d) Film-like and finger-like microstructures created by assigning different values to the morphology control design variable [100]. (e) Graded particle size arrangements created by applying morphological erosion filters on particle geometries obtained by XCT [7].

5.2 Machine learning-driven design discovery

Although machine learning methods have been widely employed in designing the molecular structures of energy materials [258], relatively fewer works can be found in designing the stochastic microstructures of Li-ion battery materials. Machine learning methods have been employed in (i) designing the compositions of the battery electrodes, and (ii) designing the microstructure features.

Applying machine learning approaches to composition design is straightforward because the input variables (composition percentages) are parameters in nature. Homma et al. [259] conducted a two-iteration Bayesian optimization to tailor the composition ratio of a ternary Li_3PO_4–Li_3BO_3–Li_2SO_4 solid-oxide electrolyte to maximize Li-ion conductivity. To explore the 2-dimensional design space, 15 samples of different composition ratios were prepared, and their Li-ion conductivities were measured experimentally as the initial training dataset. A Gaussian regression model was trained based on the initial dataset and 10 promising additional sampling locations were predicted based on the Expected Improvement (EI) and the maximum probability of improvement (PI) criteria. The additional samples were synthesized and the optimal composition (25:14:61 % mol) showed a threefold increase in Li-ion conductivity compared to binary mixtures. This work is an integration of optimization algorithm with experimental design evaluation, so a large training dataset or a large number of iterations cannot be afforded. For design search in a high dimensional design space that requires a significant amount of training data, computational design evaluation by simulation is necessary. One example of simulation-based design is presented by Joshi et al. [260]. Multiple machine learning methods, such as Deep Neural networks, Support Vector Machines (SVM), and kernel ridge regression, were investigated to predict electrode voltages for metal-ion batteries

based on chemical properties of compounds and the properties of their elemental constituents. Although stochastic microstructural features are not considered in this work, this framework can be adapted for microstructure design.

To design electrode microstructures by machine learning (Figure 20), one common practice is to parameterize the geometrical/morphological characteristics first. The choice of microstructure parameters is determined by the statistical characterization and stochastic reconstruction approach used in modeling. For example, Takagishi et al. [261] applied the stochastic particle packing algorithm to reconstruct 3D microstructures of NMC cathodes, so the input features included the volume fraction of binder/additives as well as particle volume fraction, radius, and compaction pressure, which is a process parameter which reflects the maximum overlap among the reconstructed particles. A neural network model was trained to represent the relationship between the input features and the output electrochemical properties, which included the reaction resistance, the electrolyte resistance, and the solid diffusion resistance. A Bayesian optimization targeted to achieve high capacity indicated that the optimal microstructure is composed of small active material particles packed at ca. 50 % vol. with a low fraction of binder/additives. Another work on microstructure-property learning was done by Gao et al. [262], who applied a macro-homogeneous electrochemical model to investigate a thick electrode design with a bio-inspired electrolyte channel for fast charging/discharging. The electrolyte channel geometry was parameterized by seven variables and a deep neural network was trained on simulation data to predict specific capacity, specific energy, and specific power. A gradient descent algorithm was applied to optimize the channel design, which increased by 79% the specific energy according to simulations. Duquesnoy et al. [237] established a complete workflow that spans the full spectrum of process-microstructure-property of NMC cathodes. The relationship between process parameters (calendering pressure, electrode thickness) and the microstructure features (composition, initial porosity, porosity after calendering) was obtained by fitting experimental data. A simple particle dispersion algorithm was employed to generate stochastic microstructures with after-calendering microstructural features, which were characterized in terms of effective properties such as pore and solid tortuosity factors, surface area of active material exposed to the electrolyte, percentages of current collector covered by active material or CBD phases. A training dataset was generated with the process-microstructure-property workflow and a deep neural network was trained to predict the effective properties based on input processing and microstructure parameters. A Sure Independence Screening and Sparsifying Operator (SISSO) was applied to down-select a combination of features that are highly correlated with the properties. The study produced a correlation matrix between the processing parameters and the resultant effective properties to guide the design of NMC cathodes.

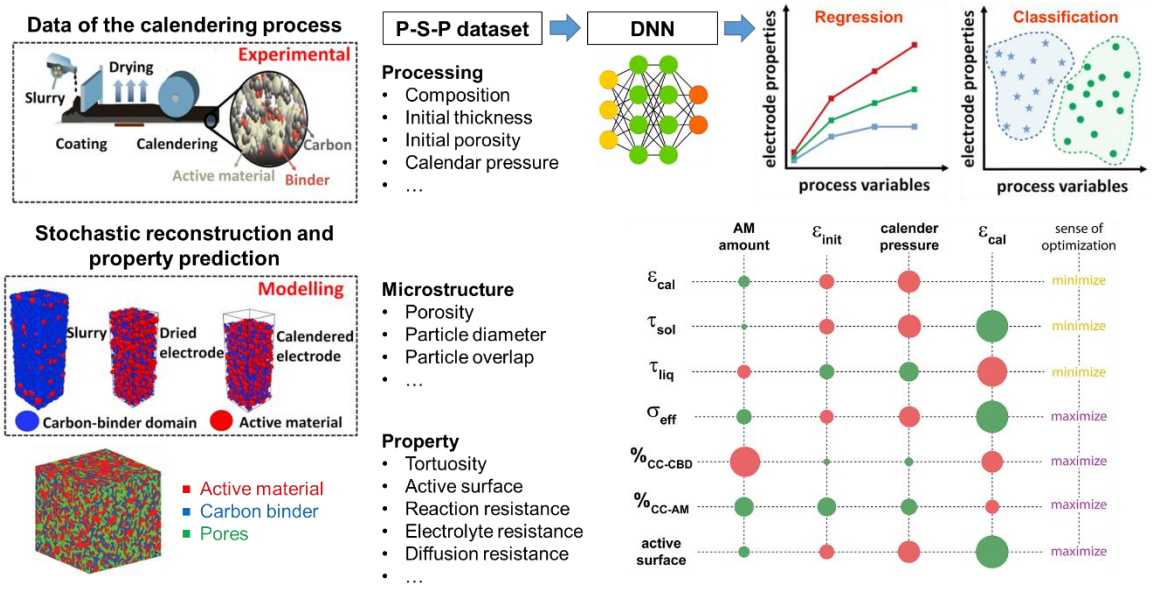

Figure 20: Machine learning framework for the design of processing parameters and microstructure features. This figure is created by adapting the figure from [237].

5.3 Deep learning-driven generative design and optimization

As discussed in Sections 3, 5.1, and 5.2, one of the major information losses in microstructure modeling and design is induced by using simplified microstructure representations. The major challenge is to fully capture the complex stochastic microstructure features. Instead of using parametric morphological descriptors that are defined *ad hoc*, one possible solution is to employ deep learning methods, which learn the key microstructural features directly from the image data and establish a supervised learning model to represent the relationship between the microstructural features and the material properties of interest. The microstructure-property supervised learning model enables both forward prediction of material properties and backward design of the microstructure. In the literature, autoencoders and GAN have been successfully applied to the design of other types of microstructural materials, and we believe they can also benefit the design of battery materials.

A general process of autoencoders/variational autoencoders-based design [132, 263, 264] is shown in Figure 21a. Taking microstructure images as the input, the encoder generates parametric latent features as the microstructure design variables. Furthermore, the latent feature-property relationship is established by another machine learning model, such as Gaussian regression for Bayesian optimization [263], convolutional residual network (ResNet) [132], etc. Microstructure design was done by searching latent feature values that lead to optimal material properties, and then mapping the optimal microstructure design from the latent space to the geometry space by decoding. However, it is also widely recognized that the autoencoder suffers from the issue of "maximum likelihood training paradigm" when combined with a conditional independence assumption on the output given the latent variables, and generate blurry samples [265]. Further open source datasets of electrode microstructures, similar to NREL's Battery Microstructure Library [76] , would complement this endeavor and ensure enough training data to generate representative electrode architectures.

GAN also provides a compressed representation of the input image data. The generative network is used to obtain the latent features of the stochastic microstructure image as the design variables. The latent features are represented by a flattened embedding layer of the generative network. New microstructure designs can

be obtained by (i) choosing one point in the latent design space, (ii) reconstructing the microstructure images by generator and judging this image as real or fake with a discriminator, and (iii) evaluating the microstructure's properties with physics modeling (e.g., FEA). To search optimal microstructure designs, Yang et al. [266] proposed using Bayesian optimization to explore the parametric latent feature space to generate new microstructure designs for polymer nanocomposites (Figure 21b). Tan et al. [267] proposed establishing a Convolutional Neural Network (CNN) model that predicts material properties directly from the input image, and integrating the CNN model with the GAN model to automate the design generation–evaluation process in optimization search. To sum up, both autoencoders and GAN are considered as promising methods for designing Li-ion battery materials. These deep feature learning methods are generally applicable to a large variety of microstructure features. By mapping the microstructure images to the latent space, the complex microstructures are represented by a small set of parametric features, which can be easily mapped to fabrication process parameters and material properties.

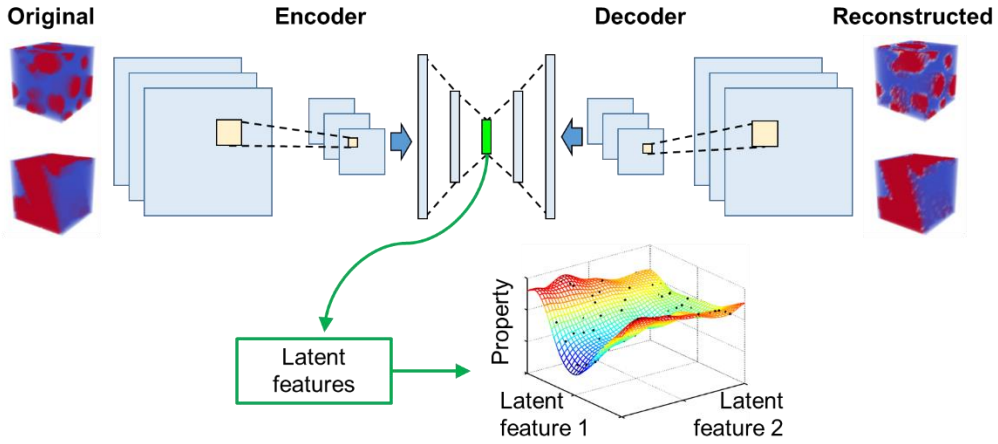

(a) Autoencoder for microstructure feature extraction and design optimization

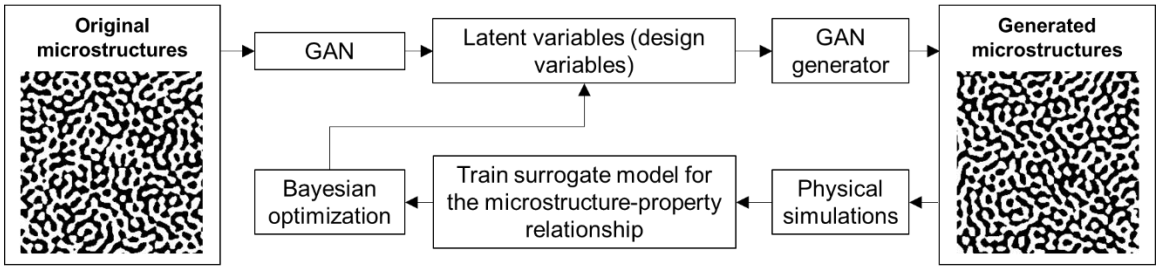

(b) Generative adversarial network-based microstructure design workflow

Figure 21: Application of deep learning models in microstructure feature extraction and design optimization. (a) An autoencoder-based method [263]. (b) An overview of GAN-based methods.

6. Conclusion and Future Prospects

In this review, we have discussed published studies of microscopic imaging, predictive modeling, and machine learning of heterogeneous microstructures and micro-scale electro-mechanical phenomena of Li-ion battery materials. Following the process of computational material design, significant achievements are summarized on data collection, battery microstructure design representation and generation, electrochemical and mechanical property evaluation, and microstructure design search. The central role of microstructural heterogeneity emerges from all these aspects, indicating that it cannot be ignored in battery

research. We expect that the integrated application of multi-physics modeling, machine learning, and advanced manufacturing technologies will lead to more innovative microstructure designs that significantly enhance the performance of Li-ion batteries, in addition to the examples reviewed in this paper. However, it is to be noted that there still exist numerous challenges to be addressed. Here, we provide our perspectives on three emerging directions related to the design and manufacturing of battery materials.

1. Microscopic image data sources. From the experiment perspective, much progress has been made in recent years on developing lab-based and synchrotron techniques that provide spatial and temporal quantifications on electrode morphologies, lithium transport phenomena, and mechanical degradation mechanisms. However, there is a clear need of further datasets that accurately capture important morphological details, like sub-particle grains and the distribution of the CBD within the pore structure of the electrode. Recent progress on leveraging respective strengths of complementary techniques such as detail of the CBD from FIB-SEM, representative volumes of electrode active materials from X-ray CT, and sub-particle grain detail from FIB-EBSD, have demonstrated a promising path towards merging multi-modal and multi-scale morphological quantifications into single 3D images. However, to develop stochastic and machine learning-based methods for guiding the design of electrode architectures, plentiful, robust, and high-quality data are needed to be openly available. Open-source data is not only needed for training and validating methods, but also for facilitating comparisons between techniques developed by different researchers as well as replication efforts. The availability of data is expected to greatly determine the pace of development of stochastic and machine learning techniques.

2. Electrochemical modeling. The electrochemical simulation of battery materials involves models for solid diffusion, electrochemical reaction, electrolyte transport, electronic conduction, chemo-mechanical coupling, and thermodynamic models of phase separation if needed, as elaborated in the main text. Over the course of fundamental studies of lithium intercalation materials, various models of porous electrodes have been proposed, starting from the earliest Newman model, which uses Nernst-Planck equation and Ohmic laws for describing the electrolyte transport and electronic conduction, respectively, and models the electrochemical reaction using Butler-Volmer kinetics. Subsequent theories refined the descriptions for phase separating materials and reaction kinetics, including phase-field models and electro-autocatalytic and Marcus-Hush-Chidsey models for electrochemical reactions, which impact the model prediction significantly but are currently not studied carefully in the context of microstructure-resolved simulations. Therefore, an appropriate model selection that matches the specific material chemistry, microstructure, level of homogenization, and physical regime of interest is essential for accurate and efficient simulations. We also envision refining electrochemical models further through inverse learning from imaging and spectroscopic data of single particles or a population of particles in a microstructure [268-270], which may yield quantitative reaction, diffusion, and thermodynamic models as well as the statistical distribution of their inhomogeneity, which are critical in the development of microstructure-resolved simulations that can faithfully reproduce experimental realities. In summary, there are plenty of opportunities to advance electrochemical modeling with the latest theoretical development, data-driven methods, and microstructural datasets.

3. Machine learning and deep learning-driven design. Computational design of Li-ion battery materials is challenging due to the complexity brought by the processing conditions, heterogeneous microstructural characteristics, material chemistry, electrochemical and mechanical properties, etc. Furthermore, how to make sense of big data collected from various information sources (experiments, simulations, open-source databases) and transfer the knowledge to a specific design problem is another challenging question. Machine learning and deep learning methods will (i) extract critical features from microstructure image data, (ii) establish the relationship of process-microstructure-property for forward prediction and inverse

design, and (iii) distill/transfer knowledge from various data sources to support the design of a specific material system. Although this review only focuses on the design of stochastic microstructures, we envision the establishment of Material Genome approaches [271-275] that consider features across multiple length scales to broaden the spectrum of achievable electrochemical and mechanical properties.

Acknowledgements

H.X. acknowledges the start-up funding by the department of mechanical engineering, University of Connecticut. J.Z. and W.L. thank the financial support from the MIT Industrial Battery Consortium, the USAID (SHERA) project, and the MIT-Indonesia Seed Fund. This work was authored in part by the National Renewable Energy Laboratory, operated by Alliance for Sustainable Energy, LLC, for the U.S. Department of Energy (DOE) under Contract No. DE-AC36-08GO28308. Funding was provided by the U.S. DOE Office of Vehicle Technology Extreme Fast Charge Program, program manager Samuel Gillard. The views expressed in the article do not necessarily represent the views of the DOE or the U.S. Government. The U.S. Government retains and the publisher, by accepting the article for publication, acknowledges that the U.S. Government retains a nonexclusive, paid-up, irrevocable, worldwide license to publish or reproduce the published form of this work, or allow others to do so, for U.S. Government purposes. M.Z.B. and H.Z. acknowledge support from the Toyota Research Institute through the D3BATT center for Data-Driven Design of Rechargeable Batteries. A.B. acknowledges support from the University of Pisa through the funding program "Progetti di Ricerca di Ateneo PRA 2020-2021", project no. PRA_2020_48. PRS and XL acknowledge funding from The Faraday Institution (EP/S003053/1, FIRG001 and FIRG003). PRS acknowledges funding from The EPSRC (EP/R020973/1 and EP/R023581/1) and The Royal Academy of Engineering (CiET1718/59). XL acknowledges support from the National Measurement System of the UK Department of Business, Energy and Industrial Strategy.

References

[1] P.R. Shearing, L.E. Howard, P.S. Jørgensen, N.P. Brandon, S.J. Harris, Characterization of the 3-dimensional microstructure of a graphite negative electrode from a Li-ion battery, Electrochemistry Communications, 2010, pp. 374-377.
[2] T. Otagawa, A.N. Jina, M.J. Madou, Three-dimensional microstructure as a substrate for a battery electrode, Google Patents, 1994.
[3] D.E. Stephenson, B.C. Walker, C.B. Skelton, E.P. Gorzkowski, D.J. Rowenhorst, D.R. Wheeler, Modeling 3D Microstructure and Ion Transport in Porous Li-Ion Battery Electrodes, Journal of The Electrochemical Society 158(7) (2011) A781.
[4] G. Crabtree, J. Sarrao, Opportunities for mesoscale science, MRS bulletin 37(11) (2012) 1079.
[5] J. Allison, D. Backman, L. Christodoulou, Integrated computational materials engineering: a new paradigm for the global materials profession, Jom 58(11) (2006) 25-27.
[6] J. Allison, Integrated computational materials engineering: A perspective on progress and future steps, Jom 63(4) (2011) 15.
[7] X. Lu, A. Bertei, D.P. Finegan, C. Tan, S.R. Daemi, J.S. Weaving, K.B. O'Regan, T.M.M. Heenan, G. Hinds, E. Kendrick, D.J.L. Brett, P.R. Shearing, 3D microstructure design of lithium-ion battery electrodes assisted by X-ray nano-computed tomography and modelling, Nature Communications 11(1) (2020).
[8] M. Ebner, D.W. Chung, R.E. García, V. Wood, Tortuosity anisotropy in lithium‐ion battery electrodes, Advanced Energy Materials 4(5) (2014) 1301278.
[9] Z. Deng, X. Lin, Z. Huang, J. Meng, Y. Zhong, G. Ma, Y. Zhou, Y. Shen, H. Ding, Y. Huang, Recent Progress on Advanced Imaging Techniques for Lithium-Ion Batteries, n/a(n/a) 2000806.

[10] O.O. Taiwo, J.M. Paz-García, S.A. Hall, T.M. Heenan, D.P. Finegan, R. Mokso, P. Villanueva-Pérez, A. Patera, D.J. Brett, P.R. Shearing, Microstructural degradation of silicon electrodes during lithiation observed via operando X-ray tomographic imaging, Journal of Power Sources 342 (2017) 904-912.
[11] M. Ebner, F. Geldmacher, F. Marone, M. Stampanoni, V. Wood, X-Ray Tomography of Porous, Transition Metal Oxide Based Lithium Ion Battery Electrodes, Advanced Energy Materials 3(7) (2013) 845-850.
[12] P. Pietsch, D. Westhoff, J. Feinauer, J. Eller, F. Marone, M. Stampanoni, V. Schmidt, V. Wood, Quantifying microstructural dynamics and electrochemical activity of graphite and silicon-graphite lithium ion battery anodes, Nature communications 7(1) (2016) 1-11.
[13] J. Paz-Garcia, O. Taiwo, E. Tudisco, D. Finegan, P. Shearing, D. Brett, S. Hall, 4D analysis of the microstructural evolution of Si-based electrodes during lithiation: Time-lapse X-ray imaging and digital volume correlation, Journal of Power Sources 320 (2016) 196-203.
[14] S. Daemi, X. Lu, D. Sykes, J. Behnsen, C. Tan, A. Palacios-Padros, J. Cookson, E. Petrucco, P. Withers, D. Brett, 4D visualisation of in situ nano-compression of Li-ion cathode materials to mimic early stage calendering, Materials Horizons 6(3) (2019) 612-617.
[15] T.M. Heenan, C. Tan, J. Hack, D.J. Brett, P.R. Shearing, Developments in X-ray tomography characterization for electrochemical devices, Materials Today 31 (2019) 69-85.
[16] V. Wood, X-ray tomography for battery research and development, Nature Reviews Materials 3(9) (2018) 293-295.
[17] C. Cao, M.F. Toney, T.-K. Sham, R. Harder, P.R. Shearing, X. Xiao, J. Wang, Emerging X-ray imaging technologies for energy materials, Materials Today (2019).
[18] S.R. Daemi, C. Tan, T. Volkenandt, S.J. Cooper, A. Palacios-Padros, J. Cookson, D.J. Brett, P.R. Shearing, Visualizing the carbon binder phase of battery electrodes in three dimensions, ACS Applied Energy Materials 1(8) (2018) 3702-3710.
[19] T. Hutzenlaub, S. Thiele, N. Paust, R. Spotnitz, R. Zengerle, C. Walchshofer, Three-dimensional electrochemical Li-ion battery modelling featuring a focused ion-beam/scanning electron microscopy based three-phase reconstruction of a LiCoO2 cathode, Electrochimica Acta 115 (2014) 131-139.
[20] J.R. Wilson, J.S. Cronin, S.A. Barnett, S.J. Harris, Measurement of three-dimensional microstructure in a LiCoO2 positive electrode, Journal of Power Sources 196(7) (2011) 3443-3447.
[21] O. Furat, D.P. Finegan, D. Diercks, F. Usseglio-Viretta, K. Smith, V. Schmidt, Mapping the architecture of single lithium ion electrode particles in 3D, using electron backscatter diffraction and machine learning segmentation, Journal of Power Sources 483 (2021) 229148.
[22] F. Lin, Y. Liu, X. Yu, L. Cheng, A. Singer, O.G. Shpyrko, H.L. Xin, N. Tamura, C. Tian, T.-C. Weng, X.-Q. Yang, Y.S. Meng, D. Nordlund, W. Yang, M.M. Doeff, Synchrotron X-ray Analytical Techniques for Studying Materials Electrochemistry in Rechargeable Batteries, Chemical Reviews 117(21) (2017) 13123-13186.
[23] T.M. Heenan, A.V. Llewellyn, A.S. Leach, M.D. Kok, C. Tan, R. Jervis, D.J. Brett, P.R. Shearing, Resolving Li‐Ion Battery Electrode Particles Using Rapid Lab‐Based X‐Ray Nano‐Computed Tomography for High‐Throughput Quantification, Advanced Science (2020) 2000362.
[24] T.M. Heenan, A. Wade, C. Tan, J.E. Parker, D. Matras, A.S. Leach, J.B. Robinson, A. Llewellyn, A. Dimitrijevic, R. Jervis, Identifying the Origins of Microstructural Defects Such as Cracking within Ni‐Rich NMC811 Cathode Particles for Lithium‐Ion Batteries, Advanced Energy Materials (2020) 2002655.
[25] S.K. Babu, A.I. Mohamed, J.F. Whitacre, S. Litster, Multiple imaging mode X-ray computed tomography for distinguishing active and inactive phases in lithium-ion battery cathodes, Journal of Power Sources 283 (2015) 314-319.
[26] M.D. Kok, J.B. Robinson, J.S. Weaving, A. Jnawali, M. Pham, F. Iacoviello, D.J. Brett, P.R. Shearing, Virtual unrolling of spirally-wound lithium-ion cells for correlative degradation studies and predictive fault detection, Sustainable Energy & Fuels 3(11) (2019) 2972-2976.

[27] J. Gelb, D.P. Finegan, D.J. Brett, P.R. Shearing, Multi-scale 3D investigations of a commercial 18650 Li-ion battery with correlative electron-and X-ray microscopy, Journal of Power Sources 357 (2017) 77-86.
[28] P. Pietsch, V. Wood, X-ray tomography for lithium ion battery research: A practical guide, Annual Review of Materials Research 47 (2017) 451-479.
[29] P. Shearing, N. Brandon, J. Gelb, R. Bradley, P. Withers, A. Marquis, S. Cooper, S. Harris, Multi length scale microstructural investigations of a commercially available Li-ion battery electrode, Journal of The Electrochemical Society 159(7) (2012) A1023.
[30] D.S. Eastwood, V. Yufit, J. Gelb, A. Gu, R.S. Bradley, S.J. Harris, D.J. Brett, N.P. Brandon, P.D. Lee, P.J. Withers, Lithiation‐Induced Dilation Mapping in a Lithium‐Ion Battery Electrode by 3D X‐Ray Microscopy and Digital Volume Correlation, Advanced Energy Materials 4(4) (2014) 1300506.
[31] C. Tan, S.R. Daemi, O.O. Taiwo, T.M. Heenan, D.J. Brett, P.R. Shearing, Evolution of electrochemical cell designs for in-situ and operando 3D characterization, Materials 11(11) (2018) 2157.
[32] F. Tariq, V. Yufit, M. Kishimoto, P. Shearing, S. Menkin, D. Golodnitsky, J. Gelb, E. Peled, N. Brandon, Three-dimensional high resolution X-ray imaging and quantification of lithium ion battery mesocarbon microbead anodes, Journal of Power Sources 248 (2014) 1014-1020.
[33] S.L. Morelly, J. Gelb, F. Iacoviello, P.R. Shearing, S.J. Harris, N.J. Alvarez, M.H. Tang, Three-dimensional visualization of conductive domains in battery electrodes with contrast-enhancing nanoparticles, ACS Applied Energy Materials 1(9) (2018) 4479-4484.
[34] C. Rahe, S.T. Kelly, M.N. Rad, D.U. Sauer, J. Mayer, E. Figgemeier, Nanoscale X-ray imaging of ageing in automotive lithium ion battery cells, Journal of Power Sources 433 (2019) 126631.
[35] R. Carter, B. Huhman, C.T. Love, I.V. Zenyuk, X-ray computed tomography comparison of individual and parallel assembled commercial lithium iron phosphate batteries at end of life after high rate cycling, Journal of Power Sources 381 (2018) 46-55.
[36] S. Frisco, A. Kumar, J.F. Whitacre, S. Litster, Understanding Li-ion battery anode degradation and pore morphological changes through nano-resolution X-ray computed tomography, Journal of The Electrochemical Society 163(13) (2016) A2636.
[37] A. Quinn, H. Moutinho, F. Usseglio-Viretta, A. Verma, K. Smith, M. Keyser, D.P. Finegan, Electron Backscatter Diffraction for Investigating Lithium-Ion Electrode Particle Architectures, Cell Reports Physical Science 1(8) (2020) 100137.
[38] L. Pillatsch, F. Östlund, J. Michler, FIBSIMS: A review of secondary ion mass spectrometry for analytical dual beam focussed ion beam instruments, Progress in Crystal Growth and Characterization of Materials 65(1) (2019) 1-19.
[39] S. Bessette, A. Paolella, C. Kim, W. Zhu, P. Hovington, R. Gauvin, K. Zaghib, Nanoscale Lithium Quantification in LiXNiyCowMnZO2 as Cathode for Rechargeable Batteries, Scientific Reports 8(1) (2018) 17575.
[40] T. Sui, B. Song, J. Dluhos, L. Lu, A.M. Korsunsky, Nanoscale chemical mapping of Li-ion battery cathode material by FIB-SEM and TOF-SIMS multi-modal microscopy, Nano Energy 17 (2015) 254-260.
[41] P. Niehoff, S. Passerini, M. Winter, Interface Investigations of a Commercial Lithium Ion Battery Graphite Anode Material by Sputter Depth Profile X-ray Photoelectron Spectroscopy, Langmuir 29(19) (2013) 5806-5816.
[42] E. Björklund, D. Brandell, M. Hahlin, K. Edström, R. Younesi, How the Negative Electrode Influences Interfacial and Electrochemical Properties of LiNi1/3Co1/3Mn1/3O2Cathodes in Li-Ion Batteries, Journal of The Electrochemical Society 164(13) (2017) A3054-A3059.
[43] C. Stetson, T. Yoon, J. Coyle, W. Nemeth, M. Young, A. Norman, S. Pylypenko, C. Ban, C.-S. Jiang, M. Al-Jassim, A. Burrell, Three-dimensional electronic resistivity mapping of solid electrolyte interphase on Si anode materials, Nano Energy 55 (2019) 477-485.

[44] C. Stetson, Z. Huey, A. Downard, Z. Li, B. To, A. Zakutayev, C.-S. Jiang, M.M. Al-Jassim, D.P. Finegan, S.-D. Han, Three-Dimensional Mapping of Resistivity and Microstructure of Composite Electrodes for Lithium-Ion Batteries, Nano Letters (2020).
[45] C. Tan, T.M. Heenan, R.F. Ziesche, S.R. Daemi, J. Hack, M. Maier, S. Marathe, C. Rau, D.J. Brett, P.R. Shearing, Four-dimensional studies of morphology evolution in lithium–sulfur batteries, ACS Applied Energy Materials 1(9) (2018) 5090-5100.
[46] L. Zielke, C. Barchasz, S. Waluś, F. Alloin, J.-C. Leprêtre, A. Spettl, V. Schmidt, A. Hilger, I. Manke, J. Banhart, Degradation of Li/S battery electrodes on 3D current collectors studied using X-ray phase contrast tomography, Scientific reports 5 (2015) 10921.
[47] J.N. Weker, N. Liu, S. Misra, J. Andrews, Y. Cui, M. Toney, In situ nanotomography and operando transmission X-ray microscopy of micron-sized Ge particles, Energy & Environmental Science 7(8) (2014) 2771-2777.
[48] L. Zielke, T. Hutzenlaub, D.R. Wheeler, I. Manke, T. Arlt, N. Paust, R. Zengerle, S. Thiele, A Combination of X‐Ray Tomography and Carbon Binder Modeling: Reconstructing the Three Phases of LiCoO2 Li‐Ion Battery Cathodes, Advanced Energy Materials 4(8) (2014) 1301617.
[49] S. Cooper, D. Eastwood, J. Gelb, G. Damblanc, D. Brett, R. Bradley, P. Withers, P. Lee, A. Marquis, N. Brandon, Image based modelling of microstructural heterogeneity in LiFePO4 electrodes for Li-ion batteries, Journal of Power Sources 247 (2014) 1033-1039.
[50] A.G. Kashkooli, S. Farhad, D.U. Lee, K. Feng, S. Litster, S.K. Babu, L. Zhu, Z. Chen, Multiscale modeling of lithium-ion battery electrodes based on nano-scale X-ray computed tomography, Journal of Power Sources 307 (2016) 496-509.
[51] D. Eastwood, R. Bradley, F. Tariq, S. Cooper, O. Taiwo, J. Gelb, A. Merkle, D. Brett, N. Brandon, P. Withers, The application of phase contrast X-ray techniques for imaging Li-ion battery electrodes, Nuclear Instruments and Methods in Physics Research Section B: Beam Interactions with Materials and Atoms 324 (2014) 118-123.
[52] D.S. Eastwood, P.M. Bayley, H.J. Chang, O.O. Taiwo, J. Vila-Comamala, D.J. Brett, C. Rau, P.J. Withers, P.R. Shearing, C.P. Grey, Three-dimensional characterization of electrodeposited lithium microstructures using synchrotron X-ray phase contrast imaging, Chemical communications 51(2) (2015) 266-268.
[53] A. Pattammattel, R. Tappero, M. Ge, Y.S. Chu, X. Huang, Y. Gao, H. Yan, High-sensitivity nanoscale chemical imaging with hard x-ray nano-XANES, Science Advances 6(37) (2020) eabb3615.
[54] D.P. Finegan, A. Vamvakeros, C. Tan, T.M.M. Heenan, S.R. Daemi, N. Seitzman, M. Di Michiel, S. Jacques, A.M. Beale, D.J.L. Brett, P.R. Shearing, K. Smith, Spatial quantification of dynamic inter and intra particle crystallographic heterogeneities within lithium ion electrodes, Nature Communications 11(1) (2020) 631.
[55] D.P. Finegan, A. Vamvakeros, L. Cao, C. Tan, T.M.M. Heenan, S.R. Daemi, S.D.M. Jacques, A.M. Beale, M. Di Michiel, K. Smith, D.J.L. Brett, P.R. Shearing, C. Ban, Spatially Resolving Lithiation in Silicon–Graphite Composite Electrodes via in Situ High-Energy X-ray Diffraction Computed Tomography, Nano Letters 19(6) (2019) 3811-3820.
[56] C. Tian, Y. Xu, D. Nordlund, F. Lin, J. Liu, Z. Sun, Y. Liu, M. Doeff, Charge Heterogeneity and Surface Chemistry in Polycrystalline Cathode Materials, Joule 2(3) (2018) 464-477.
[57] S. Li, Z. Jiang, J. Han, Z. Xu, C. Wang, H. Huang, C. Yu, S.-J. Lee, P. Pianetta, H. Ohldag, J. Qiu, J.-S. Lee, F. Lin, K. Zhao, Y. Liu, Mutual modulation between surface chemistry and bulk microstructure within secondary particles of nickel-rich layered oxides, Nature Communications 11(1) (2020) 4433.
[58] K.E. Thomas-Alyea, C. Jung, R.B. Smith, M.Z. Bazant, In Situ Observation and Mathematical Modeling of Lithium Distribution within Graphite, Journal of The Electrochemical Society 164(11) (2017) E3063-E3072.

[59] R.B. Smith, E. Khoo, M.Z. Bazant, Intercalation Kinetics in Multiphase-Layered Materials, The Journal of Physical Chemistry C 121(23) (2017) 12505-12523.
[60] R.B. Smith, M.Z. Bazant, Multiphase Porous Electrode Theory, Journal of The Electrochemical Society 164(11) (2017) E3291-E3310.
[61] M.Z. Bazant, Theory of chemical kinetics and charge transfer based on nonequilibrium thermodynamics, Accounts of chemical research 46(5) (2013) 1144-1160.
[62] Y.-S. Yu, M. Farmand, C. Kim, Y. Liu, C.P. Grey, F.C. Strobridge, T. Tyliszczak, R. Celestre, P. Denes, J. Joseph, H. Krishnan, F.R.N.C. Maia, A.L.D. Kilcoyne, S. Marchesini, T.P.C. Leite, T. Warwick, H. Padmore, J. Cabana, D.A. Shapiro, Three-dimensional localization of nanoscale battery reactions using soft X-ray tomography, Nature Communications 9(1) (2018) 921.
[63] A. Ulvestad, A. Singer, H.-M. Cho, J.N. Clark, R. Harder, J. Maser, Y.S. Meng, O.G. Shpyrko, Single Particle Nanomechanics in Operando Batteries via Lensless Strain Mapping, Nano Letters 14(9) (2014) 5123-5127.
[64] A. Ulvestad, H.M. Cho, R. Harder, J.W. Kim, S.H. Dietze, E. Fohtung, Y.S. Meng, O.G. Shpyrko, Nanoscale strain mapping in battery nanostructures, Applied Physics Letters 104(7) (2014) 073108.
[65] A. Singer, A. Ulvestad, H.-M. Cho, J.W. Kim, J. Maser, R. Harder, Y.S. Meng, O.G. Shpyrko, Nonequilibrium Structural Dynamics of Nanoparticles in LiNi1/2Mn3/2O4 Cathode under Operando Conditions, Nano Letters 14(9) (2014) 5295-5300.
[66] E.H.R. Tsai, J. Billaud, D.F. Sanchez, J. Ihli, M. Odstrčil, M. Holler, D. Grolimund, C. Villevieille, M. Guizar-Sicairos, Correlated X-Ray 3D Ptychography and Diffraction Microscopy Visualize Links between Morphology and Crystal Structure of Lithium-Rich Cathode Materials, iScience 11 (2019) 356-365.
[67] A. Ulvestad, A. Singer, J.N. Clark, H.M. Cho, J.W. Kim, R. Harder, J. Maser, Y.S. Meng, O.G. Shpyrko, Topological defect dynamics in operando battery nanoparticles, Science 348(6241) (2015) 1344.
[68] A.K.C. Estandarte, J. Diao, A.V. Llewellyn, A. Jnawali, T.M.M. Heenan, S.R. Daemi, J.J. Bailey, S. Cipiccia, D. Batey, X. Shi, C. Rau, D.J.L. Brett, R. Jervis, I.K. Robinson, P.R. Shearing, Operando Bragg Coherent Diffraction Imaging of LiNi0.8Mn0.1Co0.1O2 Primary Particles within Commercially Printed NMC811 Electrode Sheets ACS Nano (In press).
[69] S. Müller, M. Lippuner, M. Verezhak, V. De Andrade, F. De Carlo, V. Wood, Multimodal Nanoscale Tomographic Imaging for Battery Electrodes, Advanced Energy Materials 10(28) (2020) 1904119.
[70] D.P. Finegan, A. Quinn, D.S. Wragg, A.M. Colclasure, X. Lu, C. Tan, T.M.M. Heenan, R. Jervis, D.J.L. Brett, S. Das, T. Gao, D.A. Cogswell, M.Z. Bazant, M. Di Michiel, S. Checchia, P.R. Shearing, K. Smith, Spatial dynamics of lithiation and lithium plating during high-rate operation of graphite electrodes, Energy & Environmental Science (2020).
[71] K.P.C. Yao, J.S. Okasinski, K. Kalaga, I.A. Shkrob, D.P. Abraham, Quantifying lithium concentration gradients in the graphite electrode of Li-ion cells using operando energy dispersive X-ray diffraction, Energy & Environmental Science 12(2) (2019) 656-665.
[72] H. Xu, C. Bae, Stochastic 3D microstructure reconstruction and mechanical modeling of anisotropic battery separators, Journal of Power Sources 430 (2019) 67-73.
[73] H. Xu, F. Usseglio-Viretta, S. Kench, S.J. Cooper, D.P. Finegan, Microstructure reconstruction of battery polymer separators by fusing 2D and 3D image data for transport property analysis, Journal of Power Sources 480 (2020) 229101.
[74] H. Xu, R. Liu, A. Choudhary, W. Chen, A machine learning-based design representation method for designing heterogeneous microstructures, Journal of Mechanical Design 137(5) (2015) 051403.
[75] Y. Liu, M.S. Greene, W. Chen, D.A. Dikin, W.K. Liu, Computational microstructure characterization and reconstruction for stochastic multiscale material design, Computer-Aided Design 45(1) (2013) 65-76.
[76] Battery Microstructures Library, https://www.nrel.gov/transportation/microstructure.html, National Renewable Energy Laboratory.
[77] C. Yeong, S. Torquato, Reconstructing random media, Physical Review E 57(1) (1998) 495.

[78] C. Yeong, S. Torquato, Reconstructing random media. II. Three-dimensional media from two-dimensional cuts, Physical Review E 58(1) (1998) 224.
[79] Y. Jiao, F. Stillinger, S. Torquato, Modeling heterogeneous materials via two-point correlation functions: Basic principles, Physical Review E 76(3) (2007) 031110.
[80] H. Xu, Y. Li, C. Brinson, W. Chen, A Descriptor-Based Design Methodology for Developing Heterogeneous Microstructural Materials System, Journal of Mechanical Design 136(5) (2014) 051007.
[81] Y. Jiao, F. Stillinger, S. Torquato, A superior descriptor of random textures and its predictive capacity, Proceedings of the National Academy of Sciences 106(42) (2009) 17634-17639.
[82] S. Torquato, Optimal design of heterogeneous materials, Annual review of materials research 40 (2010) 101-129.
[83] J.G. Berryman, Measurement of spatial correlation functions using image processing techniques, Journal of Applied Physics 57(7) (1985) 2374-2384.
[84] F. Liu, N.A. Siddique, Microstructure Reconstruction and Direct Evaluation of Li-Ion Battery Cathodes, ECS Transactions 33(24) (2011) 25-32.
[85] N. Siddique, A. Salehi, F. Liu, Stochastic reconstruction and electrical transport studies of porous cathode of Li-ion batteries, Journal of Power Sources 217 (2012) 437-443.
[86] M. Ebner, F. Marone, M. Stampanoni, V. Wood, Visualization and Quantification of Electrochemical and Mechanical Degradation in Li Ion Batteries, Science 342(6159) (2013) 716-720.
[87] M. Ender, J. Joos, A. Weber, E. Ivers-Tiffée, Anode microstructures from high-energy and high-power lithium-ion cylindrical cells obtained by X-ray nano-tomography, Journal of Power Sources 269 (2014) 912-919.
[88] M. Kespe, H. Nirschl, Numerical simulation of lithium‐ion battery performance considering electrode microstructure, International Journal of Energy Research 39(15) (2015) 2062-2074.
[89] Z. Liu, Y.C. Chen-Wiegart, J. Wang, S.A. Barnett, K.T. Faber, Three-Phase 3D Reconstruction of a LiCoO2 Cathode via FIB-SEM Tomography, Microscopy and microanalysis : the official journal of Microscopy Society of America, Microbeam Analysis Society, Microscopical Society of Canada 22(1) (2016) 140-8.
[90] O.O. Taiwo, D.P. Finegan, D.S. Eastwood, J.L. Fife, L.D. Brown, J.A. Darr, P.D. Lee, D.J.L. Brett, P.R. Shearing, Comparison of three-dimensional analysis and stereological techniques for quantifying lithium-ion battery electrode microstructures, Journal of Microscopy 263(3) (2016) 280-292.
[91] L. Wu, X. Xiao, Y. Wen, J. Zhang, Three-dimensional finite element study on stress generation in synchrotron X-ray tomography reconstructed nickel-manganese-cobalt based half cell, Journal of Power Sources 336 (2016) 8-18.
[92] R. Xu, L. Scalco de Vasconcelos, K. Zhao, Computational analysis of chemomechanical behaviors of composite electrodes in Li-ion batteries, Journal of Materials Research 31(18) (2016) 2715-2727.
[93] C.-F. Chen, A. Verma, P.P. Mukherjee, Probing the Role of Electrode Microstructure in the Lithium-Ion Battery Thermal Behavior, Journal of The Electrochemical Society 164(11) (2017) E3146-E3158.
[94] O.O. Taiwo, M. Loveridge, S.D. Beattie, D.P. Finegan, R. Bhagat, D.J.L. Brett, P.R. Shearing, Investigation of cycling-induced microstructural degradation in silicon-based electrodes in lithium-ion batteries using X-ray nanotomography, Electrochimica Acta 253 (2017) 85-92.
[95] S. Choi, M. Jeon, J. Ahn, W.D. Jung, S.M. Choi, J.S. Kim, J. Lim, Y.J. Jang, H.G. Jung, J.H. Lee, B.I. Sang, H. Kim, Quantitative Analysis of Microstructures and Reaction Interfaces on Composite Cathodes in All-Solid-State Batteries Using a Three-Dimensional Reconstruction Technique, ACS applied materials & interfaces 10(28) (2018) 23740-23747.
[96] Z.Y. Jiang, Z.G. Qu, L. Zhou, Lattice Boltzmann simulation of ion and electron transport during the discharge process in a randomly reconstructed porous electrode of a lithium-ion battery, International Journal of Heat and Mass Transfer 123 (2018) 500-513.

[97] T. Li, H. Kang, X. Zhou, C. Lim, B. Yan, V. De Andrade, F. De Carlo, L. Zhu, Three-Dimensional Reconstruction and Analysis of All-Solid Li-Ion Battery Electrode Using Synchrotron Transmission X-ray Microscopy Tomography, ACS applied materials & interfaces 10(20) (2018) 16927-16931.
[98] W. Mai, M. Yang, S. Soghrati, A particle-resolved 3D finite element model to study the effect of cathode microstructure on the behavior of lithium ion batteries, Electrochimica Acta 294 (2019) 192-209.
[99] M. Yang, A. Nagarajan, B. Liang, S. Soghrati, New algorithms for virtual reconstruction of heterogeneous microstructures, Computer Methods in Applied Mechanics and Engineering 338 (2018) 275-298.
[100] A.N. Mistry, K. Smith, P.P. Mukherjee, Secondary-Phase Stochastics in Lithium-Ion Battery Electrodes, ACS applied materials & interfaces 10(7) (2018) 6317-6326.
[101] R. Xu, Y. Yang, F. Yin, P. Liu, P. Cloetens, Y. Liu, F. Lin, K. Zhao, Heterogeneous damage in Li-ion batteries: Experimental analysis and theoretical modeling, Journal of the Mechanics and Physics of Solids 129 (2019) 160-183.
[102] J. Park, K.T. Kim, D.Y. Oh, D. Jin, D. Kim, Y.S. Jung, Y.M. Lee, Digital Twin-Driven All-Solid-State Battery: Unraveling the Physical and Electrochemical Behaviors, Advanced Energy Materials 10(35) (2020).
[103] B. Yan, C. Lim, L. Yin, L. Zhu, Three Dimensional Simulation of Galvanostatic Discharge of LiCoO2Cathode Based on X-ray Nano-CT Images, Journal of The Electrochemical Society 159(10) (2012) A1604-A1614.
[104] S.G. Lee, D.H. Jeon, Effect of electrode compression on the wettability of lithium-ion batteries, Journal of Power Sources 265 (2014) 363-369.
[105] M. Ebner, D.-W. Chung, R.E. García, V. Wood, Tortuosity Anisotropy in Lithium-Ion Battery Electrodes, Advanced Energy Materials 4(5) (2014).
[106] L. Cheolwoong, Y. Bo, Y. Leilei, Z. Likun, Geometric Characteristics of Three Dimensional Reconstructed Anode Electrodes of Lithium Ion Batteries, Energies, 2014, pp. 2558-2572.
[107] J. Bao, W. Xu, P. Bhattacharya, M. Stewart, J.-G. Zhang, W. Pan, Discharge Performance of Li–O2 Batteries Using a Multiscale Modeling Approach, The Journal of Physical Chemistry C 119(27) (2015) 14851-14860.
[108] B. Yan, C. Lim, Z. Song, L. Zhu, Analysis of Polarization in Realistic Li Ion Battery Electrode Microstructure Using Numerical Simulation, Electrochimica acta. 185 (2015) 125-141.
[109] S. He, J. Zeng, B.T. Habte, F. Jiang, Numerical reconstruction of microstructure of graphite anode of lithium-ion battery, Science Bulletin 61(8) (2016) 656-664.
[110] S. He, B.T. Habte, F. Jiang, LBM prediction of effective electric and species transport properties of lithium-ion battery graphite anode, Solid State Ionics 296 (2016) 146-153.
[111] B.T. Habte, F. Jiang, Microstructure reconstruction and impedance spectroscopy study of LiCoO2, LiMn2O4 and LiFePO4 Li-ion battery cathodes, Microporous and Mesoporous Materials 268 (2018) 69-76.
[112] B.T. Habte, F. Jiang, Effect of microstructure morphology on Li-ion battery graphite anode performance: Electrochemical impedance spectroscopy modeling and analysis, Solid State Ionics 314 (2018) 81-91.
[113] S.A. Roberts, H. Mendoza, V.E. Brunini, B.L. Trembacki, D.R. Noble, A.M. Grillet, Insights Into Lithium-Ion Battery Degradation and Safety Mechanisms From Mesoscale Simulations Using Experimentally Reconstructed Mesostructures, J. Electrochem. En. Conv. Stor 13(3) (2016).
[114] Y. Zhang, M. Yan, Y. Wan, Z. Jiao, Y. Chen, F. Chen, C. Xia, M. Ni, High-throughput 3D reconstruction of stochastic heterogeneous microstructures in energy storage materials, npj Computational Materials 5(1) (2019) 1-8.

[115] W. Wu, F. Jiang, Simulated annealing reconstruction and characterization of the three-dimensional microstructure of a LiCoO2 lithium-ion battery cathode, Materials characterization 80 (2013) 62-68.
[116] H. Liu, J.M. Foster, A. Gully, S. Krachkovskiy, M. Jiang, Y. Wu, X. Yang, B. Protas, G.R. Goward, G.A. Botton, Three-dimensional investigation of cycling-induced microstructural changes in lithium-ion battery cathodes using focused ion beam/scanning electron microscopy, Journal of Power Sources 306 (2016) 300-308.
[117] V. Thangavel, O.X. Guerrero, M. Quiroga, A.M. Mikala, A. Rucci, A.A. Franco, A three dimensional kinetic Monte Carlo model for simulating the carbon/sulfur mesostructural evolutions of discharging lithium sulfur batteries, Energy Storage Materials 24 (2020) 472-485.
[118] B. Yan, C. Lim, L. Yin, L. Zhu, Simulation of heat generation in a reconstructed LiCoO2 cathode during galvanostatic discharge, Electrochimica Acta 100 (2013) 171-179.
[119] D.-W. Chung, P.R. Shearing, N.P. Brandon, S.J. Harris, R.E. Garcia, Particle size polydispersity in Li-ion batteries, Journal of The Electrochemical Society 161(3) (2014) A422.
[120] S. Cho, C.-F. Chen, P.P. Mukherjee, Influence of Microstructure on Impedance Response in Intercalation Electrodes, Journal of The Electrochemical Society 162(7) (2015) A1202-A1214.
[121] S. Hein, J. Feinauer, D. Westhoff, I. Manke, V. Schmidt, A. Latz, Stochastic microstructure modeling and electrochemical simulation of lithium-ion cell anodes in 3D, Journal of Power Sources 336 (2016) 161-171.
[122] Z. Jiang, J. Li, Y. Yang, L. Mu, C. Wei, X. Yu, P. Pianetta, K. Zhao, P. Cloetens, F. Lin, Y. Liu, Machine-learning-revealed statistics of the particle-carbon/binder detachment in lithium-ion battery cathodes, Nature Communications 11(1) (2020).
[123] M.E. Lynch, D. Ding, W.M. Harris, J.J. Lombardo, G.J. Nelson, W.K.S. Chiu, M. Liu, Flexible multiphysics simulation of porous electrodes: Conformal to 3D reconstructed microstructures, Nano Energy 2(1) (2013) 105-115.
[124] C.A. Milroy, S. Jang, T. Fujimori, A. Dodabalapur, A. Manthiram, Inkjet‐Printed Lithium‐Sulfur Microcathodes for All‐Printed, Integrated Nanomanufacturing, Small 13(11) (2017) 1603786.
[125] C. Huang, M. Dontigny, K. Zaghib, P.S. Grant, Low-tortuosity and graded lithium ion battery cathodes by ice templating, Journal of Materials Chemistry A 7(37) (2019) 21421-21431.
[126] B. Song, T. Sui, S. Ying, L. Li, L. Lu, A.M. Korsunsky, Nano-structural changes in Li-ion battery cathodes during cycling revealed by FIB-SEM serial sectioning tomography, Journal of Materials Chemistry A 3(35) (2015) 18171-18179.
[127] C. Chatfield, H. Xing, The analysis of time series: an introduction with R, CRC press2019.
[128] N. Berk, Scattering properties of a model bicontinuous structure with a well defined length scale, Physical review letters 58(25) (1987) 2718.
[129] A. Iyer, R. Dulal, Y. Zhang, U.F. Ghumman, T. Chien, G. Balasubramanian, W. Chen, Designing anisotropic microstructures with spectral density function, Computational Materials Science 179 (2020) 109559.
[130] L. Tan, J. Jiang, Digital signal processing: fundamentals and applications, Academic Press2018.
[131] S. Yu, C. Wang, Y. Zhang, B. Dong, Z. Jiang, X. Chen, W. Chen, C. Sun, Design of non-deterministic quasi-random nanophotonic structures using Fourier space representations, Scientific reports 7(1) (2017) 1-10.
[132] R. Cang, H. Li, H. Yao, Y. Jiao, Y. Ren, Improving direct physical properties prediction of heterogeneous materials from imaging data via convolutional neural network and a morphology-aware generative model, Computational Materials Science 150 (2018) 212-221.
[133] R. Cang, Y. Xu, S. Chen, Y. Liu, Y. Jiao, M. Yi Ren, Microstructure representation and reconstruction of heterogeneous materials via deep belief network for computational material design, Journal of Mechanical Design 139(7) (2017).

[134] E. Levina, P.J. Bickel, Texture synthesis and nonparametric resampling of random fields, The Annals of Statistics 34(4) (2006) 1751-1773.
[135] X. Liu, V. Shapiro, Random heterogeneous materials via texture synthesis, Computational Materials Science 99 (2015) 177-189.
[136] R. Bostanabad, A.T. Bui, W. Xie, D.W. Apley, W. Chen, Stochastic microstructure characterization and reconstruction via supervised learning, Acta Materialia 103 (2016) 89-102.
[137] V. Sundararaghavan, Reconstruction of three-dimensional anisotropic microstructures from two-dimensional micrographs imaged on orthogonal planes, Integrating Materials and Manufacturing Innovation 3(1) (2014) 19.
[138] I. Javaheri, V. Sundararaghavan, Polycrystalline Microstructure Reconstruction Using Markov Random Fields and Histogram Matching, Computer-Aided Design 120 (2020) 102806.
[139] S.J. Pan, Q. Yang, A survey on transfer learning, IEEE Transactions on knowledge and data engineering 22(10) (2009) 1345-1359.
[140] Y. Bengio, Deep learning of representations for unsupervised and transfer learning, Proceedings of ICML workshop on unsupervised and transfer learning, 2012, pp. 17-36.
[141] X. Li, Y. Zhang, H. Zhao, C. Burkhart, L.C. Brinson, W. Chen, A transfer learning approach for microstructure reconstruction and structure-property predictions, Scientific reports 8(1) (2018) 1-13.
[142] R. Bostanabad, Reconstruction of 3d microstructures from 2d images via transfer learning, Computer-Aided Design 128 (2020) 102906.
[143] A. Gayon-Lombardo, L. Mosser, N.P. Brandon, S.J. Cooper, Pores for thought: generative adversarial networks for stochastic reconstruction of 3D multi-phase electrode microstructures with periodic boundaries, npj Computational Materials 6(1) (2020) 1-11.
[144] J. Newman, W. Tiedemann, Porous‐electrode theory with battery applications, AIChE Journal 21(1) (1975) 25-41.
[145] P. Ramadass, B. Haran, P.M. Gomadam, R. White, B.N. Popov, Development of first principles capacity fade model for Li-ion cells, Journal of the Electrochemical Society 151(2) (2004) A196.
[146] X.-G. Yang, Y. Leng, G. Zhang, S. Ge, C.-Y. Wang, Modeling of lithium plating induced aging of lithium-ion batteries: Transition from linear to nonlinear aging, Journal of Power Sources 360 (2017) 28-40.
[147] A. Lamorgese, R. Mauri, B. Tellini, Electrochemical-thermal P2D aging model of a LiCoO2/graphite cell: Capacity fade simulations, Journal of Energy Storage 20 (2018) 289-297.
[148] M. Doyle, T.F. Fuller, J. Newman, Modeling of galvanostatic charge and discharge of the lithium/polymer/insertion cell, Journal of the Electrochemical society 140(6) (1993) 1526.
[149] S.K. Rahimian, S. Rayman, R.E. White, Comparison of single particle and equivalent circuit analog models for a lithium-ion cell, Journal of Power Sources 196(20) (2011) 8450-8462.
[150] S.J. Harris, P. Lu, Effects of Inhomogeneities ・ Nanoscale to Mesoscale ・ on the Durability of Li-Ion Batteries, The Journal of Physical Chemistry C 117(13) (2013) 6481-6492.
[151] Y. Xu, E. Hu, K. Zhang, X. Wang, V. Borzenets, Z. Sun, P. Pianetta, X. Yu, Y. Liu, X.-Q. Yang, In situ visualization of state-of-charge heterogeneity within a LiCoO2 particle that evolves upon cycling at different rates, ACS Energy Letters 2(5) (2017) 1240-1245.
[152] M. Yoshio, H. Wang, K. Fukuda, T. Umeno, T. Abe, Z. Ogumi, Improvement of natural graphite as a lithium-ion battery anode material, from raw flake to carbon-coated sphere, Journal of Materials Chemistry 14(11) (2004) 1754-1758.
[153] M. Smart, B. Ratnakumar, Effects of electrolyte composition on lithium plating in lithium-ion cells, Journal of The Electrochemical Society 158(4) (2011) A379.
[154] Y. Dai, V. Srinivasan, On graded electrode porosity as a design tool for improving the energy density of batteries, Journal of The Electrochemical Society 163(3) (2015) A406.

[155] M.M. Forouzan, B.A. Mazzeo, D.R. Wheeler, Modeling the effects of electrode microstructural heterogeneities on Li-ion battery performance and lifetime, Journal of The Electrochemical Society 165(10) (2018) A2127.
[156] E.M. Ryan, P.P. Mukherjee, Mesoscale modeling in electrochemical devices—a critical perspective, Progress in Energy and Combustion Science 71 (2019) 118-142.
[157] D. Zhang, A. Bertei, F. Tariq, N. Brandon, Q. Cai, Progress in 3D electrode microstructure modelling for fuel cells and batteries: transport and electrochemical performance, Progress in Energy 1(1) (2019) 012003.
[158] S. Cooper, A. Bertei, P. Shearing, J. Kilner, N. Brandon, TauFactor: An open-source application for calculating tortuosity factors from tomographic data, SoftwareX 5 (2016) 203-210.
[159] S. Müller, J. Eller, M. Ebner, C. Burns, J. Dahn, V. Wood, Quantifying inhomogeneity of lithium ion battery electrodes and its influence on electrochemical performance, Journal of The Electrochemical Society 165(2) (2018) A339.
[160] F.L. Usseglio-Viretta, A. Colclasure, A.N. Mistry, K.P.Y. Claver, F. Pouraghajan, D.P. Finegan, T.M. Heenan, D. Abraham, P.P. Mukherjee, D. Wheeler, Resolving the discrepancy in tortuosity factor estimation for Li-ion battery electrodes through micro-macro modeling and experiment, Journal of The Electrochemical Society 165(14) (2018) A3403.
[161] T.-T. Nguyen, A. Demortière, B. Fleutot, B. Delobel, C. Delacourt, S.J. Cooper, The electrode tortuosity factor: why the conventional tortuosity factor is not well suited for quantifying transport in porous Li-ion battery electrodes and what to use instead, npj Computational Materials 6(1) (2020) 1-12.
[162] L. Zielke, T. Hutzenlaub, D.R. Wheeler, C.W. Chao, I. Manke, A. Hilger, N. Paust, R. Zengerle, S. Thiele, Three‐Phase Multiscale Modeling of a LiCoO2 Cathode: Combining the Advantages of FIB‐SEM Imaging and X‐Ray Tomography, Advanced Energy Materials 5(5) (2015) 1401612.
[163] A.G. Kashkooli, E. Foreman, S. Farhad, D.U. Lee, K. Feng, G. Lui, V. De Andrade, Z. Chen, Morphological and electrochemical characterization of nanostructured Li4Ti5O12 electrodes using multiple imaging mode synchrotron X-ray computed tomography, Journal of The Electrochemical Society 164(12) (2017) A2861.
[164] B.L. Trembacki, A.N. Mistry, D.R. Noble, M.E. Ferraro, P.P. Mukherjee, S.A. Roberts, Mesoscale analysis of conductive binder domain morphology in lithium-ion battery electrodes, Journal of The Electrochemical Society 165(13) (2018) E725.
[165] T. Danner, M. Singh, S. Hein, J. Kaiser, H. Hahn, A. Latz, Thick electrodes for Li-ion batteries: A model based analysis, Journal of Power Sources 334 (2016) 191-201.
[166] B.L. Trembacki, D.R. Noble, V.E. Brunini, M.E. Ferraro, S.A. Roberts, Mesoscale effective property simulations incorporating conductive binder, Journal of The Electrochemical Society 164(11) (2017) E3613.
[167] A.C. Ngandjong, A. Rucci, M. Maiza, G. Shukla, J. Vazquez-Arenas, A.A. Franco, Multiscale simulation platform linking lithium ion battery electrode fabrication process with performance at the cell level, The journal of physical chemistry letters 8(23) (2017) 5966-5972.
[168] A.A. Franco, A. Rucci, D. Brandell, C. Frayret, M. Gaberscek, P. Jankowski, P. Johansson, Boosting rechargeable batteries R&D by multiscale modeling: myth or reality?, Chemical reviews 119(7) (2019) 4569-4627.
[169] D.K. Wieser, S. Fell, Micro-Scale Modeling of Li-Ion Batteries: Parameterization, Journal of The Electrochemical Society 159(6) (2012) A697-A704.
[170] M. Chouchane, E.N. Primo, A.A. Franco, Mesoscale Effects in the Extraction of the Solid-State Lithium Diffusion Coefficient Values of Battery Active Materials: Physical Insights from 3D Modeling, The Journal of Physical Chemistry Letters 11(7) (2020) 2775-2780.
[171] J. Feinauer, S. Hein, S. Rave, S. Schmidt, D. Westhoff, J. Zausch, O. Iliev, A. Latz, M. Ohlberger, V. Schmidt, MULTIBAT: Unified workflow for fast electrochemical 3D simulations of lithium-ion cells

combining virtual stochastic microstructures, electrochemical degradation models and model order reduction, Journal of Computational Science 31 (2019) 172-184.
[172] A.K. Padhi, K.S. Nanjundaswamy, J.B. Goodenough, Phospho‐olivines as positive‐electrode materials for rechargeable lithium batteries, Journal of the electrochemical society 144(4) (1997) 1188.
[173] M.S. Dresselhaus, G. Dresselhaus, Intercalation compounds of graphite, Advances in physics 51(1) (2002) 1-186.
[174] B. Horstmann, B.M. Gallant, R.R. Mitchell, A. Latz, W.G. Bessler, Y. Shao-Horn, M. Bazant, Electrochemically-driven transition of crystallization morphologies in Li-O2 batteries, 224th ECS meeting, 2013.
[175] H. Zhao, M.Z. Bazant, Population dynamics of driven autocatalytic reactive mixtures, Physical Review E 100(1) (2019) 012144.
[176] Y. Li, H. Chen, K. Lim, H.D. Deng, J. Lim, D. Fraggedakis, P.M. Attia, S.C. Lee, N. Jin, J. Moškon, Fluid-enhanced surface diffusion controls intraparticle phase transformations, Nature materials 17(10) (2018) 915-922.
[177] W.C. Chueh, F. El Gabaly, J.D. Sugar, N.C. Bartelt, A.H. McDaniel, K.R. Fenton, K.R. Zavadil, T. Tyliszczak, W. Lai, K.F. McCarty, Intercalation pathway in many-particle LiFePO4 electrode revealed by nanoscale state-of-charge mapping, Nano letters 13(3) (2013) 866-872.
[178] W. Dreyer, C. Guhlke, R. Huth, The behavior of a many-particle electrode in a lithium-ion battery, Physica D: Nonlinear Phenomena 240(12) (2011) 1008-1019.
[179] W. Dreyer, J. Jamnik, C. Guhlke, R. Huth, J. Moškon, M. Gaberšček, The thermodynamic origin of hysteresis in insertion batteries, Nature materials 9(5) (2010) 448-453.
[180] K. Märker, P.J. Reeves, C. Xu, K.J. Griffith, C.P. Grey, Evolution of structure and lithium dynamics in LiNi0. 8Mn0. 1Co0. 1O2 (NMC811) cathodes during electrochemical cycling, Chemistry of Materials 31(7) (2019) 2545-2554.
[181] A. Grenier, P.J. Reeves, H. Liu, I.D. Seymour, K. Märker, K.M. Wiaderek, P.J. Chupas, C.P. Grey, K.W. Chapman, Intrinsic Kinetic Limitations in Substituted Lithium-Layered Transition-Metal Oxide Electrodes, Journal of the American Chemical Society 142(15) (2020) 7001-7011.
[182] Y.N. Zhou, J.L. Yue, E. Hu, H. Li, L. Gu, K.W. Nam, S.M. Bak, X. Yu, J. Liu, J. Bai, High‐rate charging induced intermediate phases and structural changes of layer‐structured cathode for lithium‐ion batteries, Advanced Energy Materials 6(21) (2016) 1600597.
[183] S. Kalirai, K. Lim, B. Enders, J. Hong, W.E. Gent, A. Deva, E.R. Garcia, Y.-S. Yu, R. Celestre, M.F. Toney, Understanding Chemomechanical Li-ion Cathode Degradation through Multi-Scale, Multi-Modal X-ray Spectromicroscopy, Microscopy and Microanalysis 24(S2) (2018) 426-427.
[184] W.E. Gent, Y. Li, S. Ahn, J. Lim, Y. Liu, A.M. Wise, C.B. Gopal, D.N. Mueller, R. Davis, J.N. Weker, Persistent State‐of‐Charge Heterogeneity in Relaxed, Partially Charged Li1− xNi1/3Co1/3Mn1/3O2 Secondary Particles, Advanced Materials 28(31) (2016) 6631-6638.
[185] S. Dargaville, T.W. Farrell, Predicting active material utilization in LiFePO4 electrodes using a multiscale mathematical model, Journal of the Electrochemical Society 157(7) (2010) A830.
[186] V. Srinivasan, J. Newman, Discharge model for the lithium iron-phosphate electrode, Journal of the Electrochemical Society 151(10) (2004) A1517.
[187] Q. Zhang, R.E. White, Moving boundary model for the discharge of a LiCoO2 electrode, Journal of The Electrochemical Society 154(6) (2007) A587.
[188] T. Zhang, M. Kamlah, A nonlocal species concentration theory for diffusion and phase changes in electrode particles of lithium ion batteries, Continuum Mechanics and Thermodynamics 30(3) (2018) 553-572.
[189] B. Han, A. Van der Ven, D. Morgan, G. Ceder, Electrochemical modeling of intercalation processes with phase field models, Electrochimica Acta 49(26) (2004) 4691-4699.

[190] P. Bai, D.A. Cogswell, M.Z. Bazant, Suppression of phase separation in LiFePO4 nanoparticles during battery discharge, Nano letters 11(11) (2011) 4890-4896.
[191] D.A. Cogswell, M.Z. Bazant, Theory of coherent nucleation in phase-separating nanoparticles, Nano letters 13(7) (2013) 3036-3041.
[192] T. Hofmann, D. Westhoff, J. Feinauer, H. Andrä, J. Zausch, V. Schmidt, R. Müller, Electro-chemo-mechanical simulation for lithium ion batteries across the scales, International Journal of Solids and Structures 184 (2020) 24-39.
[193] B. Orvananos, H.-C. Yu, R. Malik, C.P. Grey, G. Ceder, K. Thornton, Interparticle Phase-Separation Dynamics in Dense Agglomerates of Lithium Iron Phosphate Nanoparticles, transition 9(6) (2006) A295-A298.
[194] B. Orvananos, H.-C. Yu, M.Z. Bazant, K. Thornton, Simulations of li-ion intercalation dynamics in 3D microstructures, 220th ECS Meeting, 2011.
[195] B. Orvananos, R. Malik, H.-C. Yu, A. Abdellahi, C.P. Grey, G. Ceder, K. Thornton, Architecture dependence on the dynamics of nano-LiFePO4 electrodes, Electrochimica Acta 137 (2014) 245-257.
[196] B. Orvananos, H.-C. Yu, A. Abdellahi, R. Malik, C.P. Grey, G. Ceder, K. Thornton, Kinetics of nanoparticle interactions in battery electrodes, Journal of The Electrochemical Society 162(6) (2015) A965.
[197] T.R. Ferguson, M.Z. Bazant, Nonequilibrium thermodynamics of porous electrodes, Journal of The Electrochemical Society 159(12) (2012) A1967.
[198] T.R. Ferguson, M.Z. Bazant, Phase transformation dynamics in porous battery electrodes, Electrochimica Acta 146 (2014) 89-97.
[199] Y. Li, F. El Gabaly, T.R. Ferguson, R.B. Smith, N.C. Bartelt, J.D. Sugar, K.R. Fenton, D.A. Cogswell, A.D. Kilcoyne, T. Tyliszczak, Current-induced transition from particle-by-particle to concurrent intercalation in phase-separating battery electrodes, Nature materials 13(12) (2014) 1149-1156.
[200] H. Mendoza, S.A. Roberts, V.E. Brunini, A.M. Grillet, Mechanical and electrochemical response of a LiCoO2 cathode using reconstructed microstructures, Electrochimica Acta 190 (2016) 1-15.
[201] N. Nadkarni, E. Rejovitsky, D. Fraggedakis, C.V. Di Leo, R.B. Smith, P. Bai, M.Z. Bazant, Interplay of phase boundary anisotropy and electro-auto-catalytic surface reactions on the lithium intercalation dynamics in Li X FePO 4 plateletlike nanoparticles, Physical Review Materials 2(8) (2018) 085406.
[202] J.-B. Caron, R.R. Gaines, C. Aria, M.G. Mángano, M. Streng, A new phyllopod bed-like assemblage from the Burgess Shale of the Canadian Rockies, Nature communications 5(1) (2014) 1-6.
[203] Y. Zeng, R.B. Smith, P. Bai, M.Z. Bazant, Simple formula for marcus–hush–chidsey kinetics, Journal of Electroanalytical Chemistry 735 (2014) 77-83.
[204] Y. Zeng, P. Bai, R.B. Smith, M.Z. Bazant, Simple formula for asymmetric Marcus–Hush kinetics, Journal of Electroanalytical Chemistry 748 (2015) 52-57.
[205] D. Fraggedakis, M. McEldrew, R.B. Smith, Y. Krishnan, Y. Zhang, P. Bai, W.C. Chueh, Y. Shao-Horn, M.Z. Bazant, Theory of coupled ion-electron transfer kinetics, Electrochimica Acta (2020) 137432.
[206] M.Z. Bazant, Thermodynamic stability of driven open systems and control of phase separation by electro-autocatalysis, Faraday discussions 199 (2017) 423-463.
[207] D. Grazioli, M. Magri, A. Salvadori, Computational modeling of Li-ion batteries, Computational Mechanics 58(6) (2016) 889-909.
[208] K. Zhao, Y. Cui, Understanding the role of mechanics in energy materials: a perspective, Extreme Mech. Lett 9 (2016) 347-352.
[209] R. Xu, K. Zhao, Electrochemomechanics of electrodes in Li-ion batteries: a review, Journal of Electrochemical Energy Conversion and Storage 13(3) (2016).
[210] Y. Zhao, P. Stein, Y. Bai, M. Al-Siraj, Y. Yang, B.-X. Xu, A review on modeling of electro-chemo-mechanics in lithium-ion batteries, Journal of Power Sources 413 (2019) 259-283.

[211] J. Zhu, T. Wierzbicki, W. Li, A review of safety-focused mechanical modeling of commercial lithium-ion batteries, Journal of Power Sources 378 (2018) 153-168.
[212] B. Liu, Y. Jia, C. Yuan, L. Wang, X. Gao, S. Yin, J. Xu, Safety issues and mechanisms of lithium-ion battery cell upon mechanical abusive loading: A review, Energy Storage Materials 24 (2020) 85-112.
[213] C.V. Di Leo, E. Rejovitzky, L. Anand, Diffusion–deformation theory for amorphous silicon anodes: the role of plastic deformation on electrochemical performance, International Journal of Solids and Structures 67 (2015) 283-296.
[214] A.F. Bower, P. Guduru, A simple finite element model of diffusion, finite deformation, plasticity and fracture in lithium ion insertion electrode materials, Modelling and Simulation in Materials Science and Engineering 20(4) (2012) 045004.
[215] S. Kim, J. Wee, K. Peters, H.-Y.S. Huang, Multiphysics coupling in lithium-ion batteries with reconstructed porous microstructures, The Journal of Physical Chemistry C 122(10) (2018) 5280-5290.
[216] R. Xu, L. De Vasconcelos, J. Shi, J. Li, K. Zhao, Disintegration of meatball electrodes for LiNi x Mn y Co z O 2 cathode materials, Experimental mechanics 58(4) (2018) 549-559.
[217] L. de Vasconcelos, N. Sharma, R. Xu, K. Zhao, In-situ nanoindentation measurement of local mechanical behavior of a Li-ion battery cathode in liquid electrolyte, Experimental Mechanics 59(3) (2019) 337-347.
[218] R. Xu, H. Sun, L.S. de Vasconcelos, K. Zhao, Mechanical and structural degradation of LiNixMnyCozO2 cathode in Li-ion batteries: an experimental study, Journal of The Electrochemical Society 164(13) (2017) A3333.
[219] B. Wu, W. Lu, A consistently coupled multiscale mechanical–electrochemical battery model with particle interaction and its validation, Journal of the Mechanics and Physics of Solids 125 (2019) 89-111.
[220] B. Wu, W. Lu, A battery model that fully couples mechanics and electrochemistry at both particle and electrode levels by incorporation of particle interaction, Journal of Power Sources 360 (2017) 360-372.
[221] W.H. Woodford, W.C. Carter, Y.-M. Chiang, Design criteria for electrochemical shock resistant battery electrodes, Energy & Environmental Science 5(7) (2012) 8014-8024.
[222] S.P. Nadimpalli, V.A. Sethuraman, D.P. Abraham, A.F. Bower, P.R. Guduru, Stress evolution in lithium-ion composite electrodes during electrochemical cycling and resulting internal pressures on the cell casing, Journal of The Electrochemical Society 162(14) (2015) A2656.
[223] J. Sheth, N.K. Karan, D.P. Abraham, C.C. Nguyen, B.L. Lucht, B.W. Sheldon, P.R. Guduru, In situ stress evolution in Li1+ xMn2O4 thin films during electrochemical cycling in li-ion cells, Journal of The Electrochemical Society 163(13) (2016) A2524.
[224] K.Y. Chung, K.-B. Kim, Investigation of structural fatigue in spinel electrodes using in situ laser probe beam deflection technique, Journal of The Electrochemical Society 149(1) (2001) A79.
[225] F.M. Kindermann, J. Keil, A. Frank, A. Jossen, A SEI modeling approach distinguishing between capacity and power fade, Journal of The Electrochemical Society 164(12) (2017) E287.
[226] P. Lu, C. Li, E.W. Schneider, S.J. Harris, Chemistry, impedance, and morphology evolution in solid electrolyte interphase films during formation in lithium ion batteries, The Journal of Physical Chemistry C 118(2) (2014) 896-903.
[227] C.R. Birkl, M.R. Roberts, E. McTurk, P.G. Bruce, D.A. Howey, Degradation diagnostics for lithium ion cells, Journal of Power Sources 341 (2017) 373-386.
[228] J. Gonzalez, K. Sun, M. Huang, J. Lambros, S. Dillon, I. Chasiotis, Three dimensional studies of particle failure in silicon based composite electrodes for lithium ion batteries, Journal of Power Sources 269 (2014) 334-343.
[229] Y. Mao, X. Wang, S. Xia, K. Zhang, C. Wei, S. Bak, Z. Shadike, X. Liu, Y. Yang, R. Xu, High‐Voltage Charging‐Induced Strain, Heterogeneity, and Micro‐Cracks in Secondary Particles of a Nickel‐Rich Layered Cathode Material, Advanced Functional Materials 29(18) (2019) 1900247.

[230] D.A. Cogswell, M.Z. Bazant, Coherency strain and the kinetics of phase separation in LiFePO4 nanoparticles, ACS nano 6(3) (2012) 2215-2225.
[231] S.A. Roberts, V.E. Brunini, K.N. Long, A.M. Grillet, A framework for three-dimensional mesoscale modeling of anisotropic swelling and mechanical deformation in lithium-ion electrodes, Journal of The Electrochemical Society 161(11) (2014) F3052.
[232] A. van Bommel, R. Divigalpitiya, Effect of calendering LiFePO4 electrodes, Journal of The Electrochemical Society 159(11) (2012) A1791.
[233] J. Zhu, W. Li, Y. Xia, E. Sahraei, Testing and modeling the mechanical properties of the granular materials of graphite anode, Journal of The Electrochemical Society 165(5) (2018) A1160.
[234] D. Schreiner, A. Klinger, G. Reinhart, Modeling of the Calendering Process for Lithium-Ion Batteries with DEM Simulation, Procedia CIRP 93 (2020) 149-155.
[235] C. Sangrós Giménez, C. Schilde, L. Froböse, S. Ivanov, A. Kwade, Mechanical, Electrical, and Ionic Behavior of Lithium‐Ion Battery Electrodes via Discrete Element Method Simulations, Energy Technology 8(2) (2020) 1900180.
[236] C.S. Giménez, B. Finke, C. Schilde, L. Froböse, A. Kwade, Numerical simulation of the behavior of lithium-ion battery electrodes during the calendaring process via the discrete element method, Powder Technology 349 (2019) 1-11.
[237] M. Duquesnoy, T. Lombardo, M. Chouchane, E.N. Primo, A.A. Franco, Data-driven assessment of electrode calendering process by combining experimental results, in silico mesostructures generation and machine learning, Journal of Power Sources 480 (2020) 229103.
[238] V. Laue, F. Röder, U. Krewer, Joint structural and electrochemical modeling: Impact of porosity on lithium-ion battery performance, Electrochimica Acta 314 (2019) 20-31.
[239] H. Kang, C. Lim, T. Li, Y. Fu, B. Yan, N. Houston, V. De Andrade, F. De Carlo, L. Zhu, Geometric and electrochemical characteristics of LiNi1/3Mn1/3Co1/3O2 electrode with different calendering conditions, Electrochimica Acta 232 (2017) 431-438.
[240] X. Lu, S.R. Daemi, A. Bertei, M.D. Kok, K.B. O'Regan, L. Rasha, J. Park, G. Hinds, E. Kendrick, D.J. Brett, Microstructural Evolution of Battery Electrodes During Calendering, Joule (2020).
[241] R. Weber, M. Genovese, A. Louli, S. Hames, C. Martin, I.G. Hill, J. Dahn, Long cycle life and dendrite-free lithium morphology in anode-free lithium pouch cells enabled by a dual-salt liquid electrolyte, Nature Energy 4(8) (2019) 683-689.
[242] V. Müller, R.-G. Scurtu, M. Memm, M.A. Danzer, M. Wohlfahrt-Mehrens, Study of the influence of mechanical pressure on the performance and aging of Lithium-ion battery cells, Journal of Power Sources 440 (2019) 227148.
[243] X. Zhang, Q.J. Wang, K.L. Harrison, K. Jungjohann, B.L. Boyce, S.A. Roberts, P.M. Attia, S.J. Harris, Rethinking how external pressure can suppress dendrites in lithium metal batteries, Journal of The Electrochemical Society 166(15) (2019) A3639.
[244] X. Zhang, Q.J. Wang, K.L. Harrison, S.A. Roberts, S.J. Harris, Pressure-driven interface evolution in solid-state lithium metal batteries, Cell Reports Physical Science 1(2) (2020) 100012.
[245] J. Zhu, W. Li, T. Wierzbicki, Y. Xia, J. Harding, Deformation and failure of lithium-ion batteries treated as a discrete layered structure, International Journal of Plasticity 121 (2019) 293-311.
[246] J. Zhu, X. Zhang, H. Luo, E. Sahraei, Investigation of the deformation mechanisms of lithium-ion battery components using in-situ micro tests, Applied energy 224 (2018) 251-266.
[247] L.S. de Vasconcelos, R. Xu, K. Zhao, Operando nanoindentation: a new platform to measure the mechanical properties of electrodes during electrochemical reactions, Journal of The Electrochemical Society 164(14) (2017) A3840.
[248] H. Sun, K. Zhao, Electronic Structure and Comparative Properties of LiNi x Mn y Co z O2 Cathode Materials, The Journal of Physical Chemistry C 121(11) (2017) 6002-6010.

[249] H. Jia, X. Li, J. Song, X. Zhang, L. Luo, Y. He, B. Li, Y. Cai, S. Hu, X. Xiao, Hierarchical porous silicon structures with extraordinary mechanical strength as high-performance lithium-ion battery anodes, Nature communications 11(1) (2020) 1-9.
[250] Y. Qi, H. Guo, L.G. Hector Jr, A. Timmons, Threefold increase in the Young's modulus of graphite negative electrode during lithium intercalation, Journal of The Electrochemical Society 157(5) (2010) A558.
[251] Y. Qi, L.G. Hector Jr, C. James, K.J. Kim, Lithium concentration dependent elastic properties of battery electrode materials from first principles calculations, Journal of the Electrochemical Society 161(11) (2014) F3010.
[252] J. Chen, J. Liu, Y. Qi, T. Sun, X. Li, Unveiling the roles of binder in the mechanical integrity of electrodes for lithium-ion batteries, Journal of The Electrochemical Society 160(9) (2013) A1502.
[253] A. Santimetaneedol, R. Tripuraneni, S.A. Chester, S.P. Nadimpalli, Time-dependent deformation behavior of polyvinylidene fluoride binder: Implications on the mechanics of composite electrodes, Journal of Power Sources 332 (2016) 118-128.
[254] H. Luo, J. Zhu, E. Sahraei, Y. Xia, Adhesion strength of the cathode in lithium-ion batteries under combined tension/shear loadings, RSC advances 8(8) (2018) 3996-4005.
[255] P. Pizette, C. Martin, G. Delette, P. Sornay, F. Sans, Compaction of aggregated ceramic powders: From contact laws to fracture and yield surfaces, Powder technology 198(2) (2010) 240-250.
[256] N. Abdelmoula, B. Harthong, D. Imbault, P. Dorémus, A study on the uniqueness of the plastic flow direction for granular assemblies of ductile particles using discrete finite-element simulations, Journal of the Mechanics and Physics of Solids 109 (2017) 142-159.
[257] C. Hendricks, N. Williard, S. Mathew, M. Pecht, A failure modes, mechanisms, and effects analysis (FMMEA) of lithium-ion batteries, Journal of Power Sources 297 (2015) 113-120.
[258] C. Chen, Y. Zuo, W. Ye, X. Li, Z. Deng, S.P. Ong, A critical review of machine learning of energy materials, Advanced Energy Materials 10(8) (2020) 1903242.
[259] K. Homma, Y. Liu, M. Sumita, R. Tamura, N. Fushimi, J. Iwata, K. Tsuda, C. Kaneta, Optimization of a Heterogeneous Ternary Li3PO4–Li3BO3–Li2SO4 Mixture for Li-Ion Conductivity by Machine Learning, The Journal of Physical Chemistry C 124(24) (2020) 12865-12870.
[260] R.P. Joshi, J. Eickholt, L. Li, M. Fornari, V. Barone, J.E. Peralta, Machine learning the voltage of electrode materials in metal-ion batteries, ACS applied materials & interfaces 11(20) (2019) 18494-18503.
[261] Y. Takagishi, T. Yamanaka, T. Yamaue, Machine learning approaches for designing mesoscale structure of Li-ion battery electrodes, Batteries 5(3) (2019) 54.
[262] T. Gao, W. Lu, Physical Model and Machine Learning Enabled Electrolyte Channel Design for Fast Charging, Journal of The Electrochemical Society 167(11) (2020) 110519.
[263] J. Jung, J.I. Yoon, H.K. Park, H. Jo, H.S. Kim, Microstructure design using machine learning generated low dimensional and continuous design space, Materialia (2020) 100690.
[264] S. Sundar, V. Sundararaghavan, Database development and exploration of process–microstructure relationships using variational autoencoders, Materials Today Communications (2020) 101201.
[265] V. Dumoulin, I. Belghazi, B. Poole, O. Mastropietro, A. Lamb, M. Arjovsky, A. Courville, Adversarially learned inference, arXiv preprint arXiv:1606.00704 (2016).
[266] Z. Yang, X. Li, L. Catherine Brinson, A.N. Choudhary, W. Chen, A. Agrawal, Microstructural materials design via deep adversarial learning methodology, Journal of Mechanical Design 140(11) (2018).
[267] R.K. Tan, N.L. Zhang, W. Ye, A deep learning–based method for the design of microstructural materials, Structural and Multidisciplinary Optimization (2019) 1-22.
[268] H. Zhao, B.D. Storey, R.D. Braatz, M.Z. Bazant, Learning the physics of pattern formation from images, Physical Review Letters 124(6) (2020) 060201.

[269] S. Effendy, J. Song, M.Z. Bazant, Analysis, Design, and Generalization of Electrochemical Impedance Spectroscopy (EIS) Inversion Algorithms, Journal of the Electrochemical Society (2020).
[270] J. Song, M.Z. Bazant, Electrochemical impedance imaging via the distribution of diffusion times, Physical review letters 120(11) (2018) 116001.
[271] J. Holdren, Materials genome initiative for global competitiveness. National Science and technology council OSTP, Washington, USA (2011).
[272] G.B. Olson, Preface to the viewpoint set on: The Materials Genome, Scripta Materialia 100(70) (2014) 1-2.
[273] G.B. Olson, Computational design of hierarchically structured materials, Science 277(5330) (1997) 1237-1242.
[274] S. Curtarolo, G.L. Hart, M.B. Nardelli, N. Mingo, S. Sanvito, O. Levy, The high-throughput highway to computational materials design, Nature materials 12(3) (2013) 191-201.
[275] H. Zhao, X. Li, Y. Zhang, L.S. Schadler, W. Chen, L.C. Brinson, Perspective: NanoMine: A material genome approach for polymer nanocomposites analysis and design, APL Materials 4(5) (2016) 053204.